FROM CANCER TO AGING: HARNESSING CAR T CELLS TO DECONSTRUCT SENESCENCE

by

Corina Amor Vegas

A Dissertation

Presented to the Faculty of the Louis V. Gerstner, Jr.

Graduate School of Biomedical Sciences,

Memorial Sloan Kettering Cancer Center

in Partial Fulfillment of the Requirements for the Degree of

Doctor of Philosophy

New York, NY

December, 2021

Scott W. Lowe, Ph.D.
Dissertation Mentor

Date

..

To my parents, Esperanza and Marcial, without whose support I would have never gotten here.

A mis padres, Esperanza y Marcial, sin cuyo apoyo nunca hubiera llegado hasta aquí.

“One evening in the late nineteen forties my wife and I were at a party […] we were all asked to sign the guest book and state our hobby […]. I put down my hobby as Biochemistry.”

The pursuit of a Hobby. Severo Ochoa

ABSTRACT

Cellular senescence is a stress response program characterized by stable cell cycle arrest. Initially described as a tumor suppressor mechanism, it involves the interplay between the tumor suppressors p53 and RB leading to a transcriptional program of gene repression that silences proliferation associated genes. Beyond their arrest, senescent cells secrete the senescence associated secretory phenotype (SASP) composed of cytokines and matrix remodeling enzymes. The SASP contributes to the induction of paracrine senescence as well as to the recruitment of immune cells, whose role is to clear the senescent cells and restore tissue homeostasis. Indeed, this is what happens in the context of wound healing or tumor suppression. However, for mechanisms that remain unclear, in certain settings such as aging or age-related diseases, senescent cells accumulate over time generating a pathological chronic pro-inflammatory milieu that plays a key role in the pathophysiology of these conditions. Here we test for the first time the therapeutic concept that chimeric antigen receptor (CAR) T cells can be engineered to target senescent cells and restore tissue homeostasis. Treatment of senescence-associated liver fibrosis with senolytic CAR T cells leads to resolution of fibrosis and enhanced liver function in both non-alcoholic steatohepatitis (NASH) and in chemical induced fibrosis. Furthermore, senolytic CAR T cells are also therapeutic in cancer models through one-two punch senogenic-senolytic approaches. These results establish the potential for using CAR T cells to interrogate senescence biology and as senolytic agents for the treatment of a broad range of senescence-associated diseases.

BIOGRAPHICAL SKETCH

Corina Amor Vegas was born in Madrid, Spain on June 13th 1993 to Asturian parents Maria Esperanza and Marcial. A middle class family, they made significant efforts to provide educational resources to Corina that they had not had. Thus, she was able to learn English from a very young age and attend an excellent private school. This hard work paid off and Corina graduated high school in 2011 with maximum qualifications and awards. Interested in the life sciences and wanting to contribute to society she enrolled in the European 6 year MD degree at the Universidad Complutense de Madrid.

It soon became apparent however, that she was more interested in understanding the mechanisms behind disease than in actual clinical practice. This led her to start spending time in research laboratories. Initially within her own university, and shortly after at the Spanish National Cancer Research Center (CNIO), where she worked in the laboratories of Mariano Barbacid and Oscar Fernández-Capetillo for a total of 4 years. This work was done every day after classes and hospital clerkships, usually well into the evenings which were followed by long study nights to maintain a good academic record on her medical degree. In addition, she was determined to understand how science was done outside of Spain, and she used all of her summers holidays those years to visit: Imperial College London, the University of Oxford, Harvard Medical School or the European Molecular Biology Laboratory (EMBL). They were years of hard work, which gave her neither academic credits for her medical degree, nor economic benefit (in fact she usually had to finance her stays through the economic awards she got for academic performance), or academic advancement (she was only co-author in one publication). But she did learn a lot of new techniques, was exposed to many scientific fields and overall these experiences only reinforced her desire to pursue science.

Upon graduation in 2017, instead of going straight into medical residency, she decided (much against everyone's advice), to come to New York and enroll in the Gerstner Sloan Kettering graduate school to earn her PhD. This proved to be a thrilling experience. For the first time her whole day was free to be spent in the lab, read papers and attend science classes. Everything that up to that point had been her "hobby" became her actual job. She did her first rotation in the lab of Scott Lowe (whom she had met at the CNIO before and had played a huge role in her decision to come to NY) and immediately made her mind to join his lab, which she officially did in 2018.

Interested in senescence, she soon realized the shortage of senolytics and surface molecules was a roadblock to the field and conceived the idea of potential senolytic CAR T cells. Having identified uPAR as a senescence surface molecule at the end of 2017, she had an initial meeting in March 2018 to decide next steps where both Scott Lowe and Michel Sadelain were highly supportive, but recognized it was a "crazy" project. She continued working on this initial side project, which eventually became her main one and the rest, as they say, it is history. After completion of her PhD Corina is moving to Cold Spring Harbor Laboratory (CSHL) to start her own laboratory as a CSHL independent fellow where she hopes she can continue investigating cool senescence biology and giving opportunities to young people interested in a career in science.

ACKNOWLEDGEMENTS

First of all I want to thank my mentor Dr.Scott W Lowe, for believing in my potential and giving me the opportunity to join his lab. Throughout the years Scott has given me unparalleled freedom, space and trust to pursue and nurture my scientific interests while at the same time being there in times of trouble when I needed him. I cannot think of a better mentor to have had and I am forever grateful for these years.

I want to especially thank Dr.Michel Sadelain for his unwavering support to the project. Despite being incredibly busy he has never hesitated to meet with me and has provided constant advice effectively becoming a second mentor to me during my PhD.

Also, I want to express my gratitude to Dr.Charles Sawyers, for agreeing to be a member of my PhD committee and for his excellent advice throughout my PhD.

A warm thank you to Dr.Charles Sherr for his advice and mentorship. Throughout these years Chuck has always had time to discuss science, grad school and life with me. He has had the patience to go over all my grants and fellowships applications and discuss all of my (often repeated) concerns. I was extremely lucky to cross paths during his sabbatical at the Lowe lab and I am extremely grateful for your time and help.

I also want to thank all the Lowe lab and Sadelain lab members who I have crossed paths with in the past four years. Special thank you to Judith Feucht and Josef Leibold for believing in the CAR T project when many others doubted it could work, for their help and for sharing with me their knowledge and experiences. Thank you to all other lab members from both labs for their help, advise and generosity over these years: Direna Alonso Curbelo, Ana Banito, Francisco Barriga, Caroline Broderick, Almudena Chaves

Perez, Chi-Chao Chen, Sean Chen, Gertrude Gunset, Katerina Hatzi, Ray Ho, Ted Kastenhuber, Margaret Kennedy, Grace Li, Eva Loizou, Amaia Lujambio, Jorge Mansilla-Soto, Riccardo Mezzadra, Scott Millman, John P.Morris IV, Bryan Ngo, Stella Paffenholz, José Reyes, Marcus Ruscetti, Kasia Rybczyk, Francisco Sánchez-Rivera, Kaloyan Tsanov, Anahi Tehuitzil, Zeda Zhang, Zhen Zhao, Changu Zhu, Wei Luan, Vincent Tem, Sha Tian, Alexandra Wuest. Very special thanks to Lynn Boss, Mei-Ling Li, Janelle Simon, Anne Trumble and Leah Zamechek for being the key structure that keeps the lab running and allow us to focus on the research.

Thank you to my current and former GSK classmates: Mariano Aufiero, Mollie Chipman, Florisela Herrejón Chávez, Ellen Horste, Sara Khalil, Buren Li, Adina Schonbrun, Zhouyang Shen and Adele Whaley. I would not have survived first year without you and your friendship these years has significantly enriched my time at GSK. Special thank you to Jordan Aronowitz, whom we always remember and miss.

I also want to thank all members of the GSK graduate school for creating a fantastic program that has allowed me to focus on the science and kept bureaucracy and economic concerns to the minimum: Mike Overholtzer (who has always been available to listen to concerns and provide advice), Ken Marians, Linda Burnley, Thomas Magaldi, David McDonagh, Stacy de la Cruz, Julie Masen and Raphaelle Chassegne. Thank you as well to Ushma Neill, Thalyana Stathis and Yaihara Fortis Santiago for all their fantastic career development advice and resources.

I want to extend my thank you to the GSK Women in Science group (GWIS): Inés Fernández Maestre, Brianna Naizir, Yanyang Chen, Florisela Herrejón Chávez and

Emily Kansler. I have truly enjoyed my time these years at GWIS and I am looking forward to what GWIS will accomplish in the years to come.

Thank you to all my friends from the old continent, especially to Susana Criado, Pablo Jerez, Javier Gomez and Maria Puig.

To Jacob Boyer, I can only say that I could not have wished for a better person to happen to show me NY and introduce me to the American life. You have been my rock these years, been there in the good and the bad, sharing science and life. When I look back at these years I treasure our time together and know it would have been very different without you. I am eager for this new chapter.

Finally, I want to wholeheartedly thank my family, who I have missed every day of these years, especially in these troubled pandemic times. My parents, Esperanza and Marcial, who have always believed in me and supported my dreams even if these took me away from them to the other side of the Atlantic. There are not enough words of appreciation to ever thank the unconditional parent love. To my sister, Sira, for her unwavering support. And lastly, to my brother, Marcial, Marta and the little tykes Paula and Enrique, who challenge my view of the world at every interaction.

THANK YOU to all of you.

TABLE OF CONTENTS

LIST OF FIGURES

LIST OF ABBREVIATIONS

Bcl-2: B cell lymphoma-2

CAR: Chimeric Antigen Receptor.

CCl_4: Carbon tetrachloride.

CDK: Cyclin-dependent kinases

cDNA: Complementary DNA

CIN: Chromosomal Instability

CNA: Copy number alterations

CRISPR/Cas9: Clustered regularly interspaced short palindromic repeats/ CRISPR-associated protein 9.

CRS: Cytokine release syndrome.

DCs: Dendritic cells.

EGFRt: Truncated epidermal growth factor receptor

EPO-GEMMs: Electroporation based genetically engineered mouse models

EBV: Epstein-Barr virus

FDA: U.S.Food and drug administration

GEMMs: Genetically engineered mouse model.

GM-CSF: Granulocyte-macrophage colony-stimulating factor

G-CSF: Granulocyte colony-stimulating factor

GS: Genomic stability

KP: $Kras^{G12V}$; $p53^{-/-}$

h.: Human

HPA: Human Protein Atlas

HMP: Human Proteome Map

HSCs: Hepatic Stellate Cells

HTVI: Hydrodynamic Tail Vein Injection

iCaspase 9: Inducible caspase 9

IFNγ: Interferon γ

ImmunoPET: Immuno-positron emission tomography

IR: Irradiation.

ITAM: Immunoreceptor tyrosine based activation domain

Luc: Luciferase

m.: Murine

MEFS: Murine embryonic fibroblasts

MSI: Microsatellite instability

NASH: Non-alcoholic steatohepatitis

NK cells: Natural killer cells

NSCLC: Non-Small Cell Lung Cancer

OIS: Oncogene Induced Senescence

PDX: Patient Derived Xenograft

PLAUR: Plasminogen activator, urokinase receptor

RNAseq: RNA sequencing

SA-β-Gal: Senescence associated β galactosidase

SAHF: Senescence associated heterochromatin foci

scFv: Single chain variable fragment

suPAR: Soluble urokinase plasminogen activator receptor

TIS: Therapy Induced Senescence

TNFα: Tumor necrosis factor α

TRAC: T cell receptor alpha constant

uPAR: Urokinase plasminogen activator receptor

UT: Untransduced

WT: Wild type

CHAPTER 1

INTRODUCTION

Age-related disorders, including cancer and chronic degenerative conditions like cardiovascular diseases, neurodegenerative pathologies, diabetes, and kidney failure constitute over 60% of all causes of death in the United States (Heron, 2021). Understanding the biology of aging is therefore a major health priority. In this regard, cellular senescence is a key determinant of organismal aging.

1.1.-Cellular senescence

1.1.1.-Concept

Senescence is a cellular program characterized by stable cell cycle arrest and resistance to both oncogenic and mitogenic stimuli. Cellular senescence is triggered in response to diverse cellular stresses that distort cellular homeostasis such as telomere erosion, unresolved DNA damage or lysosomal stress.

1.1.2.-Historical perspective

Cellular senescence was initially described by Hayflick as a phenomenon that accompanied replicative exhaustion of human cells in culture (Hayflick and Moorhead, 1961). Posterior work showed that a range of other cellular insults like telomere erosion (Harley et al., 1990), oncogenic activation (Serrano et al., 1997) and other DNA damage stimuli could induce “premature” senescence. Whether senescence was just an *in vitro* phenomenon or a process that also happened *in vivo* and had physiological relevance was a controversial topic in the field for several years. The work of the Serrano lab demonstrating the presence of senescent cells *in vivo* in premalignant Ras-driven lung

tumors provided the first evidence of its *in vivo* occurrence and relevance (Collado et al., 2005).

1.1.3.-Cell intrinsic component of cellular senescence

Initial efforts to explore the biology of cellular senescence focused on understanding the mechanisms behind the stable cell cycle arrest (Figure 1.1). These studies found that the stressors that trigger senescence could lead to the activation of p53 and RB. Activation of p53 promotes arrest through p21 and the subsequent inhibition of CDK2 which prevents phosphorylation of RB (Chicas et al., 2010). Alternatively, activation of p16INK4A inhibits CDK4/CDK6 thus preventing phosphorylation of RB ((Sharpless and Sherr, 2015)). RB in turn is linked to chromatin remodeling program that can be visualized on some cells microscopically (what is called the Senescence Associated Heterochromatic Foci or SAHF) and is also associated with the emergence of a repressive chromatin environment on E2F targets and other proliferative genes that is not observed in cells reversibly arrested during quiescence (Narita et al., 2003).

Although senescent cells undergo characteristic changes in gene expression, to date there is no single marker that proves a cell is senescent (Sharpless and Sherr, 2015). Instead, currently senescence is defined by the acquisition of several characteristics: a specific flat morphology, upregulation of the activity of senescence-associated beta-galactosidase (SA-β-gal), presence of SAHF or expression of $p16^{INK4a}$, $p15^{INK4b}$ and/or p21 cyclin-dependent kinases (Baker et al., 2011; Sharpless and Sherr, 2015). However not all senescent cells expresses each of these markers and certain normal cells (like macrophages) can present them too (Hall et al., 2017).

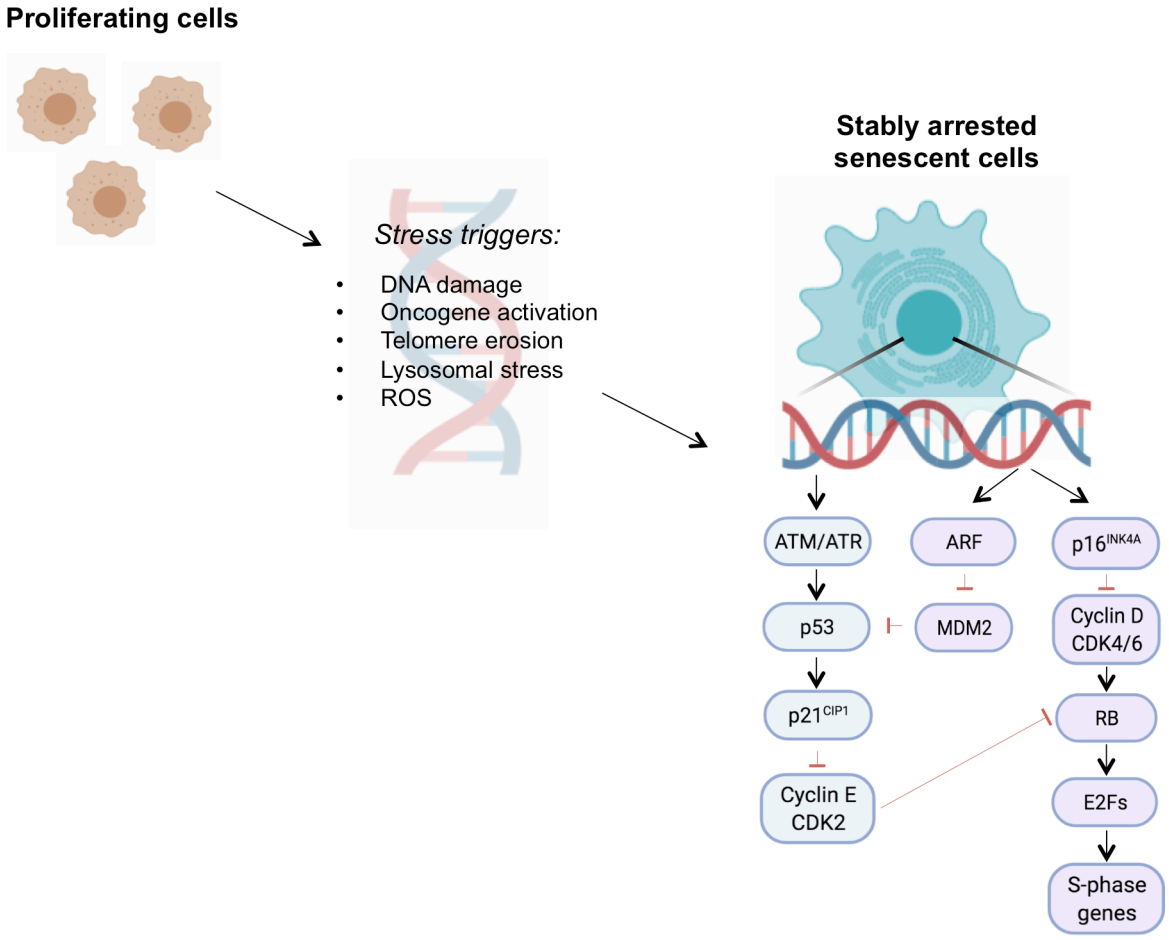

Figure 1.1. Cellular senescence is a stress response program leading to stable cell cycle arrest mediated by p53 and RB.

1.1.4.-Cell extrinsic component of cellular senescence

Besides their arrest, senescent cells activate a secretory program known as the Senescence Associated Secretory Phenotype (SASP). Key molecular mediators of the SASP are NF-κβ and BRD4 (Tasdemir et al., 2016). The SASP is composed of proinflammatory cytokines, chemokines, vascular factors and matrix metalloproteinases and its composition its highly dependent on the cell type and the trigger of senescence (Hernandez-Segura et al., 2017). It plays a key role in modulating the microenvironment of senescent cells (Lasry and Ben-Neriah, 2015). On one hand the SASP is key to propagate the senescence program in the tissue by inducing paracrine senescence of neighbor cells (Acosta et al., 2013) and on the other it plays a crucial role in recruiting immune cells that in turn can target senescent cells, a process known as senescence immune surveillance (Figure 1.2). Which components of the immune system and the mechanism they use to clear senescent cells are however, highly senescent context-depend.

NK cells are key cytolytic innate lymphoid cells that are capable of recognizing “stressed” cells, such as virus-infected and transformed cells via their ability to interact with stress ligands expressed by target cells (Murphy, 2012). They share several effector functions with conventional cytolytic CD8+ T cells such as their ability to kill target cells both through secretion of lytic granules and engagement of death receptors belonging to the TNF superfamily on the surface of target cells (Murphy, 2012). NK cells are able to target senescent cells in several contexts: 1) In age-related diseases such as liver fibrosis for example, NK cells recognize and clear senescent hepatic stellate cells (Krizhanovsky et al., 2008) in a perforin-dependent fashion (Sagiv et al., 2013). 2) Perforin production is also key to target senescent cells during ageing, as aged perforin-deficient mice, which lack cytolytic functions of both NK and T cells, display increased

accumulation of senescent cells and fibrotic tissue as compared to age-matched mice that are perforin-proficient (Ovadya et al., 2018). 3). Finally, NK cells are also able to target senescent tumor cells such as murine liver tumors that have been induced to senescence by restoration of p53 expression (Iannello et al., 2013) or lung adenocarcinoma senescent tumor cells that have been treated with combinatorial inhibition of CDK4/6 and MEK (Ruscetti et al., 2018). These processes depend on CCL2 secretion and expression of NK-activating ligand NKG2D and IL-15 by senescent cells (Iannello et al., 2013) or upregulation of ICAM-1 and the secretion of IL-15, and TNFα (Ruscetti et al., 2018) respectively.

Another immune cell involved in senescent cell clearance are macrophages. Macrophages are tissue-resident, phagocytic cells that have pleiotropic functions ranging from eliminating microbes to maintaining tissue homeostasis (Murphy, 2012). In the context of liver fibrosis, p53 drives hepatic stellate cells to senesce and secrete a SASP that polarizes macrophages to an “M1”, proinflammatory status that counteracts tumor occurrence by directly targeting senescent cells (Lujambio et al., 2013). Macrophages are also able to clear senescent cells in other contexts, such as in mouse postpartum uterus, where clearance of senescent cells helps maintaining the organ function and increase the success of second pregnancies (Egashira et al., 2017).

Finally, key players in senescence immune surveillance are T cells. T cells are immune cells characterized by a T cell receptor (TCR) which is the sole determinant of their specificity. Each alpha/beta T cell clonotype harbors a unique TCR which is able to recognize peptides presented in the context of the major histocompatibility complex (MHC) by target cells (Murphy, 2012). T cells are selected and educated to not react against self-peptides and instead recognize foreign peptides derived e.g. from viruses

infecting a cell or from missense mutations in cancer cells (Murphy, 2012). T cells have been implicated in the clearance of senescent cells especially in the setting of malignant or premalignant senescent cells. Thus, CD4+ T cells are needed for clearance of senescent Nras-mutated premalignant hepatocytes (Kang et al., 2011). Clearance of senescent cells in this setting requires macrophages that act as the effector cells (Kang et al., 2011). CD8+ T cells have also been implicated in the clearance of pancreatic tumor cells upon combined CDK4/6 and MEK inhibition and PD-1 blockade (Ruscetti et al., 2020).

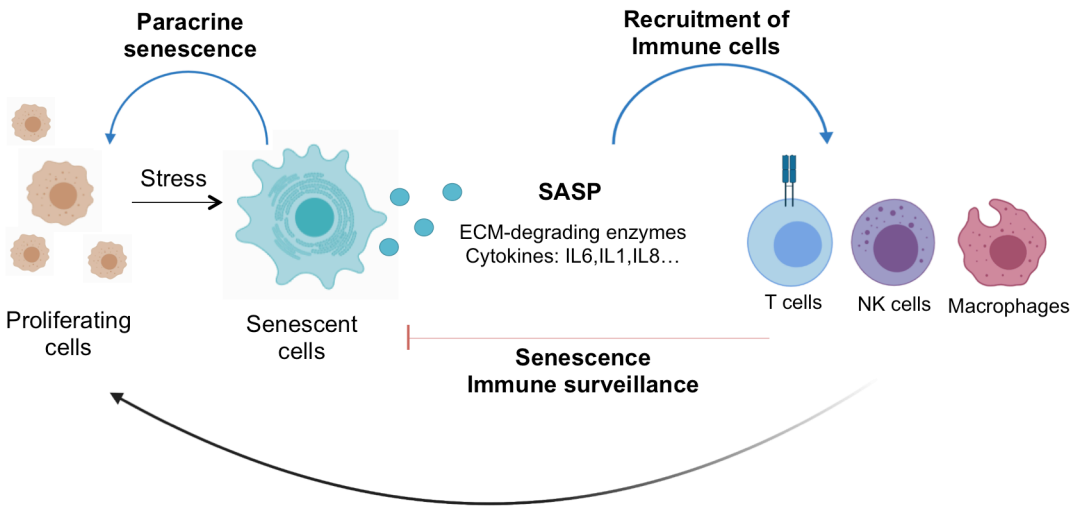

Figure 1.2. The SASP modulates the microenvironment of senescent cells.

1.2.-Implications of Cellular Senescence in Health and Disease

1.2.1.-Senescence helps restore tissue homeostasis

Cellular senescence plays a key role in restoring homeostasis in tissues that have undergone acute damage. Thus, senescent cells are integral for an optimal wound healing response where PDFG-AA secreted by senescent endothelial cells and fibroblasts induce myofibroblast differentiation (Demaria et al., 2014). Senescence also plays a key role in tumor suppression where it halts the proliferation of premalignant cells harboring oncogenic mutations and recruits the immune system to clear them (Kang et al., 2011). Inhibition of the senescence program or the immune surveillance of these cells results in a significant higher development of tumors (Kang et al., 2011).

1.2.2.-Senescence contributes to tissue damage

However senescent cells have also been shown to play a key pathogenic role in several age related diseases. This is the case of atherosclerosis, where senescent foam cells accumulate in the subendothelial space and their secreted IL1α, TNFα and Mmp3, Mmp13 contribute to plaque instability (Childs et al., 2016). Similarly, in lung fibrosis senescent fibroblasts are fibrogenic (Schafer et al., 2017) and in tau-mediated neurological diseases senescent astrocytes and microglia contribute to cognitive function decline by enhancing neurofibrillary tangle deposition (Bussian et al., 2018). In addition, GEMMs have shown that the genetic elimination of senescent cells can extend both health and lifespan suggesting a direct link between the accumulation of senescent cells and aging (Baker et al., 2011) (Baker et al., 2016).

Conciliating such opposing findings is challenging, and as a relatively novel field more research is needed. Nonetheless, one possible explanation relates to temporal dynamics (Figure 1.3). Thus, while senescence on the short term as a contained response is

beneficial and allows the tissue to recruit immune cells that help restore homeostasis; on the long term if these senescent cells are not cleared, they generate a continuous pro inflammatory milieu that is deleterious and generates tissue damage. Understanding what are the key determinants of senescence immune surveillance on the different settings and how senescent cells evade them in pathology will provide more mechanistic insight and open the door to enhanced treatments.

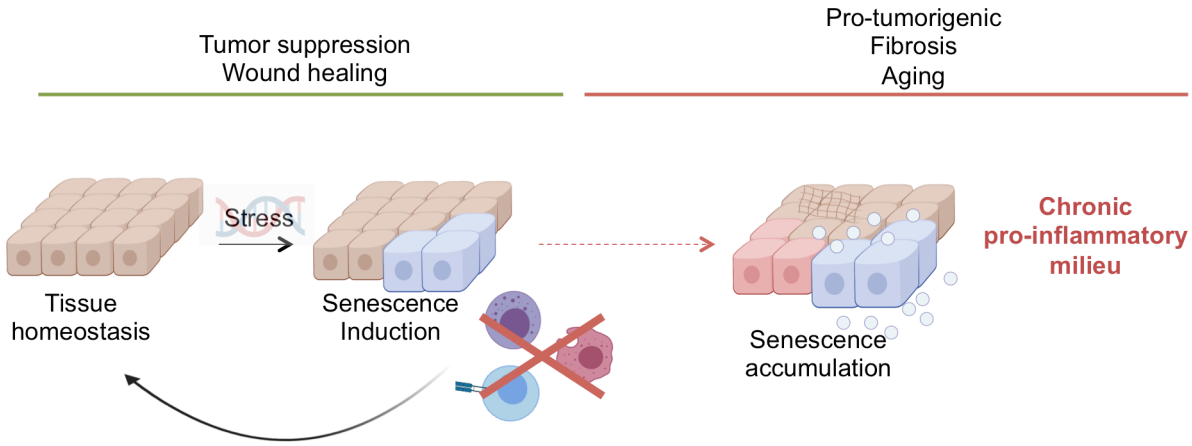

Figure 1.3. Temporal dynamics and senescence immune surveillance are key determinants of the effect of senescent cells in tissue homeostasis.

1.3.-Therapeutically targeting cellular senescence

Given the contribution of aberrantly accumulated senescent cells to pathology there has been growing interest in developing strategies to eliminate senescent cells (Kirkland and Tchkonia, 2017; Lujambio, 2016) (Figure 1.4).

Initial efforts in the field focused on inhibiting the secretion of the SASP rather than targeting the senescent cells themselves. Compounds used for this approach included glucocorticoids (Laberge et al., 2012), rapamycin (Wang et al., 2017) and JAK2 inhibitors (Xu et al., 2015).

Posterior efforts made use of a hypothesis-driven bioinformatics approach based on the resistance of senescent cells to apoptosis to identify pro-survival pathways upregulated in senescent cells (Zhu et al., 2016; Zhu et al., 2015). This strategy, coupled later to a chemical screen, led to the identification of dasatinib and quercetin and later to Bcl-2 inhibitors like navitoclax as compounds that induced apoptosis preferentially in certain senescent cells. Dasatinib is a non-selective multi-tyrosine kinase inhibitor and quercetin is a flavonoid. Dasatinib and quercetin have been usually used in combination as senolytic agents in multiple studies and clinical trials (Kirkland and Tchkonia, 2017) and their major side effects include anemia, diarrhea and can cause pulmonary edema and prolonged QT syndrome. Navitoclax targets Bcl-xl, Bcl-w and Bcl-2 and its major side effect is its dose-dependent thrombocytopenia (Kirkland and Tchkonia, 2017). Efforts to ameliorate navitoclax side effects have focused on harnessing the increased levels of SA-β-galatosidase activity of senescent cells to develop galacto-conjugation strategies to specifically release navitoclax to senescent cells (Gonzalez-Gualda et al., 2020). In any case, however, neither dasatinib or quercetin nor navitoclax can selectively induce apoptosis of all senescent cell types (Zhu et al., 2016; Zhu et al., 2015).

New research has focused on trying to identify additional characteristics of senescent cells that could be exploited to target them. In this regard, Guerrero et al and Triana-Martinez et al recently identified that senescent cells have a slightly depolarized plasma membrane and higher concentrations of H+ which sensitizes them to cardiac glycosides (Guerrero et al., 2019; Triana-Martinez et al., 2019).

A relatively unexplored angle has been that of surface proteins. Identification of surface molecules selectively (or at least preferentially) upregulated on senescent cells could enable strategies to engage the immune system to target these cells. Work by (Kim et al., 2017) identified DPP4 as a surface molecule upregulated in certain senescent cells and developed an antibody-dependent cell mediated cytotoxicity approach to target them. Further optimized strategies could involve the use of bispecific T cell engagers antibodies (BiTEs) that recruit T cells (through an anti-CD3 antibody) or the use of cellular therapy.

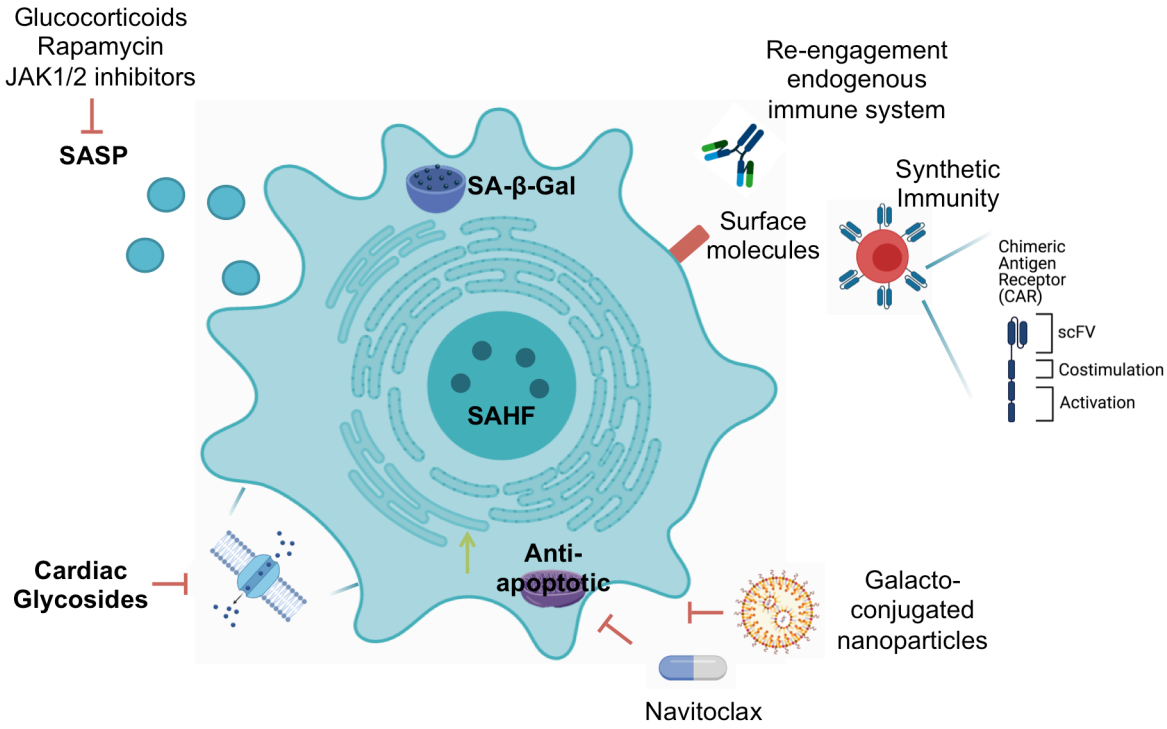

Figure 1.4. Overview of current senolytic strategies.

1.4.-Chimeric Antigen Receptor T Cells

1.4.1.-Concept and historical perspective

CAR T cells are T cells that have been engineered to express a synthetic Chimeric Antigen Receptor (CAR) to redirect their specificity against a specific antigen (Sadelain et al., 2017).

The first generation of CARs consisted of single chain fusion receptors composed of the extracellular scFV of a monoclonal antibody targeting a specific antigen linked to the intracellular CD3ζ chain or Fcγ domains (Brocker et al., 1993; Eshhar et al., 1993). It built on previous research that had tested linking the heavy or the light chain of an immunoglobulin to the constant region of the TCR α or β chains (Gross et al., 1989; Kuwana et al., 1987) or fusing the extracellular domains of CD8, CD4 or Fc receptors to the intracellular chain of the CD3ζ (Irving and Weiss, 1991; Letourneur and Klausner, 1991). However it soon became apparent that providing only the signaling of the CD3ζ chain was not enough to fully activate the CAR T cells (Brocker and Karjalainen, 1995).

Five years later, second generation CAR T cells were thus developed. These new version contained not only the scfv and the CD3ζ chain but also the intracellular domain of the costimulatory molecule CD28 which is essential for T cell growth, survival and memory formation (Finney et al., 1998). Second generation CAR T cells were found to be able to fully activate, secrete IL-2 and proliferate, and effectively target antigen expressing cells (Hombach et al., 2001; Maher et al., 2002). Additional variations of this design include the use of alternative co-stimulatory signaling domains the best studied being 4-1BB. While CD-28z based CARs mainly promote rapid T cell expansion and lead to limited T cell persistence; 4-1BB based CARs lead to a less potent initial effector

T cell but lead to longer persistence (Sadelain et al., 2017; Zhao et al., 2015).

Finally, in recent years third generation CARs have been designed that combine two costimulatory domains such as 4-1BB and CD28 (Wang et al., 2007) or OX40 and CD28z (Pule et al., 2005). While functional, clinical data has not demonstrated improved therapeutic efficacy over second generation CAR T cells (Till et al., 2012).

1.4.2.-The paradigm of CD19 CAR T cells

CD19 is a transmembrane protein specifically expressed on B cells (Murphy, 2012) and not expressed in any other vital tissues. Since B cells conserve the expression of CD19 when transformed, this made CD19 and ideal candidate for CAR T therapy in leukemia and lymphoma. Following several successful clinical trials (Brentjens et al., 2013; Davila et al., 2014; Grupp et al., 2013; Lee et al., 2015; Maude et al., 2014; Park et al., 2018) second generation CAR T cells targeting CD19 were FDA-approved for the treatment of B-ALL in children and young adults and refractory diffuse large B cell lymphoma (Maude et al., 2018; Neelapu et al., 2017).

Ongoing remaining challenges for CD19 CAR T cells are the outgrowth/relapse of CD19 negative or low tumor cells (Maude et al., 2014; Park et al., 2018) which call for the development of alternative or combinatorial antigens, lack of response of some patients to autologous CAR therapy (Park et al., 2018) and better understanding of the mechanism behind toxicities. Among the latter the most commonly described adverse events are (indeed) B cell aplasia, as well as cytokine release syndrome (CRS) and neurotoxicity. CRS is a short clinical syndrome characterized by fever, hypotension and respiratory insufficiency which correlates with high levels of IL-6, IL-1, nitric oxide and IFNγ in peripheral blood (Giavridis et al., 2018; Norelli et al., 2018). It is mediated by endogenous macrophages recruited to the tumor site and it responds to IL-6 and/or IL1

receptor blockade. CAR T related neurotoxicity is characterized by encephalopathy, aphasia, delirium and seizures and initial work suggests it is mediated by the accumulation of pro-inflammatory cytokines in the cerebrospinal fluid (Gust et al., 2017).

1.4.3.-Beyond cancer: the future of CAR T cells

Additional work has identified other antigens for hematological malignancies such as CD20, CD22 or BCMA and there are ongoing efforts to extend the efficacy of CAR T cells to solid tumors (June and Sadelain, 2018; Sadelain et al., 2017).

Interestingly, beyond oncology, there has been interest in harnessing the high potency of CAR T cells in other disease settings. Initial approaches exploited the B cell aplasia caused by CD19 CAR T cells as a therapeutic strategy in a murine model of systemic lupus erythematosus (Kansal et al., 2019) or employed CD4 ectodomain targeting CAR T cells for the treatment of HIV (Maldini et al., 2020). Posterior work has identified new targets such as FAP as potential antigens for CAR T cells in the context of cardiac fibrosis (Aghajanian et al., 2019). Although all of these initial studies were done in preclinical murine models they open the door for expanding CAR T cells in the clinic beyond the realm of oncology in the future.

1.5.-Aims

Given the lack of identified surface molecules of senescent cells and the need for potent senolytic strategies the overarching goal of this thesis is to explore the feasibility of finding surface markers of senescence and harnessing them to effectively target senescent cells through CAR T cells. Ultimately, we hypothesize and test the therapeutic potential of such a senolytic strategy. The aims are addressed in chapters 3,4 and 5.

1.5.1.-Aim 1: Identification of surface markers of senescence and development of senolytic CAR T cells.

The aim of chapter 3 is to compare the expression profile of different models of senescence to identify and subsequently validate surface molecules preferentially upregulated in senescence in both mouse and humans. In addition, chapter 3 then utilizes a found marker of senescence to engineer second generation CAR T cells targeting it. The potency and specificity of these CAR T cells against senescent cells is assessed *in vitro* and in an *in vivo* model of oncogene-induced senescence. These experiments establish uPAR as a molecule upregulated in senescence and uPAR targeting CAR T cells as *bona fide* senolytics.

1.5.2.-Aim 2: Study the therapeutic potential of senolytic CAR T cells for the treatment of age related disorders.

Chapter 4 focuses on assessing the potential of uPAR-targeting CAR T cells to eliminate senescent cells and restore tissue homeostasis in murine models of chemically or diet induced liver fibrosis and NASH. Additionally, it performs preliminary experiments on the ability of senolytic CAR T cells to revert or ameliorate age related metabolic dysfunction in aged mice.

1.5.3.-Aim 3: Exploring senogenic-senolytic approaches for the treatment of solid tumors.

Finally, chapter 5 is dedicated to study the therapeutic effect of uPAR targeting CAR T cells in both proliferating and senescent tumors. To do so it explores their activity in two different murine models of lung and ovarian cancer. Importantly, chapter 5 also describes a new approach to somatically and flexibly engineer tumors that could provide

a valuable tool to dissect determinants of senescence immune surveillance in solid tumors in future research.

CHAPTER 2

MATERIALS AND METHODS

2.1.-RNA-seq analysis

2.1.1.-RNA extraction, RNA-seq library preparation and sequencing

Total RNA was isolated from: 1) $Kras^{G12D}$; $p53^{-/-}$ cells after 8 days of treatment with vehicle (DMSO) or combined treatment with MEK inhibitor trametinib (25nM) and CDK4/6 inhibitor palbociclib (500nM). 2) Oncogene-induced senescent hepatocytes were generated in C57BL/6 mice via hydrodynamic tail vein injection (HTVI). For each mouse, 25μg of pT3-Caggs-$NRas^{G12V}$-IRES-GFP plasmids (or pT3-Caggs-$NRas^{G12V;D38A}$-IRES-GFP plasmids as control) and 5μg CMV-SB13 were suspended in saline solution at the volume of 10% of the animal's body weight for administration. Six days after HTVI, mice were anesthetized and placed on the platform for liver perfusion. Sequential perfusions of HBSS containing EGTA and HBSS containing Collagenase IV were performed, followed by passing the dissociated liver cells through a 100 μM cell strainer. The hepatocytes were further washed by low glucose DMEM and low speed centrifugation. DAPI-negative/GFP-positive hepatocytes, indicating successful transduction of mutant Nras expression, were isolated through low pressure fluorescence-activated cell sorting. 3) The datasets from senescent or proliferating hepatic stellate cells were obtained from a previous study. The datasets from proliferating, quiescent or senescent IMR-90 were obtained from a previous study(Tasdemir et al., 2016). Sequencing and library preparation were performed at the Integrated Genomics Operation (IGO) at MSKCC. RNA-seq libraries were prepared from total RNA. After RiboGreen quantification and quality control by Agilent BioAnalyzer, 100-500ng of total RNA underwent polyA selection and TruSeq library preparation according to instructions provided by Illumina (TruSeq Stranded mRNA LT Kit, RS-122-

2102), with 8 cycles of PCR. Samples were barcoded and run on a HiSeq 4000 or HiSeq 2500 in a 50bp/50bp paired end run, using the HiSeq 3000/4000 SBS Kit or TruSeq SBS Kit v4 (Illumina) at MSKCC's IGO core facility.

2.1.2.-RNA-seq read mapping, differential gene expression analysis and heatmap visualization: Resulting RNA-Seq data was analyzed by removing adaptor sequences using Trimmomatic(Bolger et al., 2014). RNA-Seq reads were then aligned to GRCm38.91 (mm10) with STAR(Dobin et al., 2013) and transcript count was quantified using featureCounts(Liao et al., 2014) to generate raw count matrix. Differential gene expression analysis and adjustment for multiple comparisons were performed using DESeq2 package(Love et al., 2014) between experimental conditions, using 2 independent biological replicates per condition, implemented in R (http://cran.r-project.org/). Differentially expressed genes (DEGs) were determined by > 2-fold change in gene expression with adjusted P-value < 0.05. For heatmap visualization of DEGs, samples were z-score normalized and plotted using pheatmap package in R. Transcripts encoding molecules defined to be located in the plasma membrane with a confidence score higher than 3 (range 0-5) as determined by UniProtKB were considered as cell suface molecules.

2.1.3.-Functional annotations of gene clusters:

Pathway enrichment analysis was performed in the resulting gene clusters with the Reactome database using enrichR(Chen et al., 2013). Significance of the tests was assessed using combined score, described as c = log(p) * z, where c is the combined score, p is Fisher exact test p-value, and z is z-score for deviation from expected rank.

2.2.-Cell lines and compounds

The following cell lines were used in this study: murine $KRAS^{G12D/+}$; $Trp53^{-/-}$ (KP) lung cancer cells (provided by Tyler Jacks and expressing luciferase (Luc)-green fluorescent protein (GFP) as described(Ruscetti et al., 2018)), NALM6 and Eμ-ALL01 cells expressing firefly luciferase (FFLuc)-GFP(Feucht et al., 2019)). Cells were maintained in a humidified incubator at 37C with 5%CO_2. KP cells were grown in DMEM supplemented with 10% FBS and 100IU/ml penicillin/streptomycin. NALM6 and Eμ-ALL01 cells were grown in complete medium composed of RPMI supplemented with 10% FBS, 1% L-glutamine, 1% MEM non-essential amino acids, 1% HEPES buffer, 1% sodium pyruvate, 0.1% beta-mercapto-ethanol and 100UI/ml penicillin/streptomycin. Human primary melanocytes were grown in dermal cell basal medium (ATCC, 200-030) supplemented with the adult melanocyte growth kit (ATCC, 200-042), 10% FBS and 100IU/ml penicillin/streptomycin. All cell lines used were negative for mycoplasma.

For drug-induced senescence experiments *in vitro*, trametinib (S2673) and palbociclib (S1116) were purchased from Selleck Chemicals and dissolved in DMSO to yield 10mM stock solutions, which were stored at -80C(Ruscetti et al., 2018). Growth medium was changed every 2 days. For *in vivo* experiments trametinib was dissolved in a 5% hydroxypropyl methylcellulose and 2% Tween-80 solution (Sigma) and palbociclib was dissolved in sodium lactate buffer (pH 4) (as published in(Ruscetti et al., 2018)). Mice were treated with 1 mg per kg body weight of trametinib and 150mg per kg body weight of palbociclib as previously described(Ruscetti et al., 2018). Cerulein was purchased from Bachem. Anakinra was purchased from sobi and administered intraperitoneally at a dose of 30mg per kg twice per day for 8 days starting 24h before CAR T cell transfer. Anti-m.IL-6R (clone MP5-20F3) was purchased from BioXcell and administered intraperitoneally once per day at 25 mg per kg body weight for the first dose and 12.5mg per kg body weight for subsequent doses for 8 days starting 24h before CAR T cell transfer as previously described(Giavridis et al., 2018).

2.3.-Senescence-associated beta galactosidase (SA-β-gal) staining

SA-β-Gal staining was performed as previously described(Ruscetti et al., 2018) at pH 6.0 for human cells and tissue and at pH 5.5 for mouse cells and tissue. Fresh frozen tissue sections or adherent cells plated in 6-well plates were fixed with 0.5% glutaraldehyde in PBS for 15 minutes, washed with PBS supplemented with 1mM $MgCl_2$ and stained for 5-8 hours in PBS containing 1mM $MgCl_2$, 1mg/ml X-Gal, 5mM potassium ferricyanide and 5mM potassium ferrocyanide. Tissue sections were counterstained with eosin. 5 high power fields per well/ section were counted and averaged to quantify the percentage of SA-β-Gal^+ cells.

2.4.-qRT-PCR

Total RNA was isolated using the RNeasy Mini Kit (Qiagen) and complementary DNA (cDNA) was obtained using TaqMan reverse transcription reagents (Applied Biosystems). Real-time PCR was performed in triplicates using SYBR green PCR master mix (Applied Biosystems) on the ViiA 7 Real-Time PCR System (Invitrogen). GAPDH or B-actin served as endogenous normalization controls for mouse and human samples.

2.5.-Mice

All mouse experiments were approved by the Memorial Sloan Kettering Cancer Center (MSKCC) Internal Animal Care and Use Committee. Mice were maintained under specific pathogen-free conditions, and food and water were provided ad libitum. The following mice were used: C57BL/6N background (purchased from The Jackson laboratory and aged mice obtained through the National Institute of Aging), NOD-scid $IL2Rg^{null}$ (NSG) mice (purchased from The Jackson laboratory) and B6.SJL-

Ptrc^{a}/BoyAiTac (CD45.1 mice) (purchased from Taconic). Mice were used at 8-12 weeks of age (5-7 weeks old for the xenograft experiments and 6-10 weeks old for T cell isolation) and 18-20 months and were kept in group housing. Mice were randomly assigned to the experimental groups.

2.6.-Transposon-mediated intrahepatic gene transfer

Transposon-mediated intrahepatic gene transfer was performed as previously described(Kang et al., 2011). In short, 8-12 week-old C57BL/6J mice received a saline solution at a final volume of 10% of their body weight containing 30ug of total DNA composed of a 5:1 molar ratio of transposon-encoding vector (containing either the sequence for *Nras*^{G12V} or the sequence for the GTPase dead form *Nras*$^{G12V;D38A}$) to transposase encoding vector (Sleeping Beauty 13) through hydrodynamic tail vein injection (HTVI). For CAR T cell studies, NSG mice were intravenously injected with 0.5x10^6 human CAR^{+} T cells or untransduced T cells 10 days after HTVI and monitored by bioluminescence imaging usinig the IVIS Imaging System (PerkinElmer) with the Living Image software (PerkinElmer). At day 15 post CAR injection, mice were euthanized, livers were removed and used for further analysis.

2.7.-Generation of murine Pancreatic Intraepithelial Neoplasias (PanIn)

The mice strain has been previously described(Livshits et al., 2018). To induce PanIn generation, KC;RIK (p48-Cre;RIK;LSLKrasG12D) male mice were treated with 8 hourly intraperitoneal injections of 80 µg/kg caerulein (Bachem) for 2 consecutive days. Mice were then harvested 21 weeks later and their pancreas used for further analysis. Age matched C;RIK mice injected with PBS were used as controls for normal pancreas.

***2.8.-In vivo* induction of CCl_4-induced liver fibrosis**

C57BL/6N mice were treated twice a week with 12 consecutive intraperitoneal (i.p.) injections of 1ml/kg tetrachloride (CCl_4) to induce liver fibrosis(Krizhanovsky et al., 2008; Lujambio et al., 2013). For murine CAR T cell studies, cyclophosphamide (200mg/kg) was administered 16-24 hours before T cell injection. Mice received 0.5-1 or 2-3x10^6 CAR^+ T cells or untransduced T cells and CCl_4 was continuously administered at the same dose and interval after T cell injection until day 20 post CAR injection, when animals were scarificed 48-72h after the last CCl_4 injection. Blood was collected by facial vein puncture or cardiac puncture.

2.9.-*In vivo* induction of NASH-induced liver fibrosis.

C57BL/6N mice were fed with NASH diet (Teklad. TD.160785 which contains 10.2% kcal from protein, 37.3% kcal from carbohydrate and 52.6% kcal from fat) and fructose containing drinking water (23.1g of fructose and 18.9 g of glucose dissolved in 1 liter of water and then filter sterilized) at 8-10 weeks of age(Wang et al., 2016; Zhu et al., 2018). Body weight was measured weekly. For murine CAR T cell studies, cyclophosphamide (200mg/kg) was administered 16 hours before T cell injection. Mice received 0.5 CAR^+ T cells or untransduced T cells and they received the same NASH diet until day 20 post CAR injection when they were euthanized. Blood was collected by facial vein puncture or cardiac puncture.

For the STAM model(Van der Schueren et al., 2015), liver tissue samples (unstained slides for immunohistochemistry) were purchased from SMC laboratories.

2.10.-Patient-derived xenografts

Experiments with patient-derived xenografts were performed as described(Ruscetti et al., 2018), using 5-7 week-old female NSG mice. MSK-LX27 was derived from a lung adenocarcinoma harboring $KRAS^{G12D}$ and p53 mutations and a deletion in CDKN2A and

was cut into pieces and inserted in the subcutaneous space. Mice were monitored daily, weighed twice weekly and caliper measurements begun when tumors became visible. Tumors were measured using the formula: tumor volume = (D x d^2)/2 and when they reached a size of 100-200 mm^3, mice were randomized based on starting tumor volume and treated with vehicle or trametinib (3 mg/kg body weight) and palbociclib (150mg/kg body weight) per os for 4 consecutive days followed by 3 days off treatment. Experimental endpoints were achieved when tumors reached a size of 2000mm^3 or became ulcerated. Tumors were harvested at the experimental endpoint and tissue was divided evenly for 10% formalin fixation and OCT frozen blocks.

2.11.-Patient samples

De-identified human samples from liver biopsies of patients with liver fibrosis from viral (HBV or HCV), alcoholic and non-alcoholic fatty liver disease were obtained through the Department of Pathology at Mount Sinai Hospital, New York, NY. Human pancreatic intraepithelial neoplasia samples (PanINs) were obtained through the Department of Pathology at Memorial Sloan-Kettering. Human atherosclerosis samples were obtained through the Department of Pathology, Weill Medical College of Cornell University, New York, NY. All human studies were approved by Mount Sinai, or Weill Medical College of Cornell University or Memorial Sloan-Kettering Institutional Review Board.

2.12.-Histological analysis

Tissues were fixed overnight in 10% formalin, embedded in paraffin, and cut into 5μm sections. Sections were subjected to hematoxylin and eosin staining, and to Sirius red staining for fibrosis detection. For fibrosis quantification, at least three whole sections from each animal were scanned and the images were quantified using NIH ImageJ software. The amount of fibrotic tissue was calculated relative to the total analyzed liver

area as previously described. Immunohistochemical and immunofluorescence stainings were performed following standard protocols. The following primary antibodies were used: human uPAR (R&D. AF807), mouse uPAR (R&D. AF534), NRAS (Santa Cruz. SC-31), SMA (abcam. Ab5694), mKATE (Evrogen. ab233), CD3 (abcam. ab5690), myc-tag (Cell Signaling. 2276), Ki-67 (abcam, ab16667), IL-6 (abcam. ab6672), p16-INK4A (Proteintech. 10883-1-AP), P-ERK$^{T202/Y204}$ (Cell Signaling.4370) and desmin (ThermoFisher Scientific . RB-9014).

2.13.-Flow cytometry

For analysis of uPAR expression in cell lines upon induction of senescence, KP cells were treated with trametinib (25nM) and palbociclib (500nM) or with vehicle (DMSO), and human primary melanocytes were continuously passaged for 15 passages and then trypsinized, resuspended in PBS supplemented with 2%FBS and stained with the following antibodies for 30 minutes on ice: PE-conjugated anti-mouse uPAR antibody (R&D. FAB531P) or APC-conjugated anti-human uPAR antibody (Thermo Fisher S.17-3879-42). The following fluorophore-conjugated antibodies were used for *in vitro* and *in vivo* experiments: ('h' prefix denotes anti-human, 'm' prefix denotes anti-mouse): hCD45 APC-Cy7 (clone 2D1, BD, #557833), hCD4 BUV395 (clone SK3, BD, #563550), hCD4 BV480 (clone SK3, BD, #566104), hCD62L BV421 (clone DREG-56, BD, #563862), hCD62L BV480 (clone DREG-56, BD, #566174), hCD45RA BV650 (clone HI100, BD, #563963), hCD25 BV650 (clone BC96, Biolegend, #302634) hPD1 BV480 (clone EH12.1, BD, #566112), hCD19 BUV737 (clone SJ25C1, BD, #564303), hCD271 PE (clone C40-1457, BD, #557196), hCD69 APC (clone FN50, Biolegend, #310910), hIL2 PE-Cy7 (clone MQ1-17H12, Invitrogen, #25-7029-42), hTNFa BV650 (clone Mab11, BD, #563418), hIFNg BUV395 (clone B27, BD, #563563), hTIM3 BV785 (clone F38-2E2, Biolegend, #345032), hCD8 PE-Cy7 (clone SK1, eBioscience, #25-0087-42), hCD8

APC-Cy7 (clone SK1, BD, #557834), hCD223 PerCP-eFluor710 (clone 3DS223H, eBioscience, #46-2239-42), hCD223 BV421 (clone 11C3C65, Biolegend, #369314), hGrB APC (clone GB12, Invitrogen, #MHGB05), hMyc-tag AF647 (clone 9B11, Cell Signaling Technology, #2233S), hCD19 PB (clone SJ25-C1, Invitrogen, #MHCD1928), hCD87 APC (clone VIM5, eBioscience, #17-3879-42), hCD87 PerCp-eFluor710 (clone VIM5, eBioscience, #46-3879-42), muPAR PE (R&D Systems, FAB531P), muPAR AF700 (R&D Systems, FAB531N), mCD45.1 APC-Cy7 (Biolegend, #110716), m.CD45.1 BV785 (Biolegend, #110743), mCD45.2 PE (Biolegend, #109868), mCD45.2 AF700 (Biolegend, #109822), mSiglec-F PerCP-Cy5.5 (BD, #565526) mI-A/I-E BV605 (Biolegend, #107639), mF4/80 (BD, #565411), mCD11b BUV395 (BD, #563553), mCD11c BV650 (Biolegend, #117339), mLY6G BV510 (Biolegend, #127633), mLY6G APC/Fire750 (Biolegend, #127652), miNOS PE-Cy7 (eBioscience, #25-5920-82), mCD19 PE (clone 1D3/CD19, Biolegend, #152408), mCD25 BV605 (Biolegend, #102035), mCD69 PerCpCy5.5 (Biolegend, #104522), mCD3 AF488 (Biolegend, #100210), mCD4 BUV395 (BD, #563790), mCD4 FITC (BD, #553729), mCD8 PE-Cy7 (Biolegend, #100722), 7-AAD (BD, #559925), DAPI (Life technologies D1306), Fixable Viability Dye eFluor 506 (65-0866-18, eBioscience) and LIVE/DEAD Fixable Violet (L34963, Invitrogen) were used as a viability dyes.

CAR staining was performed with Alexa Fluor 647 AffiniPure $F(ab)_2$ Fragment Goat Anti-Rat IgG (Jackson ImmunoResearch, #112-6606-072). For cell counting, CountBright Absolute Counting Beads were added (Invitrogen) according to the manufacturer's instructions. For in vivo experiments, Fc receptors were blocked using FcR Blocking Reagent, mouse (Miltenyi Biotec). For intracellular cytokine secretion assay, cells were fixed and permeabilized using Cytofix/Cytoperm Fixation/Permeabilization Solution Kit (BD Biosciences) or Intracelllar Fixation & Permeabilization Buffer Set Kit (eBioscience, #88-8824-00) according to the manufacturer's instructions.

Flow cytometry was performed on a LSRFortessa instrument (BD Biosciences) or Cytek Aurora (CYTEK) and data were analyzed using FlowJo (TreeStar).

For *in vivo* sample preparation, livers were dissociated using MACS Miltenyi Biotec liver dissociation kit (130-1-5-807), filtered through a 100µm strainer, washed with PBS, and red blood cell lysis was achieved with an ACK (Ammonium-Chloride-Potassium) lysing buffer (Lonza). Cells were washed with PBS, resuspended in FACS buffer and used for subsequent analysis. Lungs were minced and digested with 1mg/ml collagenase type IV and DNase type IV in RPMI at 37C and 200rpm for 45 minutes, filtered through 100µm strainer, washed with PBS, and red blood cell lysis was achieved with an ACK lysing buffer (Lonza). Cells were washed with PBS, resuspended in FACS buffer and used for subsequent analysis. For bone marrow samples, tibia and femurs were mechanically disrupted with a mortar in PBS/2mM EDTA, filtered through 40µm strainer, washed with PBS/2mM EDTA and red blood cell lysis was achieved with an ACK lysing buffer (Lonza). Cells were washed with PBS/2mM EDTA, resuspended in FACS buffer and used for subsequent analysis. Spleens were mechanically disrupted with the back of a 5-ml syringe, filtered through 40µm strainer, washed with PBS/2mM EDTA and red blood cell lysis was achieved with an ACK lysing buffer (Lonza). Cells were washed with PBS/2mM EDTA ,resuspended in FACS buffer and used for subsequent analysis.

2.14.-Cytokine measurements

Serum cytokines were measured using cytometric bead arrays (BD) as per the manufacturer's instructions.

2.15.-Detection of suPAR levels

suPAR levels from cell culture supernatant of murine plasma were evaluated by enzyme-linked immunosorbent assay (ELISA) according to the manufacturer's protocol (R&D systems, DY531 (mouse) or DY807 (human)).

2.16.-Liver function tests

Serum alanine aminotransferase (ALT) aspartate aminotransferase (AST) and albumin levels in murine serum were measured according to the manufacturer's protocol, using the EALT-100 (ALT), EASTR-100 (AST) and DIAG-250 (albumin) kits from BioAssay systems.

2.17.-Glucose Tolerance Testing

Blood samples from mice fasted overnight (12h) were collected at 0,15,30,60,90 and 120 minutes after an intraperitoneal injection of glucose (2g/kg body weight). Insulin was measured from serum collected at the 0 and 15min time points. Concentrations were determined using the Ultra Sensitive Mouse Insulin ELISA kit (Crystal Chem, 90080),

2.18.-Insulin Tolerance Testing

Mice were fasted for 4h, insulin (Humulin R, Eli Lilly,0.5 U/kg body weight) was injected intraperitoneally and blood glucose measured at 0, 15, 30 and 60 minutes.

2.19.-Exercise tolerance testing

Exercise capacity was assessed using a motorized treadmill (model 1050 EXER 3/6; Columbus Instruments, Columbus, OH). Mice was acclimatized to the treadmill for 3 days prior to testing (acclimatization involved mice walking on the treadmill at 10 min/min for 10 to 15 mins per day). Following acclimatization, all mice underwent a total of 2 separate exercise tolerance tests on consecutive days. Tolerance tests began with mice

walking at 10 ms/min with speed increased by 2 ms/min every two mins until exhaustion. The primary outcomes were time to exhaustion and total distance.

2.20.- Electroporation Based Genetically Engineered Mouse Models (EPO-GEMMs)

Eight- to 12-week old WT C57BL/6 female mice were anesthetized with isoflurane and the surgical site scrubbed with a povidone- iodine scrub (Betadine) and rinsed with 70% alcohol. After opening the peritoneal cavity, the abdominal cavity is rinsed with 300µl pre-warmed clinical grade sterile water. Subsequently, the stomach is located and exposed using a fine forceps. A 3mm incision is made in the forestomach region of the mouse. The stomach is being rinsed with 1ml of pre- warmed clinical grade sterile saline. Plasmid mix (50 µL; see specifications below) was injected directly into the epithelial compartment of the corpus of the stomach with a 30 gauge syringe, and tweezer electrodes were tightly placed around the injection bubble. Two pulses of electrical current (75 mV) given for 75-millisecond lengths at 500-millisecond intervals were then applied using an *in vivo* electroporator (Nepa Gene NEPA21 Type II Electroporator). After the procedure, the peritoneal cavity was sutured and the skin closed with skin staples. The mice were kept at 37°C until they awoke, and postsurgery pain management was done with injections of buprenorphine and/or meloxicam for the 3 following days. Tumor formation was assessed by ultrasound imaging, and mice were sacrificed following early tumor development or at endpoint. The following vectors and concentrations were used: a pT3-MYC transposon vector (5 µg), a Sleeping Beauty transposase (SB13; 1 µg), and/or a pX330 CRISPR/Cas9 vector (20 µg; Addgene #42230) targeting the respective tumor suppressor genes.

2.21.-Isolation, expansion and transduction of human T cells

All blood samples were handled following the required ethical and safety procedures.

Peripheral blood was obtained from healthy volunteers and buffy coats from anonymous healthy donors were purchased from the New York Blood Center. Peripheral blood mononuclear cells were isolated by density gradient centrifugation. T cells were purified using the human Pan T Cell Isolation Kit (Miltenyi Biotec), stimulated with CD3/CD28 T cell activator Dynabeads (Invitrogen) as described(Feucht et al., 2019) and cultured in X-VIVO 15 (Lonza) supplemented with 5% human serum (Gemini Bio-Products), 5ng/ml interleukin-7 and 5ng/ml interleukin-15 (PeproTech). T cells were enumerated using an automated cell counter (Nexcelom Bioscience).

48 hours after initiating T cell activation, T cells were transduced with retroviral supernatants by centrifugation on RetroNectin-coated plates (Takara). Transduction efficiencies were determined 4 days later by flow cytometry and CAR T cells were adoptively transferred into mice or used for *in vitro* experiments.

2.22.-Isolation, expansion and transduction of mouse T cells

B6.SJL-Ptrc^{a}/BoyAiTac mice (CD45.1 mice) were euthanized and spleens were harvested. Following tissue dissection and red blood lysis, primary mouse T cells were purified using the mouse Pan T cell Isolation Kit (Miltenyi Biotec). Purified T cells were cultured in RPMI-1640 (Invitrogen) supplemented with 10% fetal bovine serum (FBS; HyClone), 10 mM HEPES (Invitrogen), 2 mM L-glutamine (Invitrogen), MEM nonessential amino acids 1× (Invitrogen), 0.55 mM β-mercaptoethanol, 1 mM sodium pyruvate (Invitrogen), 100 IU/ mL of recombinant human IL-2 (Proleukin; Novartis) and mouse anti-CD3/28 Dynabeads (Gibco) at a bead:cell ratio of 1:2. T cells were spinoculated with retroviral supernatant collected from Phoenix-ECO cells 24 hours after initial T cell expansion as described(Davila et al., 2013; Kuhn et al., 2019) and used for functional analysis 3-4 days later.

2.23.-Genetic modification of T cells

The human and murine SFG γ-retroviral m.uPAR-28ζ plasmids were constructed by stepwise Gibson Assembly (New England BioLabs) using the SFG-1928ζ backbone as previously described(Brentjens et al., 2003; Brentjens et al., 2007; Hagani et al., 1999; Maher et al., 2002). The amino acid sequence for the single-chain variable fragment (scFv) specific for mouse uPAR was obtained from the heavy and light chain variable regions of a selective monoclonal antibody against mouse uPAR (R&D.MAB531-100) through Mass Spectometry performed by Bioinformatics Solutions,Inc. In the human SFG-m.uPAR-h28z CARs, the m.uPAR scFv is thus preceded by a human CD8a leader peptide and followed by CD28 hinge-transmembrane-intracellular regions, and CD3ζ intracellular domains linked to a P2A sequence to induce coexpression of truncated low-affinity nerve growth factor receptor (LNGFR). In the mouse SFG-m.uPAR-m28z CARs, the m.uPAR scFv is preceded by a murine CD8a leader peptide and followed by the Myc-tag sequence (EQKLISEEDL), murine CD28 transmembrane and intracellular domain and murine CD3ζ intracellular domain(Kuhn et al., 2019).

Plasmids encoding the SFGγ retroviral vectors were used to transfect gpg29 fibroblasts (H29) in order to generate VSV-G pseudotyped retroviral supernatants, which were used to construct stable retroviral-producing cell lines as described(Brentjens et al., 2003; Kuhn et al., 2019). For T cell imaging studies, murine T cells were transduced with retroviral supernatants encoding SFG-green fluorescent protein (GFP)/ click beetle red luciferase (CBRluc)(Santos et al., 2009).

2.24.-Cytotoxicity assays

The cytotoxicity of CAR T cells was determined by standard luciferase-based assays or by calcein-AM based cytotoxicity assays. For luciferase-based assays, target cells expressing firefly luciferase (FFLuc-GFP) were co-cultured with T cells in triplicates at

the indicated effector:target ratios using black-walled 96 well plates with $5x10^4$ (for NALM6 and Eμ-ALL01) or $1.5x10^4$ (for KP) target cells in a total volume of 100ul per well in RPMI or DMEM media, respectively. Target cells alone were plated at the same cell density to determine the maximal luciferase expression (relative light units (RLU)) and maximum release was determined by addition of 2% Triton-X100 (Sigma). 4 or 18 hours later, 100μl luciferase substrate (Bright-Glo; Promega) was directly added to each well. Emitted light was detected in a luminescence plate reader. Lysis was determined as (1-(RLUsample)/(RLUmax))x100. For calcein-AM based assays, target cells (NALM6) were loaded with 20μM calcein-AM (Thermo Fisher Scientific) for 30 minutes at 37C, washed twiced, and co-incubated with T cells in triplicates at the indicated effector:target ratios in 96 well-round-bottomed plates with $5x10^3$ target cells in a total volume of 200ul per well in complete medium. Target cells alone were plated at the same cell density to determine spontaneous release and maximum release was determined by incubating the targets with 2% Triton-X100 (Sigma). After 4-hours coculture, supernatants were harvested and free calcein was quantitated using a Spark plate reader (Tecan). Lysis was calculated as: ((experimental release – spontaneous release)/(maximum release – spontaneous release))x100.

2.25.-Statistical analysis and figure preparation

Data are presented as means±s.e.m. or means±s.d. Statistical analysis was performed using GraphPad Prism 6.0 (GraphPad Software). P-values <0.05 were considered to be statistically significant. Survival was determined using the Kaplan-Meier method. No statistical method was used to predetermine sample size in animal studies. Animals were allocated at random to treatment groups. Figures were prepared using Biorender.com for scientific illustrations and Illustrator CC 2019 (Adobe).

CHAPTER 3

IDENTIFICATION OF SURFACE MARKERS OF SENESCENCE AND DEVELOPMENT OF SENOLYTIC CAR T CELLS

3.1.-Introduction

Given the contribution of senescent cells to tissue damage pathologies, there is growing interest in the development of 'senolytic' agents that selectively eliminate senescent cells (Kirkland and Tchkonia, 2017).

A major limitation in the development of senolytic agents has been the fact that although senescent cells undergo characteristic changes in gene expression, there is no single marker that proves a cell is senescent (Sharpless and Sherr, 2015). Rather, senescence is currently defined by the acquisition of different characteristics: Senescent cells often times acquire a flat morphology and upregulate the activity of senescence-associated beta-galactosidase (SA-β-gal). Moreover, they often accumulate senescence-associated heterochromatin foci (SAHF), $p16^{INK4a}$, $p15^{INK4b}$ and/or p21 cyclin-dependent kinases, many of which functionally contribute to the program by engaging RB or mediating the effects of p53 (Baker et al., 2011; Sharpless and Sherr, 2015). However, not every senescent cell expresses each of these markers, certain normal cells can also stain positive (e.g. macrophages) raising questions as to whether such cells are in fact senescent or whether the markers lack specificity (Hall et al., 2017). In addition, there is significant transcriptional heterogeneity among senescent cells depending on cell type and trigger of senescence (Hernandez-Segura et al., 2017).

In recent years, several compounds have been identified based on their preferential ability to kill senescent cells. For example, the Bcl-2 antagonist ABT737 apparently acts

as a senolytic owing to the requirement for increased Bcl-2 expression to maintain the viability of senescent cells (Kirkland and Tchkonia, 2017). Additionally, the combination of quercetin and dasatinib can preferentially target senescent cells (Baar et al., 2017; Xu et al., 2018). However, all of these agents produce significant side effects (such as pleural effusion and dose-limiting thrombocytopenia) and only eliminate a fraction of senescent cells.

An alternative approach could involve CAR T cells directed against senescence-specific surface antigens. CARs are synthetic receptors that redirect T cell specificity, effector potential and other functions (Sadelain et al., 2017). CAR T cells targeting CD19 have shown remarkable efficacy in patients with refractory B-cell malignancies (Park et al., 2018) and other cell-surface antigens show promise as targets for CAR therapy in other indications (Aghajanian et al., 2019; Du et al., 2019; Pellegatta et al., 2018). Here we investigate whether CAR T cells directed against a surface protein upregulated on senescent cells could serve as senolytic agents.

3.2.-Results

3.2.1.-Identification of uPAR as a surface marker of senescence.

To identify cell surface proteins that are broadly upregulated in senescent cells, we compared RNAseq datasets derived from three independent and robust models of senescence: 1) Therapy-induced senescence (TIS) in murine lung adenocarcinoma *Kras*^{G12D}*;p53*$^{-/-}$ (KP) cells triggered to senesce by the combination of MEK and CDK4/6 inhibitors(Ruscetti et al., 2018); 2) Oncogene-induced senescence (OIS) in murine hepatocytes mediated by *in vivo* delivery of *NRAS*^{G12V} through hydrodynamic tail vein injection (HTVI)(Kang et al., 2011); and 3) Culture-induced senescence of murine hepatic stellate cells (HSCs) (Figure 3.1a). We focused on transcripts encoding

molecules located in the plasma membrane as determined by UniProtKB that were upregulated in all datasets (Figure 3.1b, c). 8 transcripts were identified, each encoding proteins linked to extracellular matrix remodeling or the coagulation cascade (Figure 3.1d).

Given that ideal antigens for CAR T cell engagement should be highly expressed on target cells but not vital tissues, we ranked each transcript according to its magnitude of upregulation (log_2 fold change), and then excluded those highly expressed in vital tissues as determined by the Human Protein Atlas (HPA) and Human Proteome Map (HPM)(Perna et al., 2017). This process identified *PLAUR,* which encodes the urokinase plasminogen activator receptor (uPAR), as a suitable candidate (Figure 3.1e). Accordingly, *PLAUR* was also upregulated in public datasets of senescent human cells (Ruscetti et al., 2018; Tasdemir et al., 2016) and immunohistochemistry confirmed that uPAR protein was absent in many vital organs (Figure 3.1g, f). Consistent with previous reports, low uPAR expression was detected in the bronchial epithelium. Other cell types that express uPAR include subsets of monocytes, macrophages and neutrophils (Simon et al., 1996; Smith and Marshall, 2010).

uPAR is the receptor for urokinase-type plasminogen activator (uPA), which promotes the degradation of the extracellular matrix during fibrinolysis, wound healing or tumorigenesis (Smith and Marshall, 2010). uPAR also functions as a signaling receptor that promotes motility, invasion and survival of tumor cells (Smith and Marshall, 2010). Nonetheless, mice lacking uPAR are viable and fertile (Bugge et al., 1995). A portion of uPAR is proteolytically cleaved upon ligand binding, generating soluble uPAR (suPAR). Interestingly, suPAR is secreted by senescent cells as part of the senescence-associated secretory phenotype (SASP)(Coppe et al., 2008) and serves as a serum

biomarker for kidney disease and diabetes (Hayek et al., 2015), two chronic pathologies linked to senescence (Hayek et al., 2015).

We next confirmed that uPAR was induced on the surface of senescent cells *in vitro* and *in vivo*. First, we evaluated therapy-induced senescence in KP lung cancer cells treated with combined MEK and CDK4/6 inhibition and replication-induced senescence in human primary melanocytes (Figure 3.2a, b and Figure 3.3a, b). In both models, cell surface uPAR expression and suPAR were markedly increased upon senescence induction (Figure 3.2a, b). Second, we examined a patient-derived xenograft (PDX) model of non-small cell lung cancer (NSCLC), in which mice were treated with combined MEK and CDK4/6 inhibitors(Ruscetti et al., 2018) (Figure 3.2c) and two different models of oncogene-induced senescence triggered either by overexpression of $Nras^{G12V}$ in murine hepatocytes transfected via hydrodynamic tail vein injection (Figure 3.2d and Figure 3.3c-e) or by endogenous $Kras^{G12D}$ expression in a murine model of senescent pancreatic intraepithelial neoplasia (PanIN) (Figure 3.3f-i). Finally, we included a mouse model of carbon tetrachloride (CCl_4)-induced liver fibrosis, in which senescent HSCs contribute to the pathophysiology (Figure 3.2e and Figure 3.3j-m) (Krizhanovsky et al., 2008). In each system, the senescence-inducing treatment increased the amount of uPAR-positive cells and serum suPAR levels. Notably, uPAR-positive cells did not express the proliferation marker Ki67, but co-expressed IL6, an established SASP component (He and Sharpless, 2017; Sharpless and Sherr, 2015).

We next confirmed that uPAR is highly expressed in tissues from patients affected by senescence-associated disorders. High uPAR expression was observed in liver fibrosis specimens from different etiologies. uPAR positive cells showed the same histological presentation as SA-β-gal positive cells and co-expressed the senescence-associated

markers p16 and IL6 (Figure 3.4a, b). uPAR was also highly expressed in atherosclerotic plaques from human carotid endarterectomy specimens and in PanIN lesions (Figure 3.4c, d). Increased uPAR and/ or suPAR levels have furthermore been noted in patients with other senescence-associated diseases including osteoarthritis, diabetes or idiopathic pulmonary fibrosis(Belcher et al., 1996; Guthoff et al., 2017; Schuliga et al., 2017). Collectively, these results nominate uPAR as a candidate target for senolytic CAR T cells.

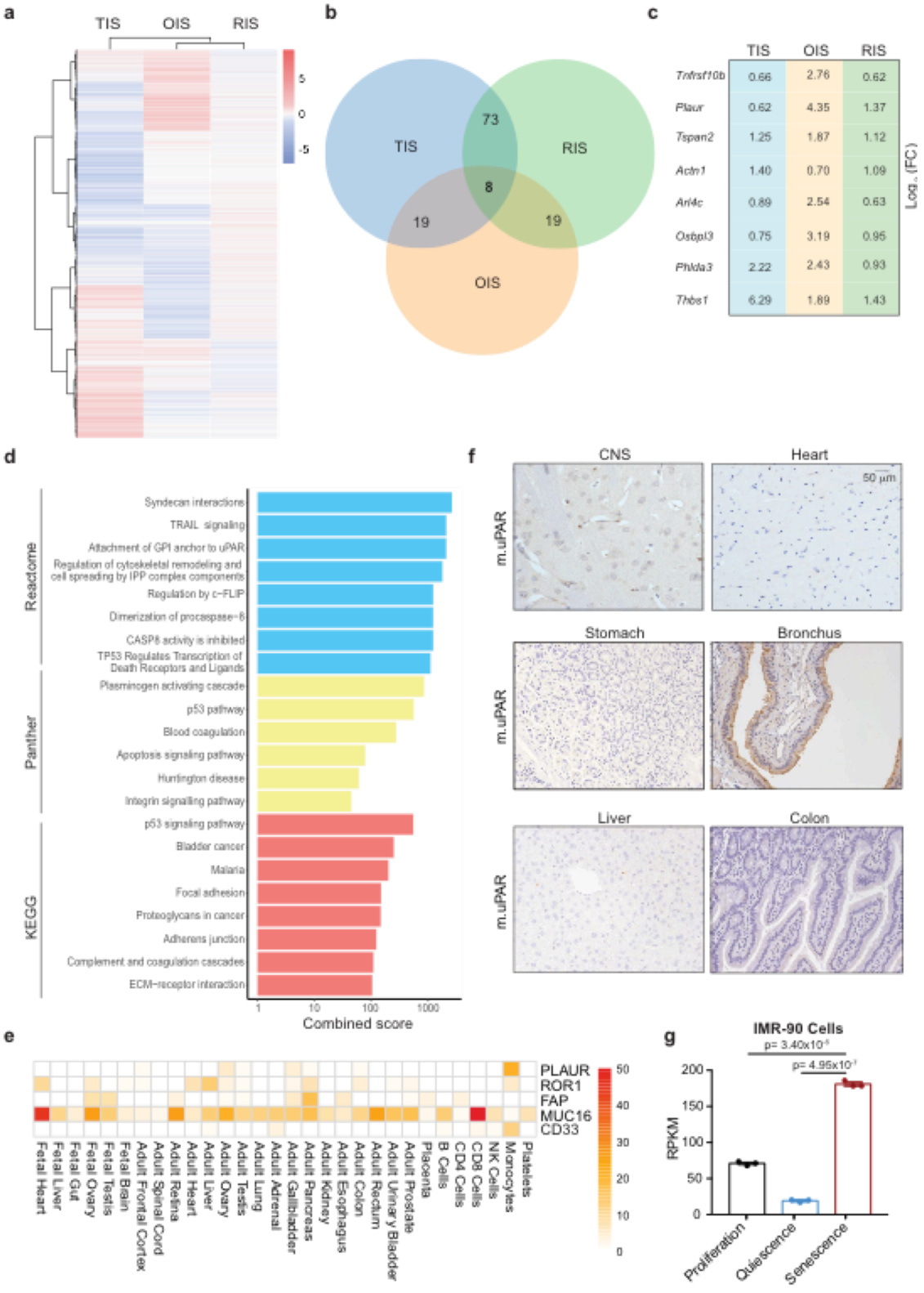

Figure 3.1. Genes coding for surface molecules commonly upregulated in senescence. (a) Heatmap of genes upregulated upon therapy-induced senescence (TIS), oncogene-induced senescence (OIS) or p-53 induced senescence in hepatic stellate cells (HSCs). **(b)** Venn diagram displaying the number of common genes upregulated in the three databases shown in (a). **(c)** Log_2 fold change of the eight commonly upregulated genes in the three different datasets shown in (a). **(d)** Combined

enrichment score of significantly enriched gene sets among the 8 commonly upregulated genes in senescence. **(e)** Heatmap showing the expression profile of human uPAR (*PLAUR*) in human vital tissues as determined by the Human Proteome Map (HPM) compared to the expression profiles of other targets of CAR T cells in current clinical trials. **(f)** Immunohistochemical staining of murine uPAR (m.uPAR) in vital tissues of C57BL/6J mice. Representative results of 2 independent experiments. **(g)** Reads Per Kilobase (RPKM) of *PLAUR* mRNA in proliferating, quiescent (induced by serum starvation) or senescent (triggered by $HRAS^{G12V}$ overexpression) human fibroblasts IMR-90. Results of 1 independent experiment with n=3 replicates for proliferating, quiescent and senescent conditions. Data represent mean± SEM. Two-tailed unpaired Student's t-test.

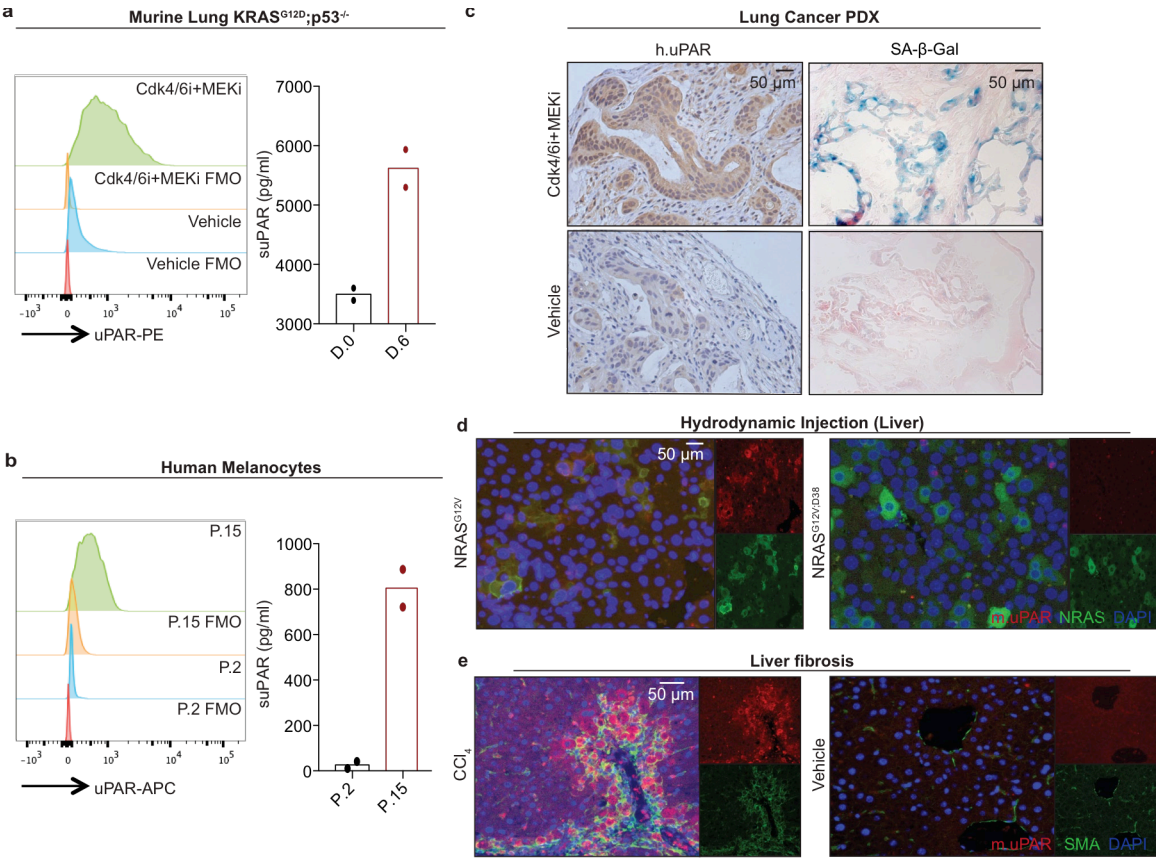

Figure 3.2. uPAR is a cell surface and secreted biomarker of senescence. (a) Flow cytometric analysis of mouse uPAR (m.uPAR) expression on *Kras^{G12D};p53$^{-/-}$* murine lung adenocarcinoma cells (KP) induced to senesce by treatment with MEK and CDK4/6 inhibitors as compared to controls. Representative results of n=3 independent experiments. Levels of soluble uPAR (suPAR) as determined by ELISA in the supernatant of senescent or proliferating KP cells. Representative results of n=2 independent experiments. **(b)** Flow cytometric analysis comparing human uPAR (h.uPAR) expression on primary human melanocytes induced to senesce by continuous passage with proliferating controls**.** Representative results of n=2 independent experiments. Levels of suPAR in the supernatant of senescent (Passage 15 = P.15) or proliferating (Passage 2 = P.2) primary human melanocytes. Representative results of n=2 independent experiments. **(c)** Immunohistochemical stainings of h.uPAR and SA-β-Gal of a patient-derived xenograft (PDX) from human lung adenocarcinoma orthotopically injected into NSG mice after treatment with vehicle or combined MEK and CDK4/6 inhibitors; representative of n=2 independent experiments (n=3 mice per group). **(d)** Co-immunofluorescence (IF) staining of m.uPAR (red) and NRAS (green) in the livers of mice 6 days after hydrodynamic tail vein injection of a plasmid encoding *NRAS^{G12V}* or *NRAS$^{G12V;D38A}$*. Representative results of n=3 independent experiments (n=5 mice per group). **(e)** Co-IF staining of m.uPAR (red) and smooth muscle actin (green) in the livers of mice 6 weeks after semi-weekly i.p. treatment with CCl_4 (n=7 mice) or vehicle (n=4 mice). Representative results of n=3 independent experiments.

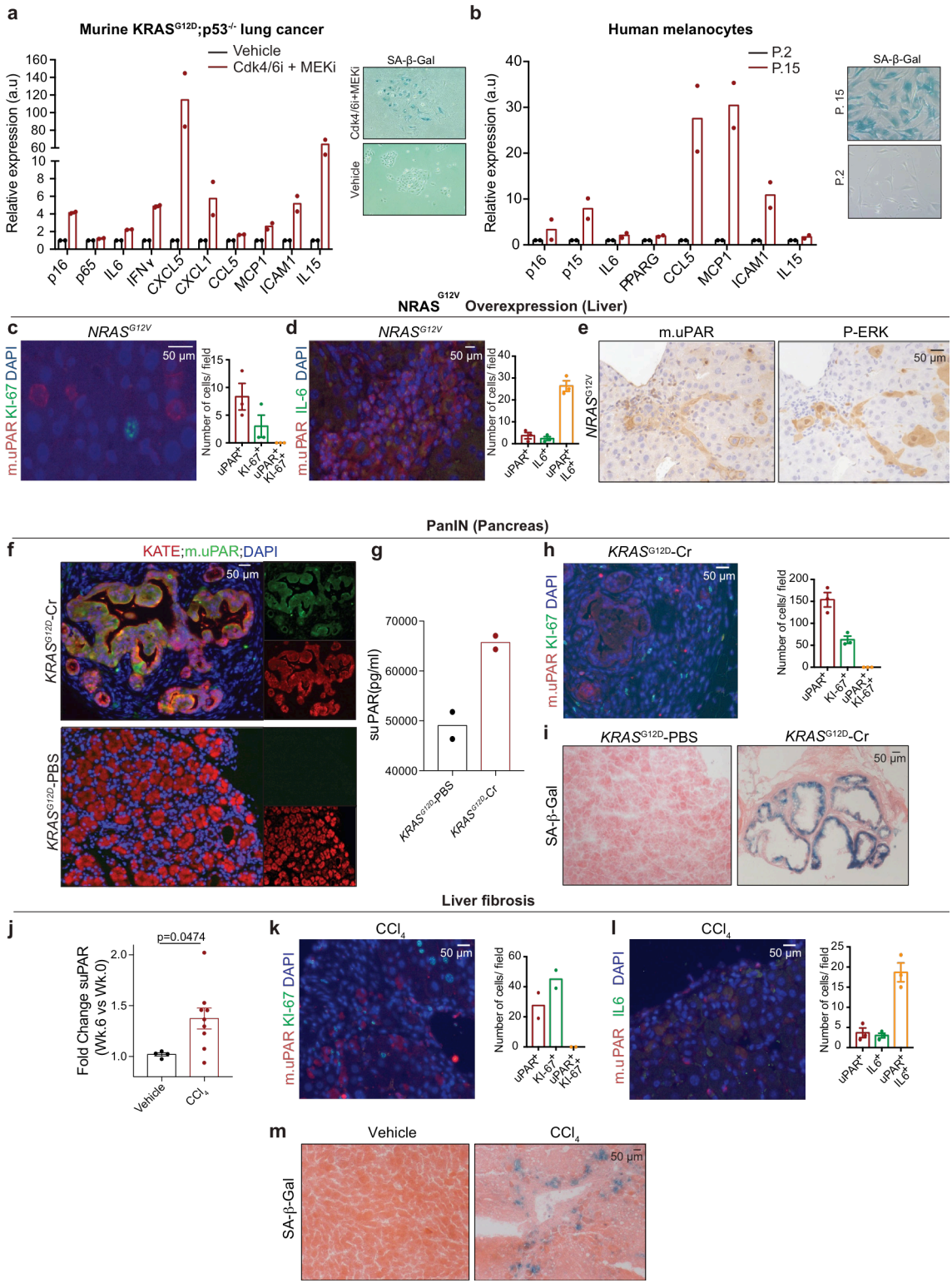

Figure 3.3. uPAR expression is upregulated on senescent cells. (a-b) qRT-PCR of SASP gene expression in senescent versus proliferating **(a)** KRAS$^{G12D;p53-/-}$ (KP) tumor cells or **(b)** human primary melanocytes and representative SA-β-Gal stainings. **(c-e)** Co-immunofluorescence stainings and quantifications of **(c)** m.uPAR (red) and ki-67 (green) or **(d)** m.uPAR (red) and IL6 (green) and **(e)** immunohistochemical staining of m.uPAR or P-ERK in serial sections in murine livers 6 days after hydrodynamic tail vein injection (HTVI) with a plasmid encoding NRAS^{G12V}. Representative results of 2

independent experiments (n=3 mice per group). (**f-i)** Mice expressing endogenous $KRAS^{G12D}$ in pancreatic epithelial cells were treated with cerulean (Cr) and harvested 21 weeks afterwards when they had developed PanINs. Mice with normal pancreas (KRAS WT PBS) were used as controls. **(f)** Co-immunofluorescence staining of KATE (red) and m.uPAR (green). Representative results of 2 independent experiments (n=3 mice per group). **(g)** Levels of soluble uPAR (suPAR) in the mice shown in (f). Representative results of 2 independent experiments (n=2 mice per group). **(h)** Co-immunofluorescence stainings and quantifications of m.uPAR (red) and ki-67 (green). Representative results of 2 independent experiments (n=3 mice per group). **(i)** Representative SA-β-Gal staining. Representative results of 1 independent experiment (n=3 mice per group). **(j-m)** Mice were treated with either vehicle or CCl_4 semiweekly for 6 weeks to induce liver fibrosis. **(j)** Fold change in the serum levels of suPAR. Representative results of 2 independent experiments (Vehicle: n=4, CCl_4: n=9 mice per group). **(k)** Co-immunofluorescence staining and quantification of m.uPAR (red) and ki-67 (green). Representative results of 2 independent experiments (n=2 mice per group). **(l)** Co-immunofluorescence staining and quantification of m.uPAR (red) and IL-6 (green). Representative results of 2 independent experiments (n=3 mice per group). **(m)** Representative SA-β-Gal staining. Representative results of 2 independent experiments (n=3 mice per group). **(j)** Two-tailed unpaired Student's t-test. Data represent mean± SEM **(c,d,h,j,l).**

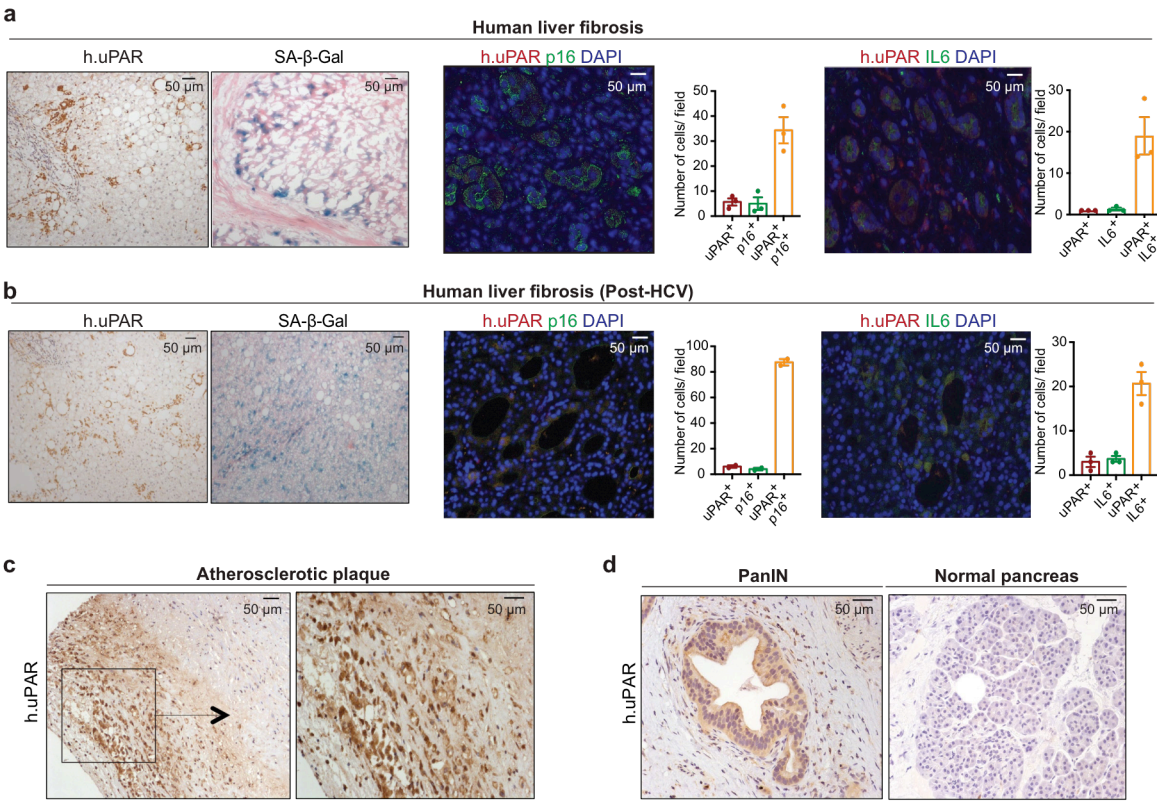

Figure 3.4. uPAR is a marker of senescence in senescence-associated human pathologies. (a) Immunohistochemical expression of human uPAR (h.uPAR) and SA-β-Gal in human samples of hepatitis-induced liver fibrosis (n=7 patients). Co-immunofluorescence staining and quantification of human uPAR (red) and p16 (green) or human uPAR (red) and IL6 (green) in human samples of hepatitis-induced liver fibrosis (n=3). **(b)** Immunohistchemical expression of human uPAR (h.uPAR) and SA-β-Gal in human samples from patients with eradicated hepatitis C virus (HCV) and residual liver fibrosis (n=7 patients). Co-immunofluorescence staining and quantification of human uPAR (red) and p16 (green) or human uPAR (red) and IL6 (green) in human samples of HCV-induced liver fibrosis (n=3). **(c)** Immunohistochemical stainings of human uPAR (h.uPAR) in human carotid endarterectomy samples (n= 5 patients). **(d)** Immunohistochemical stainings of human uPAR (h.uPAR) in human pancreas bearing pancreatic intraepithelial neoplasia (PanINs) compared to normal pancreas controls (n= 3 patients). **(a,b)** Data represent mean± SEM.

3.2.2.-Engineering anti-uPAR CAR T cells.

We constructed a uPAR-specific CAR comprising an anti murine uPAR (m.uPAR) single chain variable fragment (scFv) linked to human CD28 costimulatory and CD3ζ (h.28z) signaling domains (m.uPAR-h.28z), transduced human T cells, and performed cytotoxicity assays using target cells expressing a murine uPAR cDNA (Figure 3.5a-d). To enable comparisons to well-characterized CAR T cells directed against CD19 (Brentjens et al., 2003), murine uPAR was introduced into the human $CD19^{+}$ pre-B acute lymphoblastic leukemia cell line (B-ALL) NALM6 (Figure 3.5c). m.uPAR-h.28z CAR T cells showed no cytotoxicity towards uPAR negative NALM6 cells, but comparable activity to CD19 CAR (h.19-h.28z) T cells when targeting uPAR-expressing NALM6 cells (Figure 3.5d and Figure 3.6a). m.uPAR-h.28z, but not h.19-h.28z, CAR T cells efficiently eliminated senescent KP cells expressing endogenous uPAR, which was accompanied by antigen-specific granzyme B and IFNγ secretion (Figure 3.5.e). Hence, m.uPAR-h.28z CAR T cells can selectively and efficiently target senescent cells.

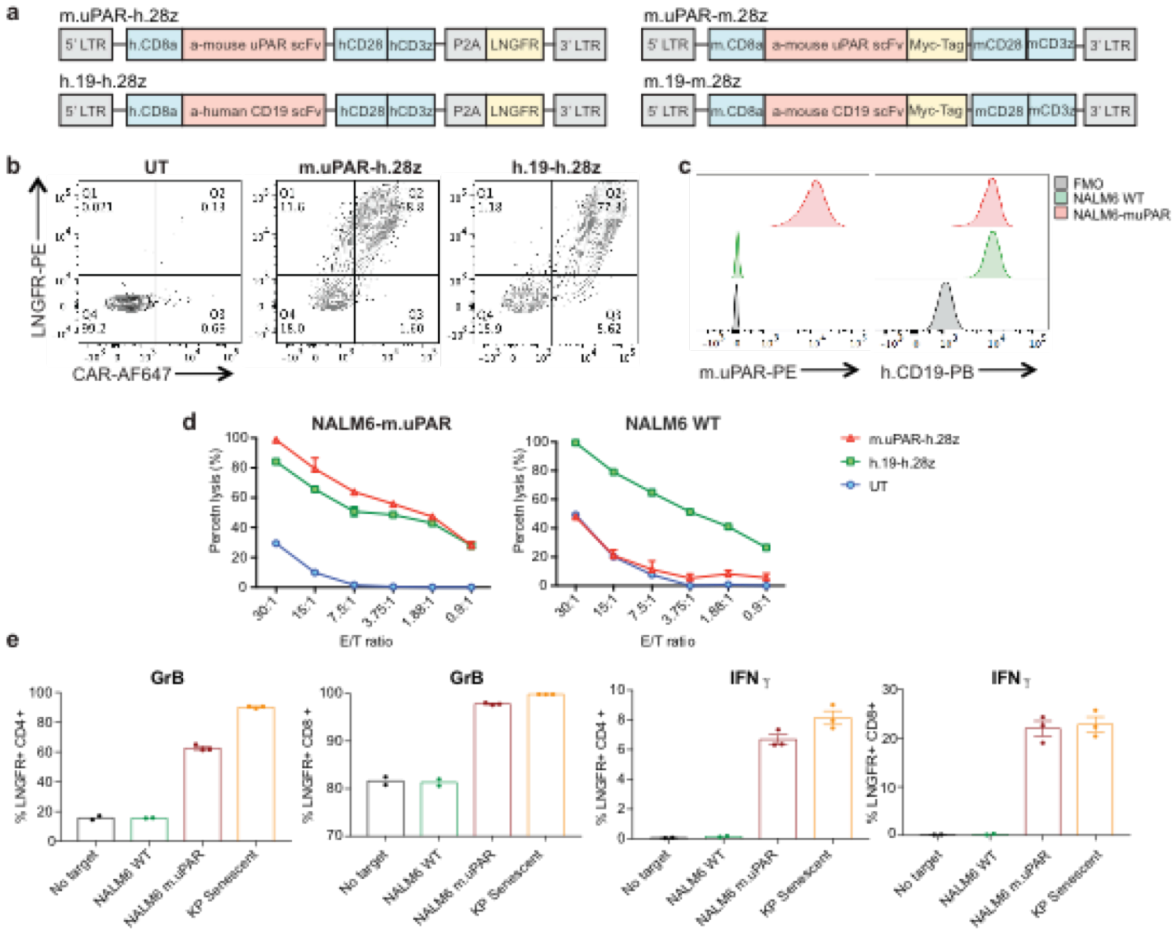

Figure 3.5. uPAR-28z CAR T cells selectively target uPAR positive cells. (a) Construct maps encoding human m.uPAR-h.28z and h.CD19-h.28z CAR T cells or murine m.uPAR-m.28z and m.CD19-m.28z CARs. **(b)** Flow cytometric analysis showing expression levels of CAR and LNGFR for m.uPAR-h.28z and h.19-h.28z CAR T cells compared to untransduced (UT) T cells. Representative results of 4 independent experiments. **(c)** Flow cytometric analysis of murine uPAR and human CD19 expression on wild type NALM6 cells and on NALM6 cells overexpressing murine uPAR (NALM6-m.uPAR). Representative results of 3 independent experiments. **(d)** Cytotoxic activity of m.uPAR-h.28z, h.19-h.28z and untransduced (UT) T cells as determined by 4hr-Calcein assay with firefly luciferase (FFL)-expressing NALM6 WT or NALM6-m.uPAR as targets. Representative results of n=3 independent experiments performed in triplicates. Data are mean± SEM. **(e)** Granzyme B (GrB) and Interferon γ (IFNγ) expression on CD4+ and CD8+ m.uPAR-h.28z or h.19-h.28z CAR T cells 18 hours after co-culture with NALM6 WT, NALM6-m.uPAR or senescent Kras$^{G12D;p53-/-}$ (KP) cells as determined by intracellular cytokine staining. Results of n=1 independent experiment (no target: n=2, NALM6 WT: n=2, NALM6-m.uPAR: n=3 and KP senescent: n=3 replicates). Data are mean± SEM.

3.2.3.-Senolytic activity of anti-uPAR CAR T cells.

To study whether m.uPAR-h.28z CAR T cells could function as *bona fide* senolytics *in vivo*, we took advantage of the well-characterized model of oncogene-induced senescence triggered by hepatic overexpression of $NRAS^{G12V}$-Luciferase used above (Kang et al., 2011). While these senescent cells normally undergo immune clearance (Kang et al., 2011), they are retained in the livers of immunodeficient NOD-Scid-gamma (NSG) mice (Kang et al., 2011). Successful transfection of murine hepatocytes in NSG mice was confirmed by bioluminescence imaging and followed by administration of $0.5x10^6$ m.uPAR-h.28z CAR^+ T cells or untransduced (UT) T cells as controls.

Treatment with m.uPAR-h.28z CARs led to a profound decrease in bioluminescence signal within 10 days (Figure 3.6b), suggesting effective clearance of senescent hepatocytes. Histological analyses confirmed that livers from m.uPAR-h.28z CAR T cell treated mice had significantly reduced numbers of NRAS ($p<0.01$) and SA-β-gal positive cells ($p<0.001$) compared to controls (Figure 3.6d, e). Furthermore, m.uPAR-h.28z CAR T cells (but not UT T cells) accumulated around senescent hepatocytes within 7 days of infusion (Figure 3.6f) and displayed an effector memory phenotype ($CD62L^-CD45RA^-$) with little evidence of T cell exhaustion (<2% $PD1^+TIM3^+LAG3^+$ CAR T cells) 15 days after their administration (Figure 3.6g, h). These data suggested that indeed, uPAR-28z CAR T cells can eliminate senescent cells *in vivo*.

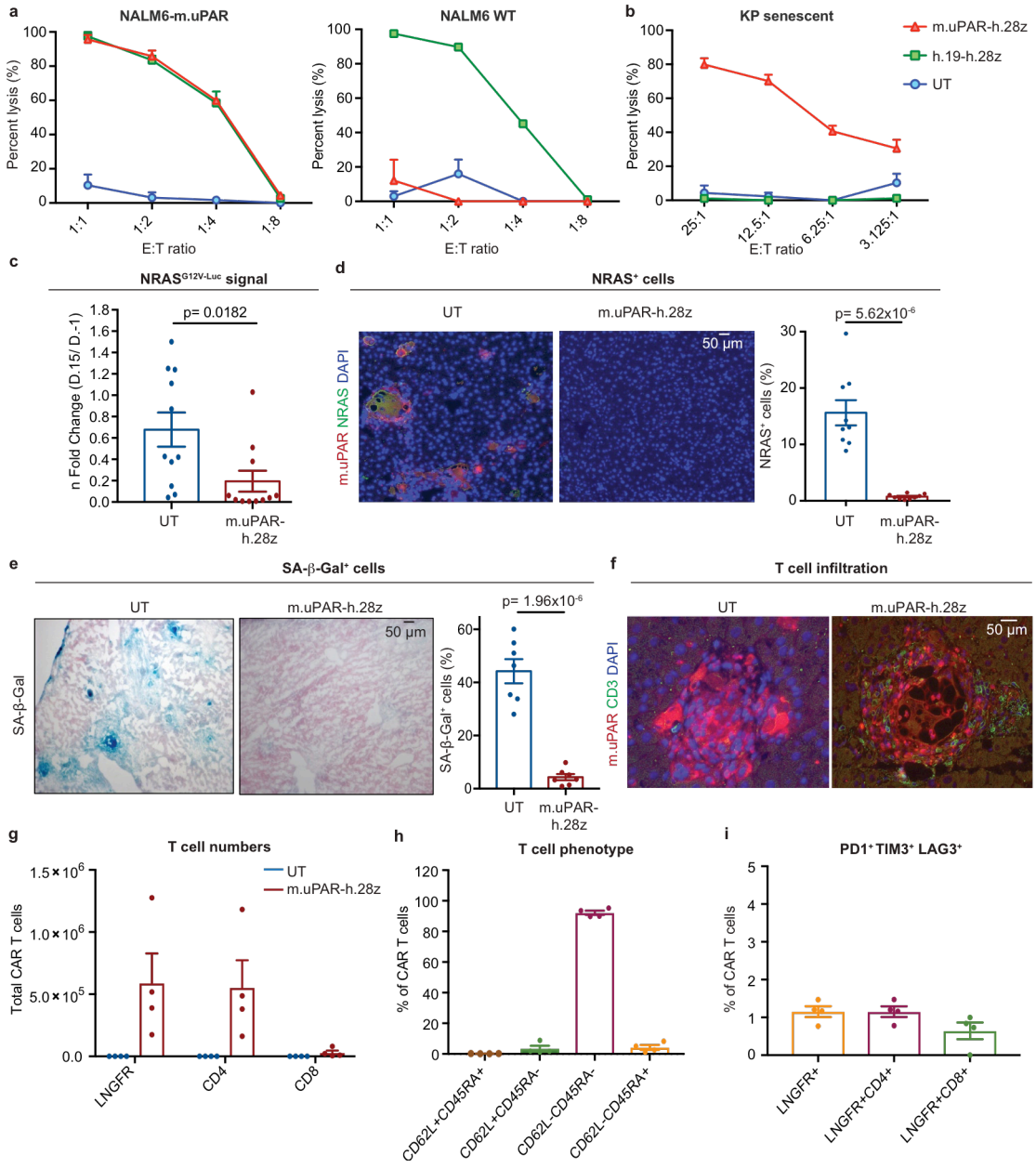

Figure 3.6. uPAR-CAR T cells are bona fide senolytics. (a) Cytotoxic T cell activity as determined by a 18hr-bioluminescence assay with luciferase-expressing NALM6 wild type (WT) or NALM6 overexpressing m.uPAR (NALM6-m.uPAR) as targets. Data representative of n=3 independent experiments, each performed in triplicates. **(b)** Cytotoxic T cell activity as determined by a 4hr-bioluminescence assay with MEK/Cdk4/6 inhibitor-induced senescent KP cells as targets; representative of n=2 independent experiments, each performed in triplicates. **(c-i)** NSG mice were injected with a plasmid encoding *NRAS*^{G12V}-GFP-Luciferase and treated with 0.5x10^6 m.uPAR-h.28z CAR T cells or untransduced (UT) T cells 10 days after injection. Mice were euthanized 15 days later and livers were analyzed. **(c)** n fold change in luciferase signal in mice (calculated as average radiance on day 15 divided by average radiance on day -1) (n=11 mice per group). **(d)** Co-immunofluorescence (IF) staining of m.uPAR (red) and NRAS (green) and quantification of NRAS-positive cells (n=9 mice per group). **(e)** Representative stainings and quantification of SA-β-Gal positive cells (n=7 mice per group). **(f)** Co-IF

staining of m.uPAR (red) and human CD3 (green) (n=5 mice per group). **(g-i)** Number of liver infiltrating T cells (g), expression of CD62L/CD45RA (h) and PD1+TIM3+LAG3+ (i) on m.uPAR-h.28z CAR T cells as determined by flow cytometry (n=4 mice per group). **(c-e)** Representative results of n=2 independent experiments. Data are mean± SEM. Two-tailed unpaired Student's t-test.

3.3.-Discussion

Herein we identify uPAR as a surface protein and suPAR as a secreted biomarker broadly induced on senescent cells. While it is true that uPAR can also be expressed by a certain subset of immune cells like macrophages and monocytes, the identification of a surface molecule of senescence opens the senescence field to further advancement. For example, using surface uPAR (and excluding CD45+ immune cells) it could now be possible to isolate senescent cells from *in vivo* settings and study the molecular characteristics of the senescence program in different settings. In addition, it will also open the door for more precise *in vivo* detection models to study the dynamics of these cells through intravital antibody- based imaging strategies such as immunoPET. Ultimately, it also facilitates the development of more specific senolytics by harnessing either antibody-mediated approaches or cellular therapy.

In this regard, our work also shows for the first time the feasibility of engineering CAR T cells as senolytic agents *in vitro* and *in vivo*. While further work is needed to determine whether uPAR-targeting CAR T cells have the required safety profile to be developed clinically, appropriately dosed senolytic CAR T cells can infiltrate the areas of senescence, efficiently target senescent cells, and produce a therapeutic benefit without notable toxicities in mice.

One of the outstanding questions pertains to CAR T persistence. Since senescent cells do not divide, these initial senolytic CAR T cells were developed using a second generation SFG vector with 28z as co-stimulatory domain. This approach maximized safety and efficacy in models in which the senescence stimulus was transient and if needed, left the door open for a second CAR T injection at a later time point. However, in contexts where the senescence stimulus is continuous such as ageing, CAR T

persistence might be preferred. In this regard future work should compare how CAR T cells with enhanced functional persistence perform in terms of safety and efficacy. If persistent CAR T designs are preferred in the setting of diseases with continuous senescence inducing stimuli the incorporation of safety switches such as iCaspase-9 (iCasp9) (Gargett and Brown, 2014) or EGFRt (Paszkiewicz et al., 2016) could minimize and provide control over the potential for adverse effects. Another possibility could entail the incorporation of CARs with dual specificities using AND/OR logic gate approaches (Eyquem et al., 2017; Srivastava et al., 2019). uPAR was initially chosen as an antigen upregulated across various senescent cells and triggers of senescence, but future CAR designs could be focused on surface proteins upregulated on specific senescent cells. This would increase the pool of potential targets which could be combined using AND logic gates to increase specificity and using OR logic gates to decrease targeting to essential tissues (Srivastava et al., 2019).

Finally, we have seen in the introduction how senescent cells modulate their microenvironment and affect the recruitment of immune cells aimed to clear them (Ruscetti et al., 2020; Tasdemir et al., 2016). Similar mechanisms could apply to senolytic cell therapy and thus potentially different immune cell types would be better suited for cellular therapy depending on the context. For example, while CAR T cells are particularly well suited for liver diseases and previous studies have shown that senescent cells are preferentially targeted by T cells in this organ (Kang et al., 2011), CAR-NK cells might provide a more potent effect in the lung, where they have been shown to be the main senescence targeting immune cell (Ruscetti et al., 2018). Future studies will also help to elucidate the mechanisms whereby senescent cells influence the activity of cellular therapy and inform the generation of enhanced CAR designs that

could secrete specific cytokines (Giavridis et al., 2018) or express receptors that would turn inhibitory signals into stimulatory ones (Giavridis et al., 2018).

CHAPTER 4

THERAPEUTIC POTENTIAL OF SENOLYTIC CAR T CELLS FOR THE TREATMENT OF AGE RELATED DISORDERS

4.1.-Introduction

Over the past 150 years life expectancy has significantly increased with an average lifespan in the USA of 78.8 years in 2020 vs 39.41 in 1870. Nowadays, 16.9% of the USA population is over 65 years old and expected to reach 22% by 2050. Healthspan, however, has remained more constant (Scott, 2021) and there has been an increase in chronic “age-related diseases” such as vascular disease, diabetes, cancer and dementias (Scott, 2021). Importantly, research has shown that the biggest health and economic impact will result from targeting the aging process itself rather than any individual disease (Scott, 2021), highlighting the need to understand aging biology. In this regard, cellular senescence is a key determinant of organismal aging (Baker et al., 2011).

Genetically engineered mouse models (GEMMs) that eliminate senescent or $p16^{+}$ cells in aging have shown that eliminating these cells can ameliorate symptoms and expand health and lifespan (Baker et al., 2016; Baker et al., 2011). Recapitulating these results with current senolytics has been more challenging owing to limited efficacy as compared to highly efficient mouse models. Nonetheless, initial work by (Xu et al., 2018) with dasatinib and quercetin show the potential for this approach. In addition, targeting senescent cells has been shown to be highly effective in the treatment of age-related pathologies such as lung fibrosis, atherosclerosis, or neurodegenerative conditions (Bussian et al., 2018; Childs et al., 2016; Munoz-Espin et al., 2018).

In this chapter we explore the efficacy and safety profile of senolytic CAR T cells to treat age related disorders.

4.2.-Results

4.2.1.-Therapeutic preclinical activity of senolytic CAR T cells in liver fibrosis

To evaluate the senolytic capacity of uPAR CAR T cells in immunocompetent settings, we transduced T cells derived from C57BL/6 mice with a fully murinized CAR (m.uPAR-m.28z). We confirmed CAR expression and showed that they displayed a similar cytolytic profile to m.uPAR-h.28z when targeting the mouse $CD19^+$ B-ALL cell line Eμ-ALL01 expressing exogenous uPAR or senescent KP cells (Figure 4.1a).

Besides cancer, senescence contributes to a range of chronic tissue pathologies including liver fibrosis, a condition that can evolve into cirrhosis and produces a microenvironment that favors hepatocellular carcinoma development (He and Sharpless, 2017; Sharpless and Sherr, 2015). Since genetic ablation of senescent cells ameliorates liver fibrosis (Puche et al., 2013; Schnabl et al., 2003), we performed dose-escalation studies using m.uPAR-m.28z CAR T cells in the well-defined model involving CCl_4 exposure, which leads to the accumulation of senescent HSCs, fibrosis, and liver damage within 6 weeks (Krizhanovsky et al., 2008). m.uPAR-m.28z, m.19-m.28z CARs or UT T cells were infused at either the previously effective dose of 0.5-1x10^6 CAR T cells or higher dosage (2-3x10^6) into mice with established liver fibrosis (Kuhn et al., 2019) (Figure 4.1 and 4.2). In some experiments, mice were treated with either m.uPAR-m.28z, m.19.-m.28z or control T cells expressing click-beetle red luciferase to track T cells *in vivo* using bioluminescence (Dobrenkov et al., 2008) (Figure 4.2a).

At either dosage, m.uPAR-m.28z CAR T cells produced a striking reduction in liver fibrosis. Hence, liver samples obtained 20 days after treatment with m.uPAR-m.28z CAR T cells displayed fewer senescent cells and less fibrosis as assessed by SA-β-Gal and Sirius red staining compared to controls ($p<0.001$), which was associated with an

accumulation of adoptively transferred T cells (Figure 4.1c and 4.2c). Consistent with on-target activity and a therapeutic benefit, mice treated with m.uPAR-m.28z CAR T cells displayed reduced serum levels of suPAR and of the liver enzymes ALT and AST (Figure 4.1d,e,f and 4.2e,f,g), indicating efficient elimination of pro-inflammatory senescent HSCs (Puche et al., 2013; Schnabl et al., 2003) and a reduction in liver damage, respectively. Bioluminescence imaging revealed that transferred T cells initially transited through the lungs as expected. Eventually, m.uPAR-specific, but not m.CD19-directed CARs or UT T cells, accumulated in the livers of CCl_4-treated mice, showing expansion over a few days followed by rapid contraction (Figure 4.1g,h). The high senolytic activity of uPAR CAR T cells was corroborated by efficient reduction of fibrosis under aggravated conditions produced by prolonged CCl_4 exposure as well as sustained fibrosis resolution in long-term follow up studies (Figure 4.2h,i).

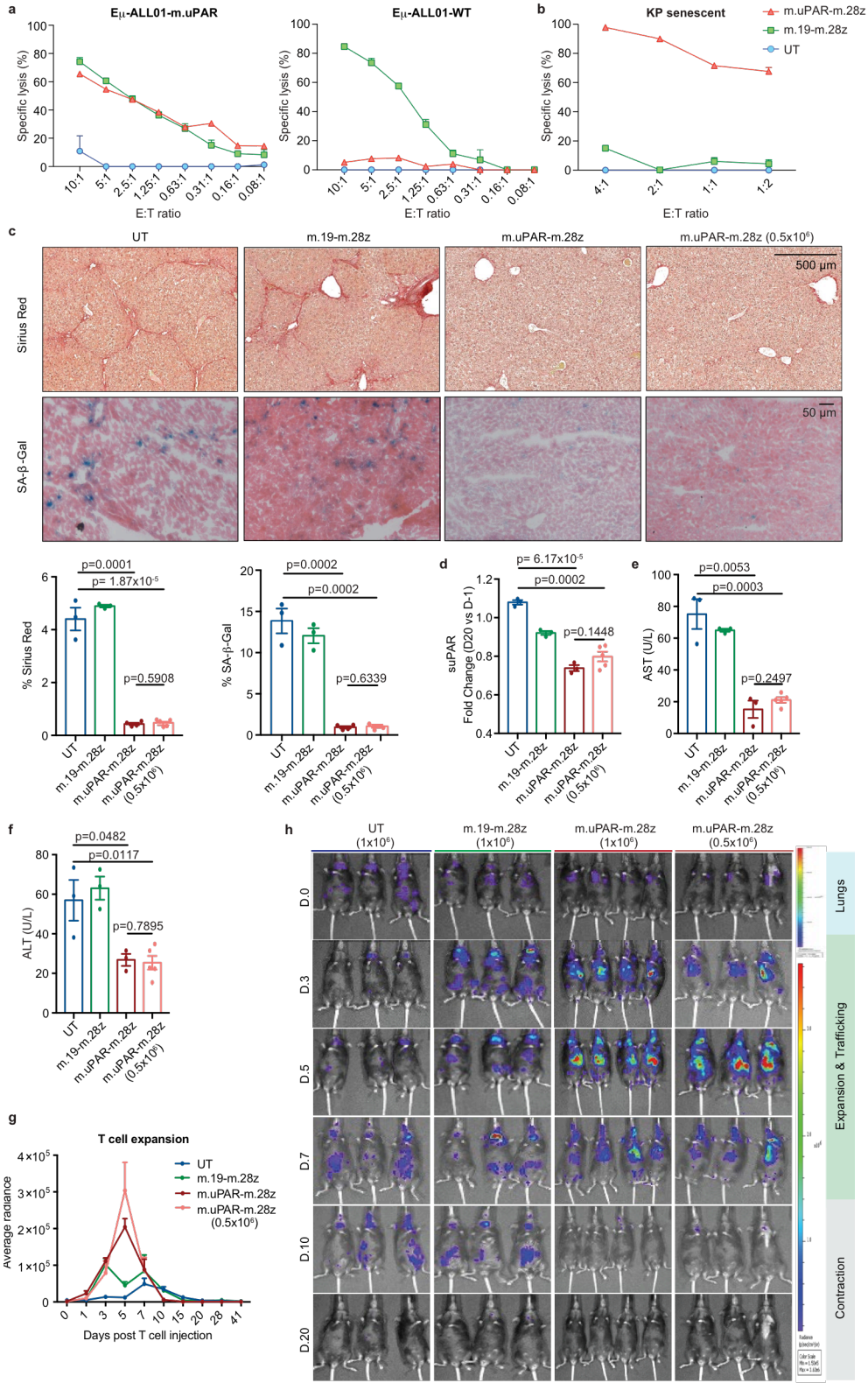

Figure 4.1. Senolytic CAR T cells at low doses show therapeutic efficacy in CCl_4-induced liver fibrosis. (a) Cytotoxicity of murine CAR T cells as determined by a 18hr-bioluminescence assay with luciferase-expressing Eμ-ALL01 WT or Eμ-ALL01-m.uPAR as targets. Representative results of n=3 independent experiments, each performed in

triplicates. **(b)** Cytotoxic activity as determined by a 18hr-bioluminescence assay using MEKi/CDK4/6i–treated KP cells as targets. Results of n=2 independent experiments, each performed in triplicates. **(c-f)** Mice with CCl_4-induced liver fibrosis were treated with 0.5x10^6 or 1x10^6 m.uPAR-m.28z, 1x10^6 m.19-m.28z or untransduced (UT) T cells and euthanized 20 days after. Livers were used for further analyses. (c) Representative levels of fibrosis as evaluated by Sirius red staining, SA-β-Gal expression and respective quantifications (UT and m.19-m.28z: n=3, m.uPAR-m.28z: n=4, m.uPAR-m.28z at 0.5x10^6: n=5). **(d-f)** Fold change differences in serum levels of suPAR (d), AST (e) and ALT (f) 20 days after T cell infusion (UT, m.19-m.28z and m.uPAR-m.28z: n=3; m.uPAR-m.28z at 0.5x10^6: n=5). **(g)**-**(h)** Mice with CCl_4-induced liver fibrosis were injected with 0.5x10^6 or 1x10^6 click beetle red luciferase-expressing CAR T cells or UT T cells. **(g)** Luciferase signal (average radiance) of treated mice after T cell administration (UT and m.19-m.28z: n=3, m.uPAR-m.28z: n=4, m.uPAR-m.28z at 0.5x10^6: n=3). **(h)** Representative bioluminescence images of mice at different time points after injection. Signal in control mice at day 10 indicates abdominal peritonitis induced by CCl_4 injections as confirmed by pathology. **(c-h)** Results of n=1 independent experiment. Data are mean± SEM. Two-tailed unpaired Student's t-test.

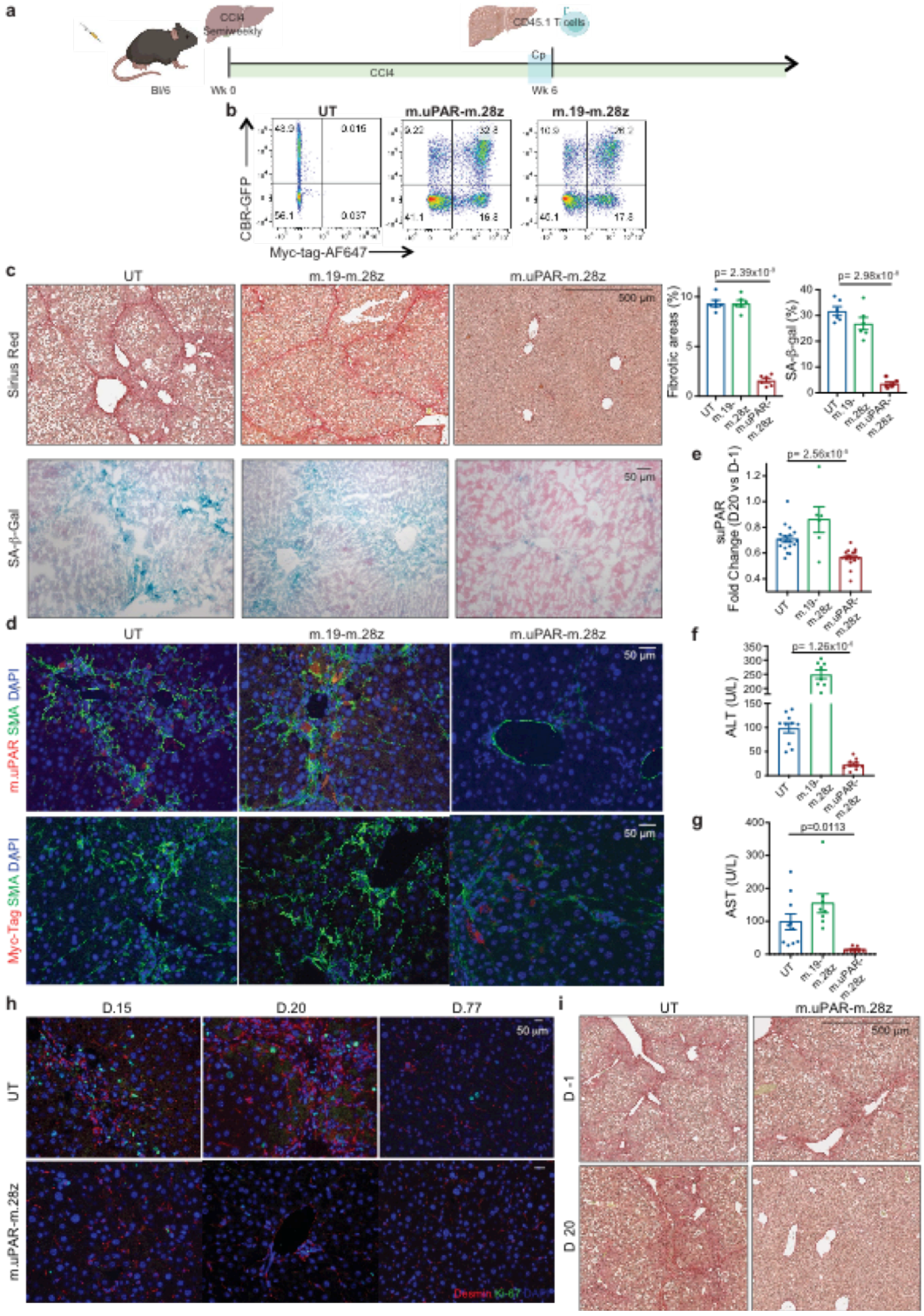

Figure 4.2. Senolytic CAR T cells show therapeutic activity in CCl_4-induced liver fibrosis. (a) Layout for experiments performed using the CCl_4-induced liver fibrosis model: C57BL/6N mice received semiweekly intraperitoneal infusions of CCl_4 for 6 weeks and were intravenously infused with 0.5-1x10^6 (Fig. 3) or 2-3x10^6 (Extended Data Fig. 6c-i) murine m.uPAR-m.28z CAR T cells, m.19-m.28z CAR T cells or untransduced (UT) T cells 16-24hr after cyclophosphamide (200mg/kg) administration. Mice were euthanized 20 days after CAR infusion to assess liver fibrosis. Images were created with

Biorender.com. **(b)** Expression of GFP/click beetle red (CBR) luciferase and Myc-tag for m.uPAR-m.28z and m.19-m.28z CAR T cells used for T cell imaging experiments (Fig. 3g-h) as compared to control T cells. Representative results of 2 independent experiments. **(c)** Sirius red and SA-β-Gal staining and quantifications of livers from treated mice (n=6 mice per group). **(d)** Co-immunofluorescence of m.uPAR (red) and smooth muscle actin (green) or Myc-tag (red) and smooth muscle actin (green) in the livers of treated mice. **(e)** Fold change difference in serum levels of soluble (suPAR) 20 days after CAR T cell treatment as compared to day -1 before CAR T cell injection (UT: n=18 mice, m.19-m.28z: n=6, m.uPAR-m.28z: n=17). **(f-g)** Levels of serum alanine aminotransferase (ALT) (U/L) **(f)** and levels of serum aspartate aminotransferase (AST) (U/L) **(g)** 20 days after CAR treatment (UT: n=10 mice, m.19-m.28z: n=8, m.uPAR-m.28z: n=10). **(h)** Co-immunofluorescence staining of desmin (red) and ki-67 (green) in the livers of mice 15, 20 and 77 days after CAR T cell treatment. CCl_4 treatment was stopped 20 days after T cell infusion (n=3 mice per group). **(i)** Mice were treated with CCl_4 for 10 weeks. Sirius red staining of the livers of mice before (d.-1) and 20 days after T cell administration (UT: n=4 mice, m.uPAR-m.28z: n=2). **(c-g)** Representative results of 2 independent experiments. All data represent mean± SEM. **(c, e-g)** Two-tailed unpaired Student's t-test.

4.2.2.-Safety profile of senolytic CAR T cells in liver fibrosis

Mice treated at the supratherapeutic doses presented with hypothermia and weight loss, which was accompanied by a rise in serum cytokines including IL6, GM-CSF, G-CSF and IFNy (Figure 4.3a-e). Similar to CAR T cell-associated cytokine release syndrome (CRS) (Giavridis et al., 2018; Norelli et al., 2018), this early toxicity was transient, associated with local accumulation and activation of macrophages and could be mitigated by lower CAR T cell doses or CRS-prevention using IL6R and IL1R inhibitors (Figure 4.3f and 4.4). Importantly, mice treated at the lower effective dose remained highly active and did not display observable signs of morbidity, changes in temperature or weight, or relevant alterations in cell blood counts (Figure 4.5). Moderate macrophage infiltration was noted in the lungs after 20 days, which also occurred in mice treated with m.19-m.28z or UT T cells (Figure 4.5d).

Altogether, these findings indicate that appropriately-dosed uPAR-directed CAR T cells can deplete senescent cells without precipitating severe CRS-like symptoms and highlight the potential of short acting CD28/CD3z-based CAR T cells (Feucht et al., 2019) in senescence-associated indications.

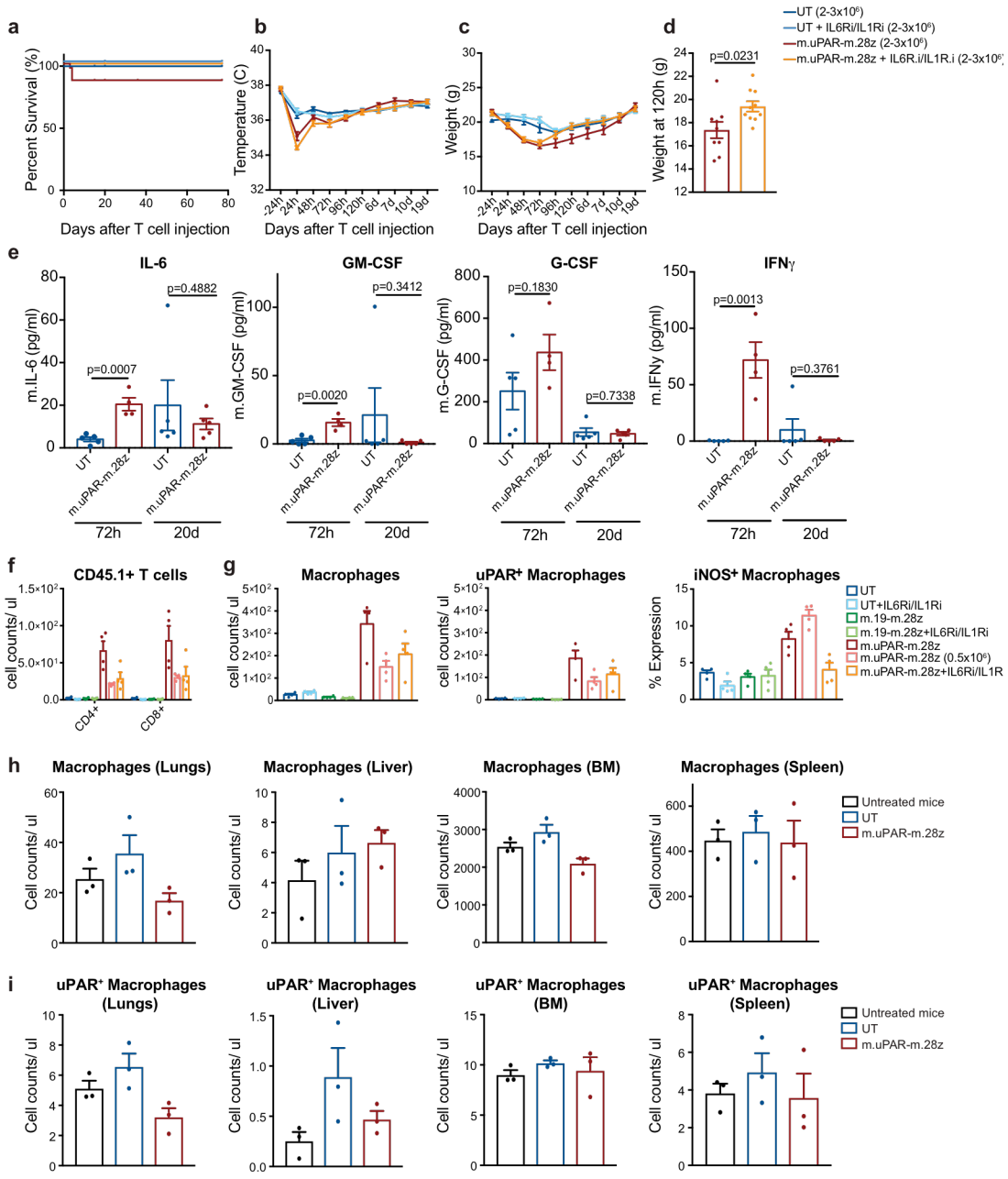

Figure 4.3. Safety profile of m.uPAR-m.28z CAR T cells at supratherapeutic T cell doses. C57BL/6N mice received semiweekly intraperitoneal (ip) infusions of CCl_4 for 6 weeks followed by intravenous (iv) infusion of 2-3x10^6 murine m.uPAR-m.28z CAR T cells or untransduced (UT) T cells 16-24hr after cyclophosphamide (200mg/kg) administration. A subset of mice (as specified in the figures) received additional treatment with IL6R blocking antibodies (IL6Ri) and Anakinra (IL1Ri), starting 24h before T cell infusion and continued daily until 6 days after T cell infusion. Mice were euthanized 12 weeks after CAR infusion to assess potential toxicities. **(a)** Kaplan-Meier curve showing survival of mice after CAR T cell injection (UT: n=19 mice, UT + IL6Ri/IL1Ri: n=7, m.uPAR-m.28z: n=30, m.uPAR-m.28z + IL6Ri/IL1Ri: n=19). **(b-c)** Temperature **(b)** and weight **(c)** of treated mice (UT: n=7 mice, UT + IL6Ri/IL1Ri: n=8, m.uPAR-m.28z: n=11, m.uPAR-m.28z + IL6Ri/IL1Ri: n=10). **(d)** Weight (g) of mice 120h after infusion with either m.uPAR-m.28z or m.uPAR-m.28z and additional treatment with

IL6Ri and IL1Ri (m.uPAR-m.28z: n=11, m.uPAR-m.28z + IL6Ri/IL1Ri: n=10). **(e)** Serum levels of murine IL-6, GM-CSF, G-CSF and IFNy in mice treated with either m.uPAR-m.28z or UT T cells 72h or 20 days after T cell infusion (UT: n=5, m.uPAR-m.28z: n=4 at 72h and n=5 at 20d). **(f-g)** Number of adoptively transferred CD45.1 positive T cells **(f)**, macrophages, uPAR-positive and iNOS-positive macrophages **(g)** in the lungs of mice treated with m.uPAR-m.28z, m.19-m.28z or UT T cells alone or in combination with combined IL6Ri and ILR1i 3 days after T cell infusion (n=4 mice per group). **(h-i)** Numbers of macrophages **(h)** and uPAR positive macrophages **(i)** in lungs, liver, bone marrow (BM) and spleen of untreated mice or mice treated with either m.uPAR-m.28z or UT T cells 12 weeks after T cell infusion (n=3 mice per group). **(a-e)** Representative results of 3 independent experiments. All data represent mean± SEM. Two-tailed unpaired Student's t-test. **(f-i)** Representative results of 1 independent experiment. All data represent mean± SEM. Two-tailed unpaired Student's t-test.

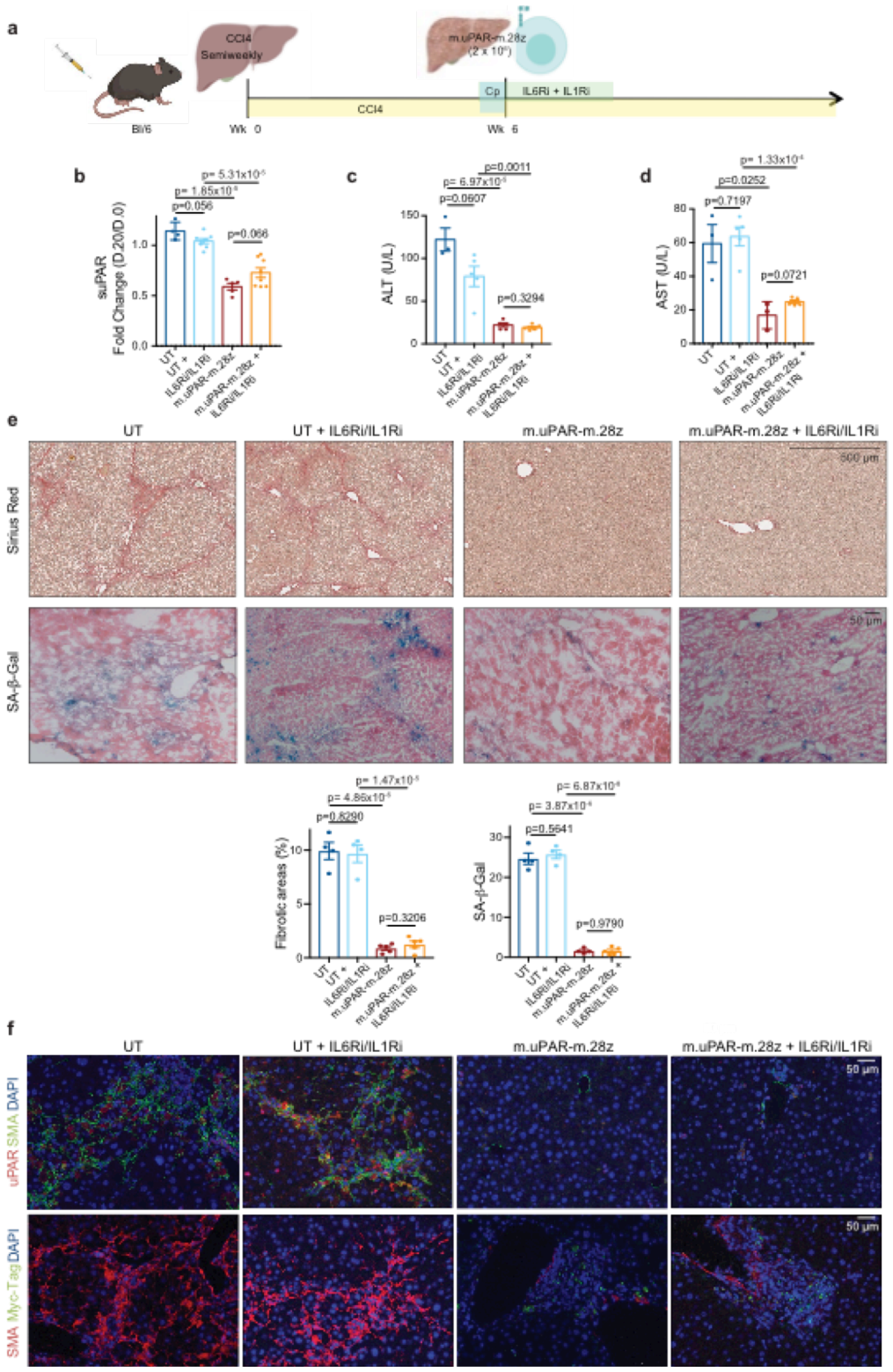

Figure 4.4. Therapeutic intervention with IL6R and IL1R inhibitors does not decrease therapeutic efficacy of senolytic CAR T cells in CCl_4-induced liver fibrosis. (a) Experimental layout: C57BL/6N mice received semiweekly intraperitoneal (ip) infusions of CCl_4 for 6 weeks and were intravenously (iv) infused with 2-3x10^6 murine m.uPAR-m.28z CAR T cells or UT T cells 24hr after cyclophosphamide (200mg/kg) administration. IL6R blocking antibodies (IL6Ri) and Anakinra (ILRi) were

first administered 24h before T cell infusion followed by daily (IIL6Ri) or twice a day (Anakinra) injections for the first 6 days until treatment was stopped. Mice were euthanized 20 days after T cell infusion to assess liver fibrosis. Images were created with Biorender.com. **(b)** Fold change difference in serum levels of soluble (suPAR) 20 days after CAR T cell treatment as compared to day -1 before CAR T cell injection (UT: n=4 mice, UT+IL6Ri/IL1Ri: n=8, m.uPAR: n=5, m.uPAR+IIL6Ri/IL1Ri: n=8). **(c-d)** Levels of serum alanine aminotransferase (ALT) (U/L) **(c)** and of serum aspartate aminotransferase (AST) (U/L) **(d)** in treated mice 20 days after T cell infusion (UT: n=3 mice, UT+IL6Ri/IL1Ri: n=5, m.uPAR-m.28z: n=5 (ALT) and n=3 (AST), m.uPAR-m.28z+IIL6Ri/IL1Ri: n=5). **(e)** Representative levels of fibrosis evaluated by Sirius red staining and SA-β-Gal staining of livers from treated mice and quantification of liver fibrosis and SA-β-Gal+ cells in the respective livers 20 days after treatment (UT: n=4 mice, UT+IL6Ri/IL1Ri: n=4, m.uPAR-m.28z: n=4, m.uPAR-m.28z+IIL6Ri/IL1Ri: n=5). **(f)** Co-immunofluorescence staining of either murine uPAR (red) and smooth muscle actin (green) or Myc-tag (red) and smooth muscle actin (green) in the livers of treated mice. **(b,c,d,e,f)** Representative results of 1 independent experiment. All data represent mean± SEM. Two-tailed unpaired Student's t-test.

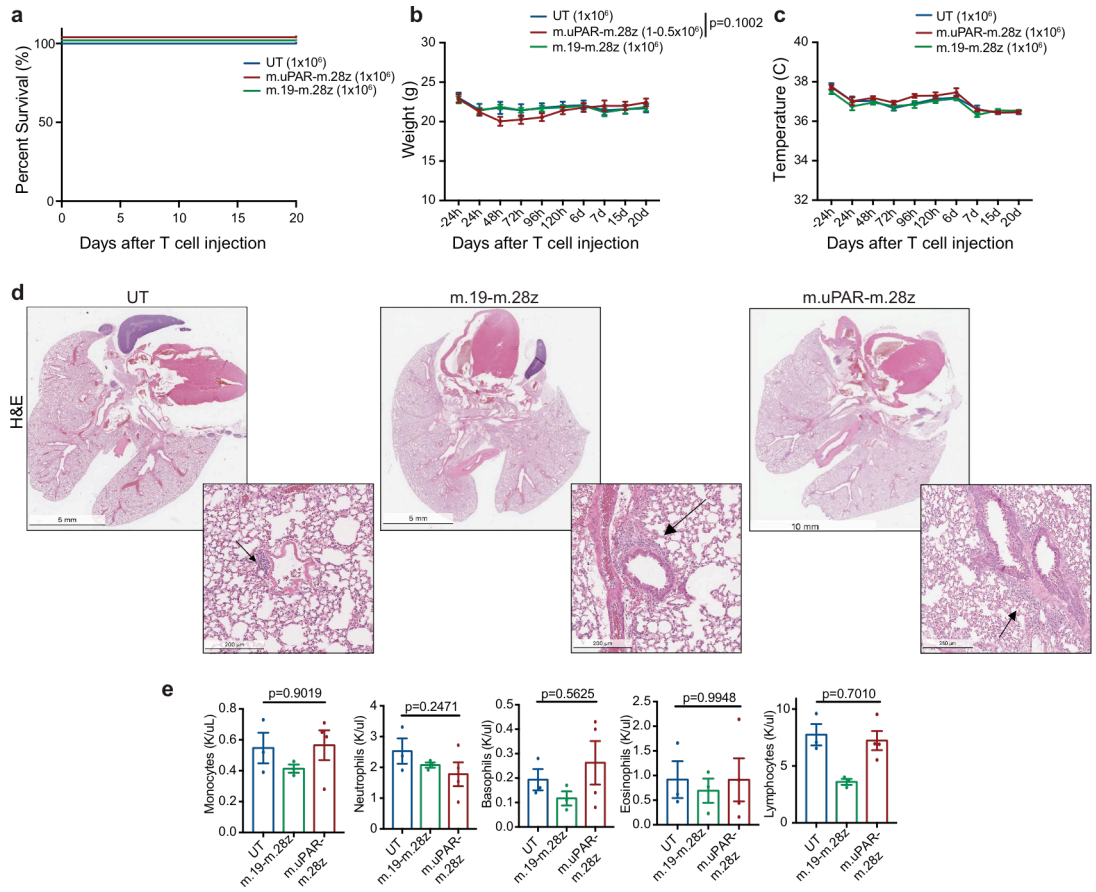

Figure 4.5. Safety profile of m.uPAR-m.28z CAR T cells at therapeutic T cell doses. (a)-(e) C57BL/6N mice received semiweekly intraperitoneal (ip) infusions of CCl_4 for 6 weeks and were intravenously (iv) injected with 0.5-1x10^6 murine m.uPAR-m.28z CAR T cells, 1x10^6 murine m.19-m.28z CAR T cells or untransduced (UT) T cells 16hr after cyclophosphamide (200mg/kg) administration. Mice were euthanized 20 days after T cell administration to assess potential toxicities and lung histopathology. **(a)** Kaplan-Meier curve showing survival of mice after treatment with either m.uPAR-m.28z (n=16 mice), m.19-m.28z CAR T cells (n=6) or UT T cells (n=6). **(b-c)** Weight (g) shown in **(b)** and temperature (C) shown in **(c)** of mice as measured before and at different time points after T cell infusion (UT and m.19-m.28z: n=6 mice; m.uPAR-m28z: n=7). P value in **(b)** refers to differences in weight at 48h. **(d-e)** Representative hematoxylin and eosin (H&E) stainings of lungs **(d)** and complete blood counts **(e)** of treated mice 20 days after T cell infusion (UT and m.19-m.28z: n=3-4 mice; m.uPAR-m28z: n=4). Increased macrophage accumulation was observed in the immunodeficient setting. **(a-e)** Representative results of 1 independent experiment. All data represent mean± SEM. **(b, e)** Two-tailed unpaired Student's t-test.

4.2.3.-Therapeutic preclinical activity of senolytic CAR T cells in NASH

We also tested whether uPAR-targeting CAR T cells could be effective against fibrosis induced by non-alcoholic steatohepatitis (NASH), a condition of growing incidence in which effective therapeutic options are lacking (Brunt et al., 2015). Although the contribution of cellular senescence to NASH pathology is poorly understood, its role in other fibrosis settings prompted us to test for the presence of senescent cells in two well-established murine NASH models. Indeed, senescent cells were prevalent around the fibrotic areas (Figure 4.6a) and co-expressed uPAR and either markers of HSCs ($uPAR^+$ and $desmin^+$) or macrophages ($uPAR^+$ and $F4/80^+$) (Figure 4.6b). Accordingly, treatment of mice with diet-induced NASH using $0.5x10^6$ m.uPAR-m.28z CAR T cells (but not UT controls) efficiently eliminated senescent cells, reduced fibrosis and improved liver function (as assessed by serum albumin levels) without eliciting detectable toxicity (Figure 4.6c,d and 4.7). Thus, senolytic CAR T cells are effective against liver fibrosis of different etiologies.

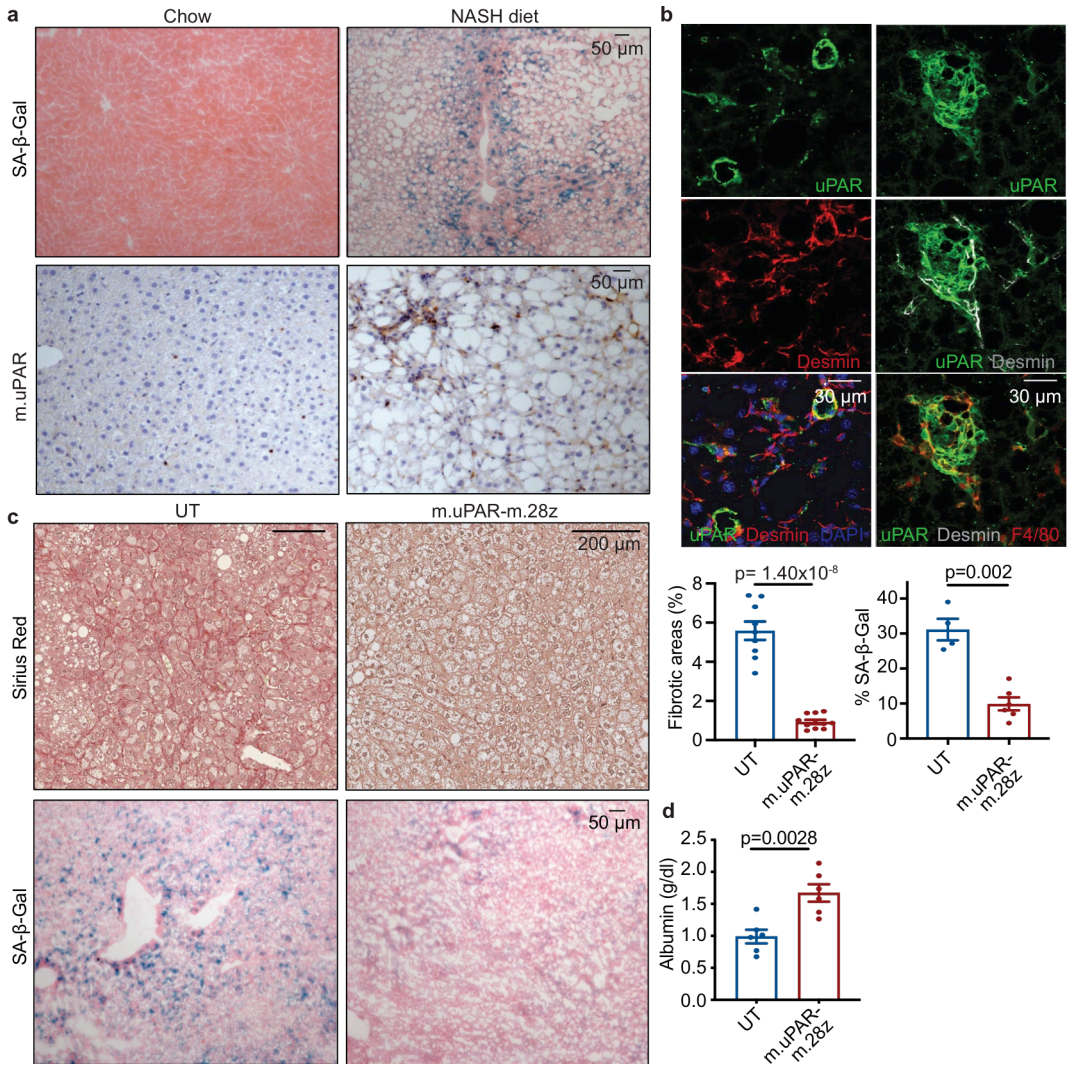

Figure 4.6. Senolytic CAR T cells are therapeutic in NASH-induced liver fibrosis. **(a,b)** Representative stainings in the livers of mice treated with chow or NASH diet for 3-4 months. **(a)** Immunohistochemical staining of m.uPAR and SA-β-Gal (n=3 mice per group) **(b)** Co-immunofluorescence staining of m.uPAR (green), desmin (red in left panel, gray in right panel) and F4/80 (red). Representative results of n=2 independent experiments (n=3 mice per group). **(c-d)** Mice treated with NASH diet for 3 months were injected with 0.5x10^6 m.uPAR-m.28z CAR T cells or untransduced (UT) T cells. Liver and serum analyses were performed 20 days later. **(c)** Representative Sirius red staining, SA-β-Gal expression and quantifications (Sirius red: UT: n=9 mice, m.uPAR-m.28z: n=11. SA-β-Gal: UT: n= 4 mice, m.uPAR-m.28z: n=6). **(d)** Serum albumin levels (UT and m.uPAR-m.28z: n=6). **(c-d)** Results of n=2 independent experiments. Data are mean± SEM. Two-tailed unpaired Student's t-test.

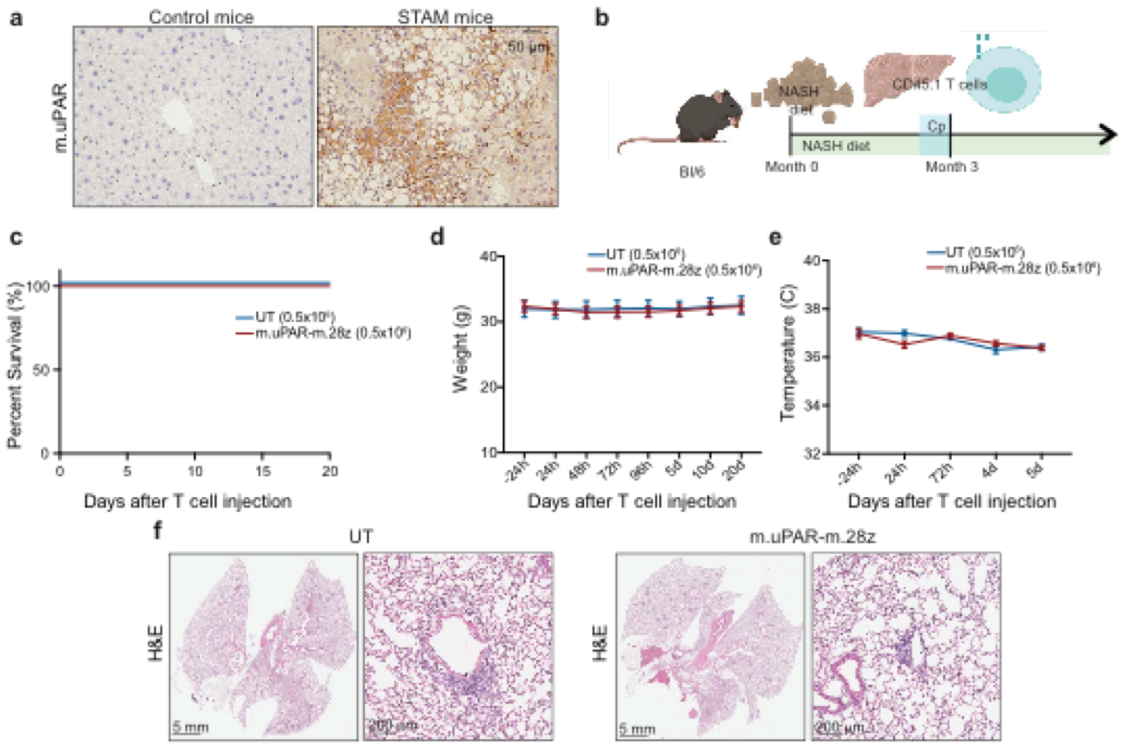

Figure 4.7. Safety profile of senolytic CAR T cells at therapeutic doses in a murine NASH-induced liver fibrosis model. (a) Immunohistochemical expression of murine uPAR in samples from the "STAM™" model(Fujii et al., 2013; Van der Schueren et al., 2015) (n=3 mice). **(b)** Experimental layout for experiments performed using the model of diet-induced NASH (Fig. 4, Extended Data Fig. 10): C57BL/6N mice received normal chow or NASH diet(Zhu et al., 2018) for 3 months, followed by intravenous (iv) infusion with $0.5x10^6$ murine m.uPAR-m.28z CAR T cells or UT T cells 16 hours after cyclophosphamide (200mg/kg) administration. Mice were euthanized 20 days after CAR infusion to assess liver fibrosis. Images were created with Biorender.com. **(c)** Kaplan-Meier curve showing survival of mice after treatment with either m.uPAR-m.28z or UT T cells (m.uPAR-m.28z: n=16 mice and UT: n=10). **(d-e)** Weight **(d)** and temperature **(e)** of mice before and at different time points after T cell infusion (m.uPAR-m.28z: n=11 mice and UT: n=9). Data represent mean± SEM. **(f)** Representative H&E stainings of the lungs of treated mice (m.uPAR-m.28z: n=6 mice and UT: n=4**). (c-f)** Representative results of 2 independent experiments.

4.2.4.-Harnessing senolytic CAR T cells to deconstruct aging

We wondered whether uPAR would also be upregulated in senescent cells generated as a result of natural aging. Indeed, uPAR was highly upregulated in the liver, adipose tissue, pancreas and muscle of aged (20 months) but not young (3months) mice (Figure 4.8a), where it co-localized with other markers of senescence such as p16, IL6, SA-B-Gal (data not shown). Importantly, in these settings uPAR was expressed on the cell surface allowing us to use antibodies against uPAR to sort senescent cells from dissociated tissues (Figure 4.8.b). In addition, cell surface-bound uPAR can be cleaved releasing a soluble fraction called suPAR, whose levels were significantly upregulated in the serum of aged mice (Figure 4.8c), recapitulating the observation that suPAR increases with age in humans and correlates with healthspan (Hartmann Rasmussen).

To test whether senolytic CAR T cells could effectively and safely target senescent cells in aging we tested the uPAR CAR T cells in a syngeneic model of natural aging. For this, we injected CD45.2 Bl/6N mice of 3 months old (young) or 20 months old (aged) with $0.5x10^6$ m.uPAR-m.28z murine CAR Ts generated from CD45.1 mice or with irrelevant CAR T cells targeting human CD19 (h.19-m.28z) or untransduced T cells as controls and monitored the mice until their natural death (Figure 4.9a). The injected uPAR CAR Ts in the 20m mice expanded and persisted and we were able to detect them by flow cytometry in several organs such as spleen, bone marrow, liver and muscle by day 20 post infusion (Figure 4.9c) where they presented an effector memory phenotype (data not shown). This correlated with a significant decrease in the number of senescent cells detected in the tissues both by histology as well as by whole body luminescence in $p16^{Luc}$ mice (Figure 4.9b). Moreover, infusion of the uPAR CAR Ts led to an improvement in metabolic function as measured by improved glucose tolerance testing, insulin tolerance testing and pancreatic beta cell function (Figure 4.9d-g) as well as by

decreased levels of cholesterol and triglycerides in plasma (Figure 4.9h). These results correlated with improved fitness of aged mice, which displayed enhanced exercise capacity and strength (Figure 4.9i,j). Notably, these effects on fitness and metabolism could be observed by day 20 post-infusion and were maintained up to 5 months post-treatment. Importantly, treatment with the uPAR CAR Ts in aging did not result in any obvious comorbidities with the mice presenting no changes in body weight or temperature, or secretion of cytokines associated with cytokine release syndrome (data not shown). In addition, whole body autopsy performed by trained veterinary pathologists at MSKCC 20 days post CAR Ts injection did not reveal any markers of organ damage (data not shown).

Overall, these initial results suggest that uPAR CAR Ts are safe and effective in targeting senescent cells in aging and they are able to improve the fitness and metabolic healthspan of aged mice.

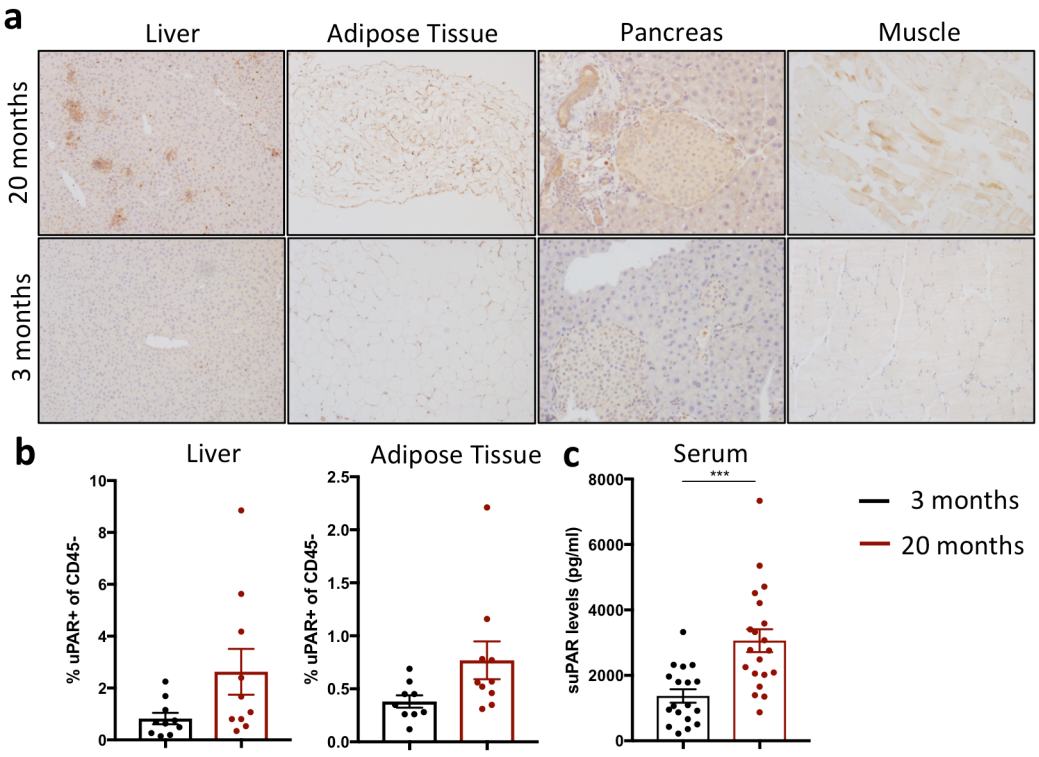

Figure 4.8. uPAR is upregulated in aging. (a) uPAR expression by immunohistochemistry in muscle, gonadal adipose tissue, liver and endocrine pancreas of 20 and 3 months old Bl/6 mice. **(b)** Surface uPAR expression on non-immune cells ($CD45^-$) in the gonadal adipose tissue and liver of 20 and 3 months old Bl/6N mice. **(c)** Serum levels of suPAR in 20 and 3 months old Bl/6N mice.

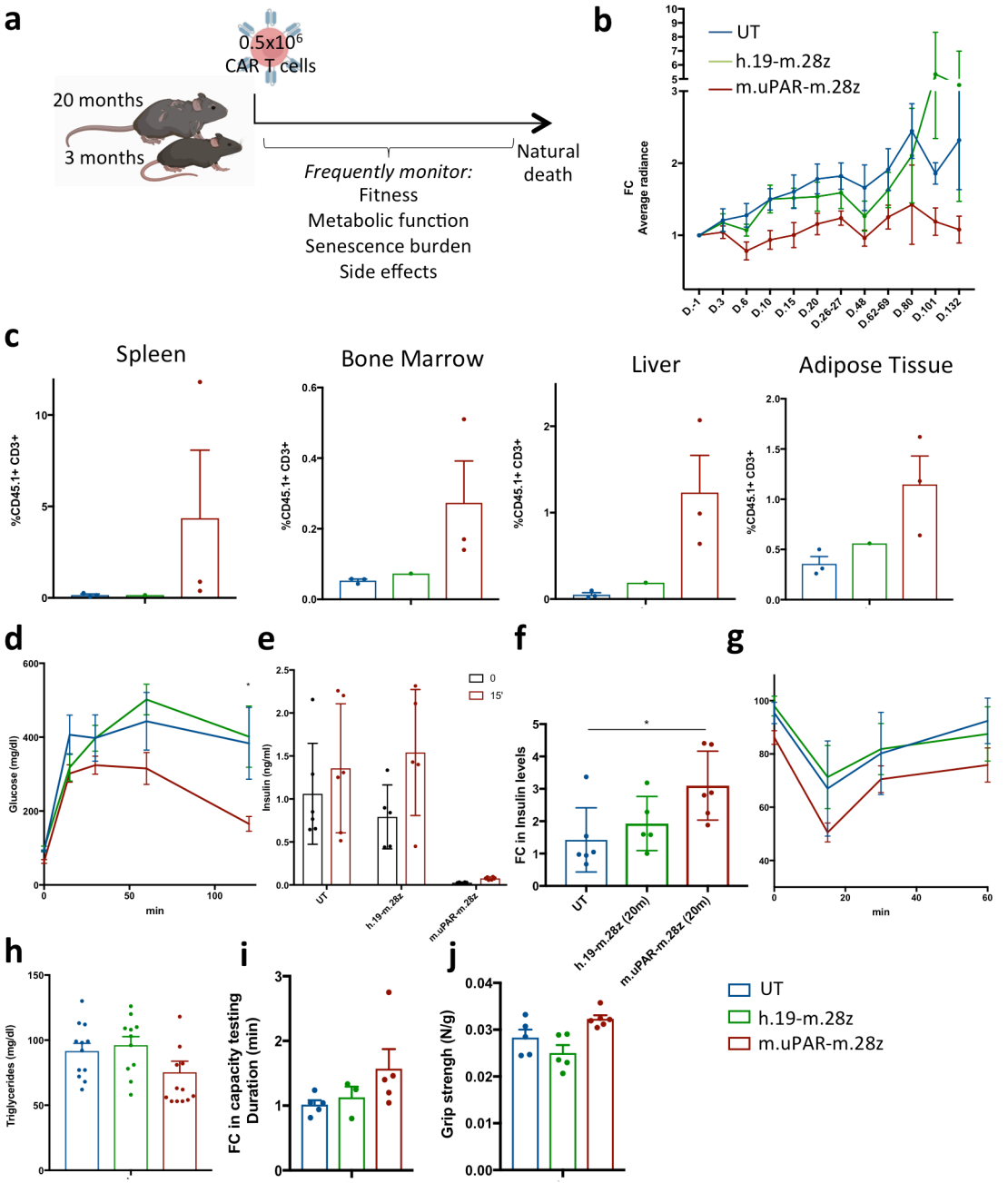

Figure 4.9. Senolytic uPAR CAR T cells are effective in natural aging. (a) Experimental scheme. **(b)** Fold change in the levels of luciferase in 13 months old $p16^{Luc}$ mice after treatment with $0.5x10^6$ m.uPAR-m.28z or h.19-m.28z CAR Ts or untransduced T cells. **(c)** Percentage of CAR Ts or untransduced T cells in spleen, bone marrow, liver or gonadal adipose tissue in 20 months old Bl/6 mice 2.5months after infusion. **(d)** Glucose tolerance testing 2.5 months after treatment in the 20 months old mice. **(e)** Basal levels of insulin and 15 minutes after administration of glucose (2g/kg) **(f)** fold change in insulin levels 15 minutes after administration of glucose (2g/kg) in 20 months old Bl/6 mice 2.5months after administration of CAR Ts or untransduced T cells. **(g)** Insulin tolerance test 2.5 months after treatment in the 20 months old mice. **(h)** Levels of triglycerides in plasma 2.5 months after treatment in the 20 months old mice. **(i)** Fold change in capacity testing 4 months after treatment in the 20 months old mice. **(j)** Grip strength 4 months after treatment in the 20 months old mice.

4.3.-Discussion

Our results provide proof-of-principle of the therapeutic potential of senolytic CAR T cells in senescence-associated pathologies. Indeed additional work is needed and future iterations could target other cell surface molecules specific to particular senescence contexts, incorporate 'safety switches (Paszkiewicz et al., 2016)'(Gargett and Brown, 2014) or combinatorial strategies to maximize efficacy while minimizing side-effects (Gargett and Brown, 2014; Sadelain et al., 2017). Nonetheless, these initial results open the field to a new senolytic approach. Beyond fibrosis, senescence has been linked to many disorders of chronic tissue damage associated with aging such as severe atherosclerosis, diabetes, or osteoarthritis consequently, senolytic CAR T cells may have broad therapeutic potential.

The fact that uPAR is upregulated on the surface of senescent cells in physiological aging and that senolytic CAR T cells are effective in this setting could potentially allow for studies that address several bottlenecks in the study of cellular senescence in aging:

First, by using uPAR as a surface marker of senescence we could, in an unprecedented manner, isolate senescent cells from *in vivo* models of aging and characterize their molecular program. Understanding the peculiarities of the senescence program in aging versus other settings of senescence would help us to better understand the mechanisms underlying their accumulation in aging and to tailor strategies to target these cells. This research is particularly relevant because most previous studies characterizing senescent cells have employed only models of senescence in young organisms, omitting age as an additional key variable in senescence despite the fact that most senescence-associated diseases occur in elderly individuals. In addition, it would also enable precise intravital imaging studies to understand the dynamics of senescent cells in vivo.

Second, by using cellular therapy to target senescent cells *in vivo*, we generate a versatile tool for the effective elimination of senescent cells in models of aging. They could be used to rapidly perform functional studies to understand the contribution of senescent cells to the aging phenotypes without extensive breeding and aging of mouse colonies. The flexibility of cellular therapy will allow us to optimize target, CAR design, dose and timing to the different experimental needs providing a valuable resource to streamline aging studies.

Finally, senolytic CAR T cells not only eliminate senescent cells, but could also have the potential to modulate the endogenous immune system, “retraining” it to target senescent cells providing a two-fold therapeutic advantage through CD40L CAR designs (Kuhn et al., 2019). Of course, our work will also study and optimize the safety profile of using such approaches in aged organisms. This information in turn will be highly relevant not only for the senescence field but also for cellular engineering. CAR T cells are used in elderly cancer patients but to date little efforts have been focused in understanding how their activities might be differentially regulated in this setting and tailoring them for aging.

CHAPTER 5

SENOGENIC-SENOLYTIC APPROACHES FOR THE TREATMENT OF SOLID TUMORS

5.1.-Introduction

Initially described as a tumor suppressive mechanism that is ultimately bypassed by tumors, induction of senescence in established tumors can lead to potent tumor regressions ((Wang et al., 2019a; Xue et al., 2007). On one hand, reintroducing senescence leads to cell cycle arrest of the tumor cells halting tumor growth. On the other, induction of senescence has been shown to lead to the recruitment of immune cells through cytokines secreted by the SASP ((Ruscetti et al., 2018; Tasdemir et al., 2016)) as well as by modulation of the vasculature ((Ruscetti et al., 2020)). These recruited immune cells target the senescent cells and potentially could restore targeting to the proliferating neighbor cells.

Interestingly, induction of senescence in tumors through conventional chemotherapeutic approaches has also been described to lead to tumor progression and metastasis (Demaria et al., 2017; Kawaguchi et al., 2021). Although this area still requires further investigation it is possible that failure to clear the senescent cells would lead to their deleterious accumulation and the generation of a chronic proinflammatory milleu that could mediate these effects (Figure 5.1a). A therapeutic possibility to avoid this would be combining senescence inducing therapies (senogenics) with potent senolytic strategies to ensure senescent cell clearance (Figure 5.1b). In this context, we set out to explore whether uPAR targeting CAR T cells could be effective senolytics.

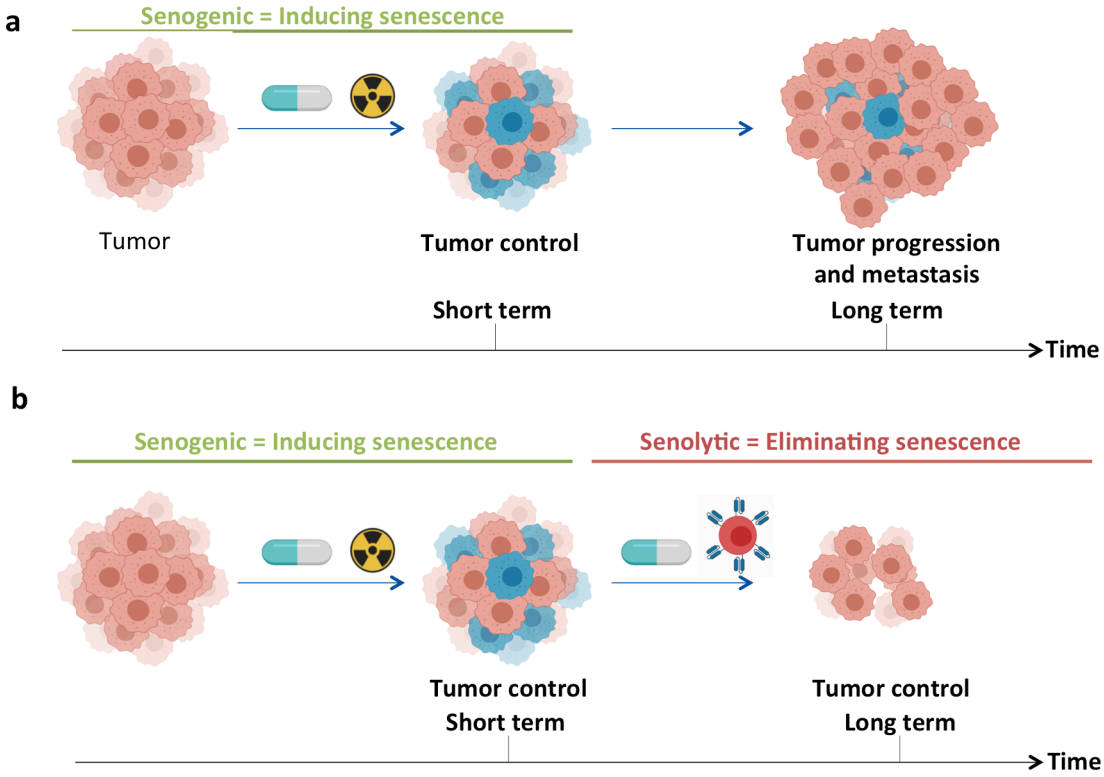

Figure 5.1. Rationale for senogenic-senolytic therapeutic approaches in cancer. **(a)** Induction of senescence in tumors (senogenic approaches) can lead to growth arrest and tumor control. Failure of clearance of the senescent cells leads to their accumulation and the constant secretion of SASP factors that can ultimately promote the proliferation of neighbor proliferating cells. **(b)** Combining senogenic approaches with senolytic strategies to eliminate the senescent cells could potentially prove an effective therapeutic avenue.

5.2.-Results

5.2.1.-Therapeutic potential of senolytic CAR T cells for the treatment of lung cancer.

As described in chapter 3, uPAR is highly upregulated in a model of *Kras*^{G12V}*;p53*$^{-/-}$ driven lung adenocarcinoma upon senescence induction with combined MEK and CDK4/6 inhibitors. Induction of senescence in this model has been shown to lead to senescent tumor cell clearance by endogenous NK cells (Ruscetti et al., 2018). We wondered however, if it could be possible to further improve the survival benefit by combining senescence induction with senogenic CAR T cells as uPAR was highly upregulated in these senescent cells. To test this concept, mice harboring orthotopic KP lung adenocarcinomas were treated with combined MEK and CDK4/6 inhibitors followed by administration of either uPAR- or CD19-specific CAR T cells or UT T cells (Figure 5.2a). Treatment with uPAR-targeted CAR T cells significantly prolonged survival without eliciting signs of toxicity (Figure 5.2b-d). Lungs harvested from these mice showed a substantial decrease in senescent tumor cells accompanied by enhanced infiltration of adoptively transferred $CD4^+$ and $CD8^+$ T cells expressing activation markers (Figure 5.2e,f). In addition to confirming the senolytic properties of uPAR-directed CAR T cells, these results point towards the potential of combinatorial strategies using senolytic CAR T cells for the treatment of solid tumors.

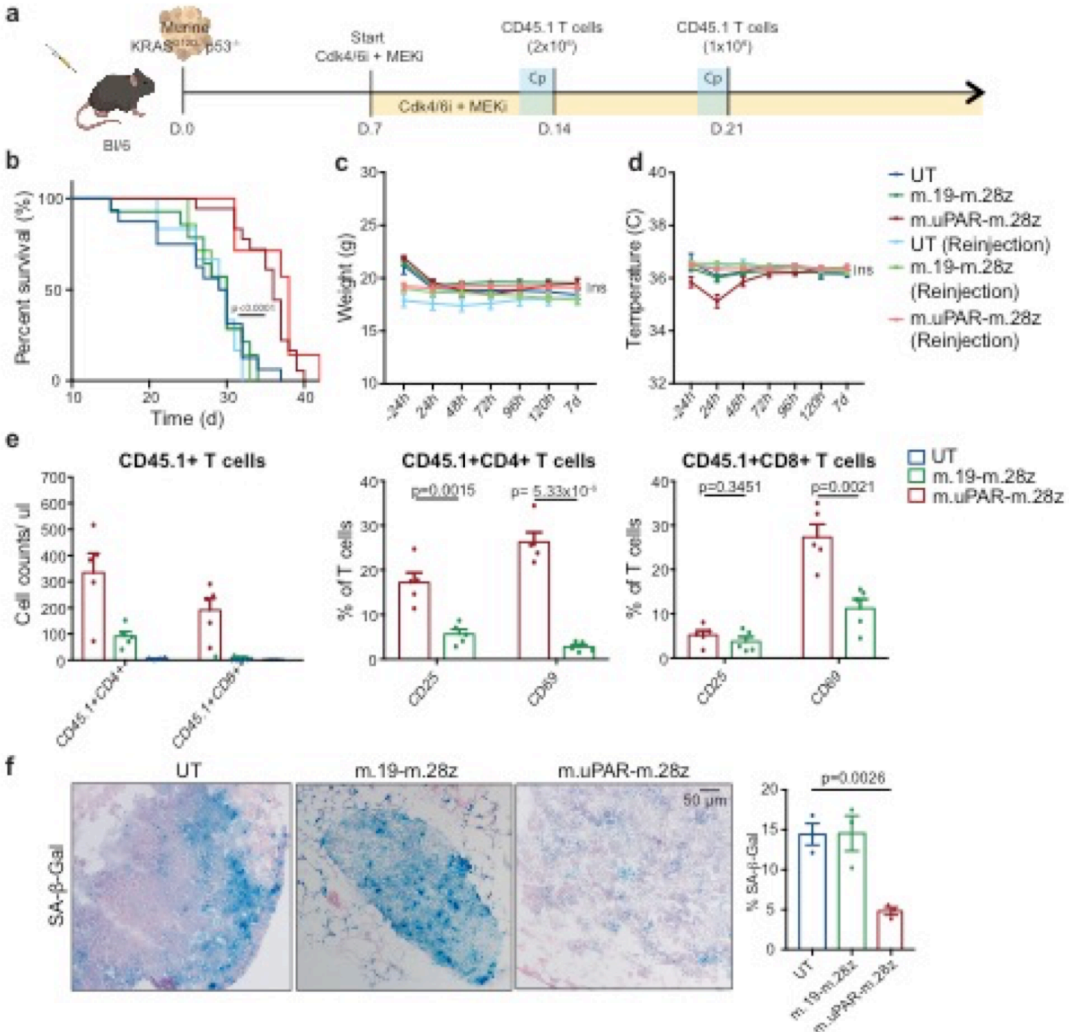

Figure 5.2. Senolytic CAR T cells target senescent cells in a Kras^{G12D}-driven model of lung cancer. (a) Experimental layout: C57BL/6N mice were tail vein injected with 10.000 Kras^{G12D};p53$^{-/-}$ cells. Treatment with combined MEK (1mg/kg body weight) and Cdk4/6 inhibitors (100 mg/kg body weight) was initiated 7 days later, followed by adoptive transfer of 2x10^6 CD45.1+ T cells (m.uPAR-m.28z CAR T cells, m.19-m.28z CAR T cells or untransduced (UT) T cells) one week later. A subset of mice received a second infusion of either 1x10^6 m.uPAR-m.28z CAR T cells, m.19-m.28z CAR T cells or UT T cells 7 days after the first T cell injection. Images of the mouse, tumor cells and CAR T cells were created with Biorender.com. **(b)** Kaplan-Meier curve showing survival of mice and log-rank (Mantel Cox) test. Results of 2 independent experiments (UT: n=16, m.19-m.28z: n=14, m.uPAR-m.28z: n=18, UT reinjection: n=6, m.19-m.28z reinjection: n=7 and m.uPAR-m.28z reinjection: n=7 mice). **(c-d)** Weight (g) **(c)** and temperature (C) **(d)** as measured 24h before and at different time points after CAR T cell infusion. P values refer to the comparison between UT and m.uPAR-m.28z injected mice at 48h (weight: p=0.9329; temperature: p=0.1534). Results of 1 independent experiment (UT: n=5, m.19-m.28z: n=5, m.uPAR-m.28z: n=8, UT reinjection: n=5, m.19-m.28z reinjection: n=7 and m.uPAR-m.28z reinjection: n=7 mice). **(e)** Cell counts of CD45.1+ T cells and expression of activation markers CD25 or CD69 (UT: n=4, m.19-m.28z: n=5, m.uPAR-m.28z: n=5 mice) on CD45.1+ T cells in the lungs of mice 7 days after administration of m.uPAR-m.28z, m.19-m.28z or UT T cells. **(f)** Representative SA-β-Gal

staining and quantification in the lungs of mice 7 days after treatment with m.uPAR-m.28z CAR T cells compared to mice treated with m.19-m.28z CAR T cells or UT T cells (n=3 mice per group). **(b)** Log-rank (Mantel Cox) test one-sided. **(c-g)** Data represent mean± SEM. Two-tailed unpaired Student's t-test.

5.2.2.-Therapeutic potential of senolytic CAR T cells in ovarian cancer.

In addition to being upregulated upon senescence induction, some tumors have been described to express high basal levels of uPAR, which have been hypothesized to be related to enhanced metastatic potential (Smith and Marshall, 2010). One of such tumor types is ovarian cancer (Wang et al., 2019b). Work in the Lowe laboratory by Stella Paffenholz and Josef Leibold led to the development of a mouse model of ovarian cancer with the genotypes *Myc;p53*$^{-/-}$ (MP) or *Myc;p53*$^{-/-}$*Brca*$^{+/-}$ (MPB). Cell lines derived from these tumors express high basal levels of uPAR (Figure 5.3a). To test the therapeutic potential of uPAR targeting CAR T cells in ovarian cancer we treated mice harboring orthotopic ovarian tumors resulting from intraperitoneal injection of MPB ovarian cell lines. Mice were intraperitoneally injected with 1.5x10^6 uPAR CAR T cells or untransduced T cells as controls. Treatment with the uPAR CAR T cells led to a significant survival advantage without signs of toxicity (Figure 5.3c-e).

A remaining question in our experiments was how the soluble factors secreted by senescent tumor cells affect the activity of senolytic CAR T cells. To try to explore this concept we exploited the fact that MPB ovarian tumors senesce in response to treatment with cisplatin (data not shown) without changing their already high expression of uPAR (Figure 5.3a). *In vitro* cytotoxicity assays suggested a stimulatory effect of the SASP on CAR T activity as CAR T cells presented higher killing activity at all effector:target ratios when co-cultured with senescent instead of proliferating cells (Figure 5.3b). Recent preliminary *in vivo* data however has failed to replicate the *in vitro* results with no statistically significant differences in the survival of mice treated with cisplatin and untransduced T cells or mice that received cisplatin and uPAR CAR T cells. Current efforts in the laboratory are focused on increasing the sample size as well as testing higher doses of uPAR CAR T cells. It could be possible however, that the secreted

factors are different *in vitro* than *in vivo* and/or that the tumor microenvironment differentially modulates CAR T activity *in vivo.*

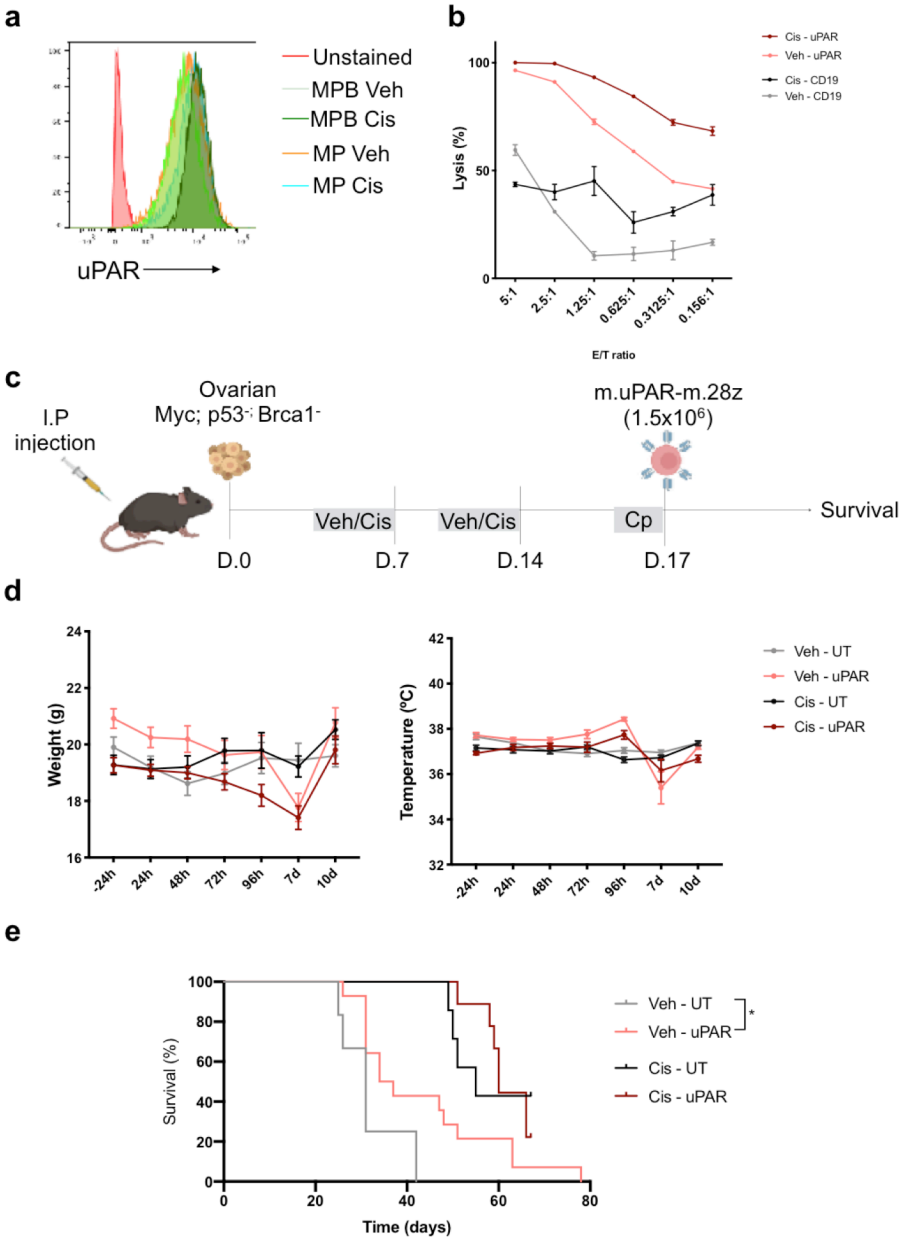

Figure 5.3. Therapeutic activity of uPAR CAR T cells in a Myc-driven model of ovarian cancer (a) Expression of surface uPAR on *Myc;p53*$^{-/-}$ (MP) or *Myc;p53*$^{-/-}$ *Brca1*$^{+/-}$ (MPB) cell lines treated with Vehicle (DMSO) or cisplatin (1μM) **(b)** Cytotoxic activity as determined by a 18hr-bioluminescence assay using Cisplatin or vehicle–treated MPB cells as targets and m.uPAR-m.28z or m.19-m.28z CAR T cells. **(c)** Experimental layout: C57BL/6N mice were tail vein injected with 10.000 MPC cells. Treatment with cisplatin (5mg/kg) or vehicle was initiated 7 days later and the mice received a second dose 14 days after cell injection followed 3 days later by adoptive transfer of 1.5x10^6 m.uPAR-m.28z CAR T cells or untransduced (UT) T cells. Images of the mouse, tumor cells and CAR T cells were created with Biorender.com. **(d)** Weight (g) and temperature (C) **(d)** as measured 24h before and at different time points after CAR T cell infusion **(e)** Kaplan-Meier curve showing survival of mice and log-rank (Mantel Cox) test one-sided. Results of 2 independent experiments (UT-vehicle: n=13, m.uPAR-m.28z vehicle: n=14, UT-cisplatin: n=10, m.uPAR-m.28z cisplatin: n=10)

5.2.3.-Development of Electroporation-Based Genetically Engineered Mouse Models (EPO-GEMMs):

Owing to their ability to capture tumor development in the complexity of the whole organism, genetically engineered mouse models (GEMMs) have proven to be a valuable tool for understanding genotype-phenotype relationships or evaluating new therapeutic concepts like senogenic-senolytic approaches in a range of tumor types. However, due to the cost and waste of intercrossing various germline strains, traditional GEMMs are time-consuming and expensive, making it difficult to model and interrogate the spectrum of tumor genotypes that exist in patients or conduct large-scale preclinical studies (Leushacke et al., 2017; Seidlitz et al., 2019; Till et al., 2017).

To address these issues, Josef Leibold, a postdoc of the Lowe lab devised a method to somatically introduce cancer predisposing lesions or other genetic elements into murine tissues using electroporation, thereby producing Electroporation-based Genetically Engineered Mouse Models (EPO-GEMMs) (Leibold et al., 2020; Seehawer et al., 2018). In this approach, transposon-based vectors encoding cDNAs or CRISPR/Cas9 constructs targeting endogenous genes are introduced into the tissue following survival surgery followed by a brief electric pulse, where they are taken up by a subset of cells. In circumstances where a particular lesion or combination of lesions provides a selective advantage, focal tumors arise at the electroporation site. This approach was initially successfully developed in prostate tumors (Leibold et al., 2020). When I joined the Lowe lab, we wondered whether it could potentially be used to model other malignancies that were severily understudied such as gastric cancer and, between Josef Leibold and later Kaloyan Tsanov, we started to develop a EPO-GEMM approach to model gastric cancer.

Gastric cancer is the fourth leading cause of cancer-associated deaths and the fifth most commonly diagnosed cancer worldwide (Sung et al., 2021). While localized disease can be successfully treated, the survival rate of gastric cancer patients drops dramatically in the advanced and especially at the metastatic stages (Ajani et al., 2016; Smyth et al., 2020; Verdecchia et al., 2007). Despite recent advances in our understanding of the molecular features of this cancer, effective treatment strategies are currently lacking, particularly for patients with metastatic disease (Ajani et al., 2017; Wagner et al., 2017).

Genome sequencing studies have classified gastric cancer into four major genetic subtypes defined by: (1) chromosomal instability (CIN); (2) genomic stability (GS); (3) microsatellite instability (MSI); and (4) Epstein-Barr Virus (EBV) infection (Cristescu et al., 2015; Huang et al., 2018; Wang et al., 2014). The CIN tumor subtype is the largest, and is characterized by *TP53* mutations and a high frequency of copy number alterations (CNAs) targeting recurrently gained and lost genomic regions (Cancer Genome Atlas Research, 2014). In contrast, tumors of the GS subtype show far fewer chromosomal aberrations and are devoid of *TP53* mutations, rather harboring alterations in *CDH1* or the Wnt signaling pathway. Not only do CIN and GS tumors display distinct mutational profiles, but they also differ in their histopathology, showing prominent features of intestinal differentiation or diffuse histological features, respectively (Lauren, 1965). The MSI subtype is defined by the presence of microsatellite instability (MSI) and mutations in mismatch repair genes such as *MLH1* or *MSH2*. Presumably due to their increased mutational load and potential for neoantigen production, these tumors elicit a T cell-dominated immune response (Germano et al., 2017; Le et al., 2017) and frequently respond to immune checkpoint blockade (Chao et al., 2021; Kim et al., 2018; Kwon et al., 2021; Le et al., 2017; Le et al., 2015). Finally, the EBV tumor subtype is a uniquely different entity that is characterized by alterations in the PI3K/AKT signaling pathway

(Cancer Genome Atlas Research, 2014; Liang et al., 2014), and can display both a diffuse and intestinal histology (Tavakoli et al., 2020). This subtype also frequently responds to immunotherapy (Panda et al., 2018). Interestingly, mutational gains and amplifications of the *MYC* gene are associated with early progression of intestinal metaplasia to gastric cancer and can be found in all gastric cancer subtypes (Cancer Genome Atlas Research, 2014; Huang et al., 2018).

To generate gastric cancer EPO-GEMMs, we developed a survival surgery technique coupled with direct tissue electroporation to deliver genetic elements to the murine stomach epithelium. A transposase-transposon vector pair was used to express a defined oncogene and a plasmid co-expressing Cas9 with an sgRNA to knock out a tumor suppressor gene of interest (Figure 5.4a). Since *MYC* is a potent oncogene that is frequently amplified across gastric cancers (Cancer Genome Atlas Research, 2014; Huang et al., 2018), we used a transposon vector containing human *MYC* cDNA as the universal oncogene, and adapted sgRNAs to target different tumor suppressor genes in accordance with their mutation in distinct subtypes of gastric cancer (Figure 5.4b).

We initially first set out to develop a model of the most common subtype observed in patients, CIN gastric cancer, which is characterized by a high frequency of *TP53* mutations (Cancer Genome Atlas Research, 2014; Cristescu et al., 2015). The *MYC* transposon-transposase system was combined with a Cas9-sgRNA vector targeting *Trp53* (hereafter referred to as *p53*), to recapitulate a genotype commonly seen in patients (Ding et al., 2018) (Figure 5.4b). Mice electroporated with all three plasmids consistently developed lethal tumors (90% penetrance; 45 day medium survival) that harbored the predicted disruptions of the *p53* locus (Figure 5.5a). In contrast, mice electroporated with either the *MYC* or Cas9-sgp53 vector alone did not develop tumors

within a year of follow-up (Figure 5.5a). Histologically, tumors displayed a mixture of well-differentiated adenocarcinoma, representing the intestinal phenotype according to the Lauren classification (Lauren, 1965), and poorly differentiated gastric carcinoma at late stage (Figure 5.5c). The well-differentiated areas expressed E-cadherin, cytokeratin-8 (CK8), high levels of the proliferation marker Ki67, and partially stained positive for the parietal cell marker H^+/K^+ ATPase, in accordance with human CIN gastric tumors.

Next, we proceeded to model the GS subtype of gastric cancer. Since human GS tumors frequently harbor alterations in *CDH1* (encoding E-cadherin) and/or WNT pathway genes (Figure 5.4b), we replaced the *p53* sgRNA with an sgRNA targeting *Cdh1* or *Apc*. Delivery of the MYC-sgCdh1 or MYC-sgApc configurations to the gastric epithelium consistently produced tumors with a median survival of 68 and 44 days post-electroporation, respectively (Figure 5.5b). Histological characterization of the *MYC-Apc*$^{-/-}$ tumors revealed an undifferentiated histology while largely retaining expression of the epithelial markers E-cadherin and CK8, and partially stained positive for H^+/K^+ ATPase, as seen in human gastric cancer (Figure 5.5d). On the other hand, the *MYC-Cdh1*$^{-/-}$ tumors displayed undifferentiated histology and, as expected, showed a complete absence of E-Cadherin expression (data not shown). Interestingly, this diffuse undifferentiated histopathology was remarkably similar to focal regions of advanced CIN tumors that appeared to dedifferentiate and also became E-cadherin negative.

To molecularly characterize the CIN and GS EPO-GEMM tumors, we performed RNA and whole-genome sequencing of *MYC-p53*$^{-/-}$, *MYC-Apc*$^{-/-}$, and *MYC-Cdh1*$^{-/-}$ tumors. Importantly, *MYC-p53*$^{-/-}$ but not *MYC-Apc*$^{-/-}$ or *MYC-Cdh1*$^{-/-}$ tumors harbored recurrent genomic rearrangements that showed synteny to their human counterparts, consistent with the CIN subtype of human gastric cancer (Figure 5.5e-g). This was accompanied by

relative depletion of p53 signatures at the transcriptional level in *MYC-p53*$^{-/-}$ tumors, providing a further validation of the molecular fidelity of EPO-GEMM tumors to their corresponding human subtype (Figure 5.5h) (Cancer Genome Atlas Research, 2014). Taken together, the above data establish gastric cancer EPO-GEMMs as fast and flexible models that recreate fundamental histological and molecular features of the CIN and GS genetic subtypes of the human disease.

Alterations in DNA mismatch repair genes are frequently found in patients and lead to microsatellite instability (MSI) gastric cancer, a subtype that has not been produced using traditional GEMMs (Figure 5.4b) (Cancer Genome Atlas Research, 2014; Cristescu et al., 2015). To generate such models, we combined the *MYC* transposon-transposase system with a CRISPR vector targeting both *p53* and the mismatch repair gene *Msh2*. This approach allows for direct comparison of MSI (*MYC; p53*$^{-/-}$*; Msh2*$^{-/-}$) and MSS (*MYC; p53*$^{-/-}$) gastric cancers that harbor identical driver genes except for *Msh2* loss. Consistent with the less aggressive nature of MSI compared to MSS tumors in human gastric cancer patients, the median survival of mice electroporated with *Msh2* sgRNAs was longer compared to MP controls (53 vs. 45 days, respectively) (Figure 5.6a). Importantly, despite this extended survival, *Msh2* disruption appeared to confer a selective advantage during tumorigenesis, as the resulting tumors harbored genetic alteration of the *Msh2* locus, lacked Msh2 expression in the tumor, and the combination of *MYC* overexpression and *Msh2* disruption alone also led to tumor development (Figure 5.6b).

Disruption of DNA repair pathway genes leads to an overall increase in genetic alterations (Germano et al., 2017; Lengauer et al., 1998), including a particular base substitution signature that has been reported in patients with mismatch repair-deficient

cancers (Alexandrov et al., 2013). Accordingly, whole-exome sequencing of EPO-GEMM tumors revealed a significantly higher amount of genetic alterations in MSI vs. MSS tumors, and a base substitution signature that closely resembled the one seen in patients with MSI cancers (Figure 5.66c,d).

While genetic disruption of the mismatch repair pathway is a driver of gastric cancer, it also generates unique therapeutic vulnerabilities (Lord and Ashworth, 2012). In particular, the high mutational burden arising from microsatellite instability is thought to produce an increased level of neoantigens presented by MHC molecules and facilitate a T cell-mediated anti-tumor response (Germano et al., 2017; Mandal et al., 2019), thus rendering MSI gastric and colon cancers more responsive to immune-modulatory drugs (Andre et al., 2020; Chao et al., 2021; Kwon et al., 2021; Le et al., 2017). Interestingly, we did observe an overall increase of infiltrating $CD45^+$ and $CD3^+$ cells in MSI EPO-GEMMs compared to their MSS counterparts, yet this phenotype was heterogeneous within the MSI tumor population possibly reflecting the random process of generating immunogenic and non-immunogenic neoantigens (Figure 5.6.e). Moreover, a comparison of immune signaling pathways and infiltrates imputed from bulk RNA sequencing data of murine and human MSI vs. MSS tumors indicated strong correlation between human and mouse tumors (Figure 5.6f). MSI tumors were markedly enriched in signatures of most immune cell subtypes as well as inflammatory pathways, consistent with increased immune infiltration and an immune-stimulatory microenvironment (Figure 5.6f). Finally, treatment of MSI tumor-bearing mice with CTLA4 inhibitory antibodies led to a significant survival benefit, while MSS tumors did not respond to this checkpoint blockade therapy (Figure 5.6g). Overall, these data show that MSI EPO-GEMMs mimic human MSI gastric cancers on the molecular and microenvironmental levels, including their therapeutic susceptibility to immune checkpoint blockade.

Overall, these data illustrate the power of EPO-GEMMs to faithfully model different tumor types in this case, of an understudied disease like gastric cancer. The flexibility provided by EPO-GEMMs could provide an ideal platform to gain a better understanding of the determinants of senescence restoration and immune surveillance in solid tumors.

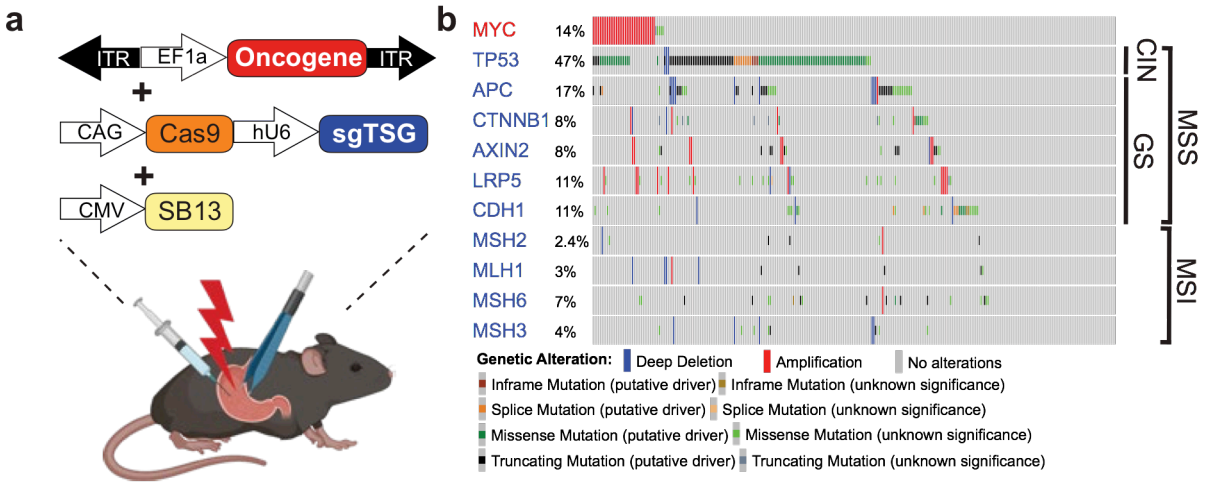

Figure 5.4. Somatic induction of oncogenic lesions by *in vivo* electroporation of the stomach. (a) Schematic of the EPO-GEMM of gastric cancer. **(b)** OncoPrint displaying frequent mutations in gastric cancer patient samples isolated from primary tumors (TCGA dataset). CIN (Chromosomal instability), GS (Genomic stability), MSS (Microsatellite stable), MSI (Microsatellite instable).

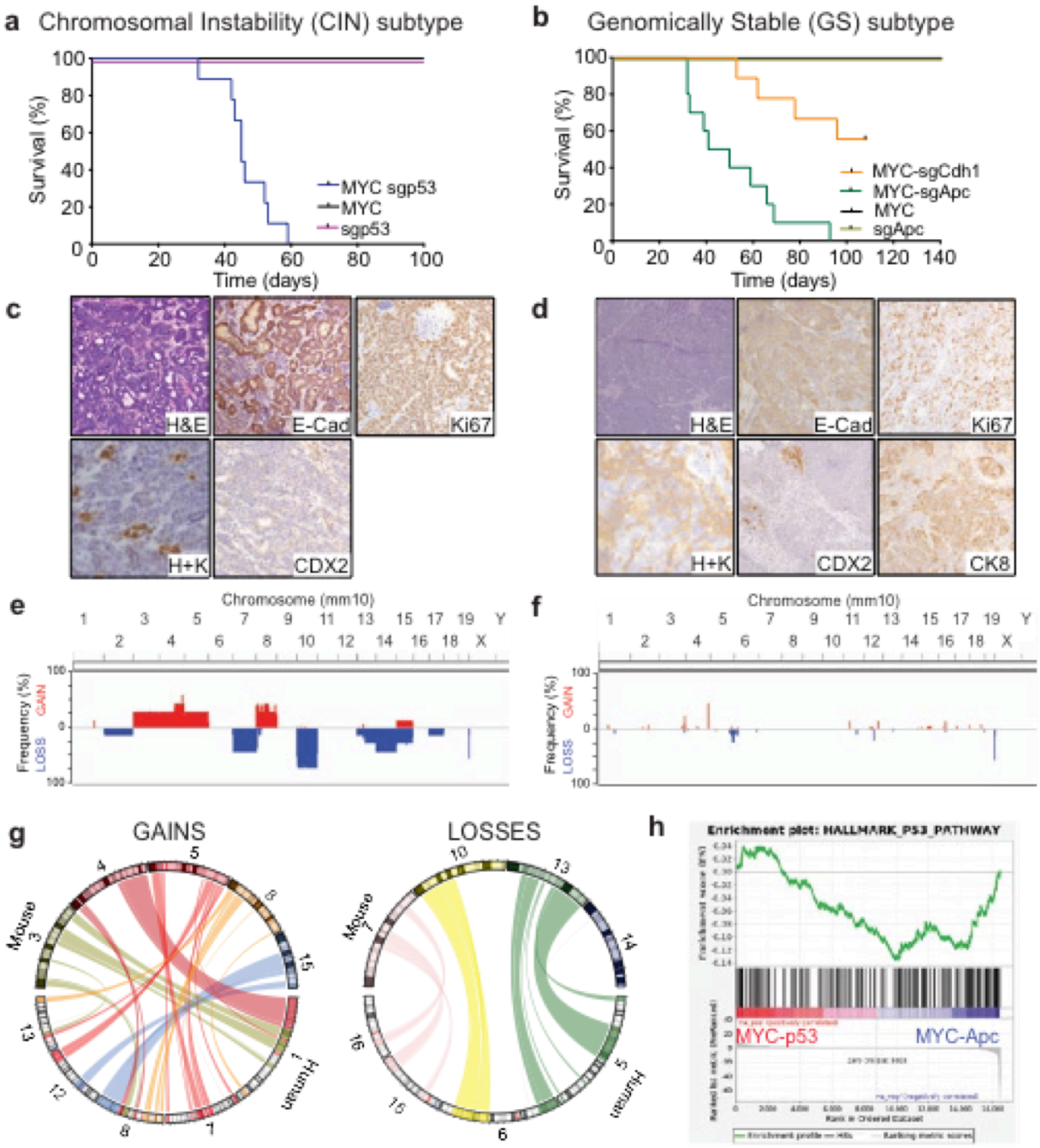

Figure 5.5. Engineering CIN and GS gastric cancer de novo using EPO-GEMMs (a) Kaplan-Meier survival curve of mice electroporated with the *MYC* transposon vector and a Sleeping Beauty transposase (MYC, black) or a CRISPR/Cas9 vector targeting p*53* (sgp53, red) or with the *MYC* transposon vector and a Sleeping Beauty transposase and a CRISPR/Cas9 vector targeting *p53* (MYC sgp53,blue).**(b)** Kaplan-Meier survival curve of mice electroporated with the *MYC* transposon vector and a Sleeping Beauty transposase (MYC, black) or a CRISPR/Cas9 vector targeting *Apc* (sgAPC, grey) or with the *MYC* transposon vector and a Sleeping Beauty transposase and a CRISPR/Cas9 vector targeting *Apc* (MYC sgAPC,green) or with the *MYC* transposon vector and a Sleeping Beauty transposase and a CRISPR/Cas9 vector targeting *Cdh1* (MYC sgCdh1,orange). **(c)** and **(d)** Representative immunohistochemistry of CIN (c) and

GS (d) tumors. **(e)** and **(f)** Frequency plot of CNV analysis of CIN (e) and GS (f) EPO-GEMM tumors. **(g)** Circos plots of genomic rearrangements in murine EPO-GEMM CIN tumors compared to human gastric cancer (TCGI dataset) **(h)** GSEA for p53 signaling pathway of MP tumors.

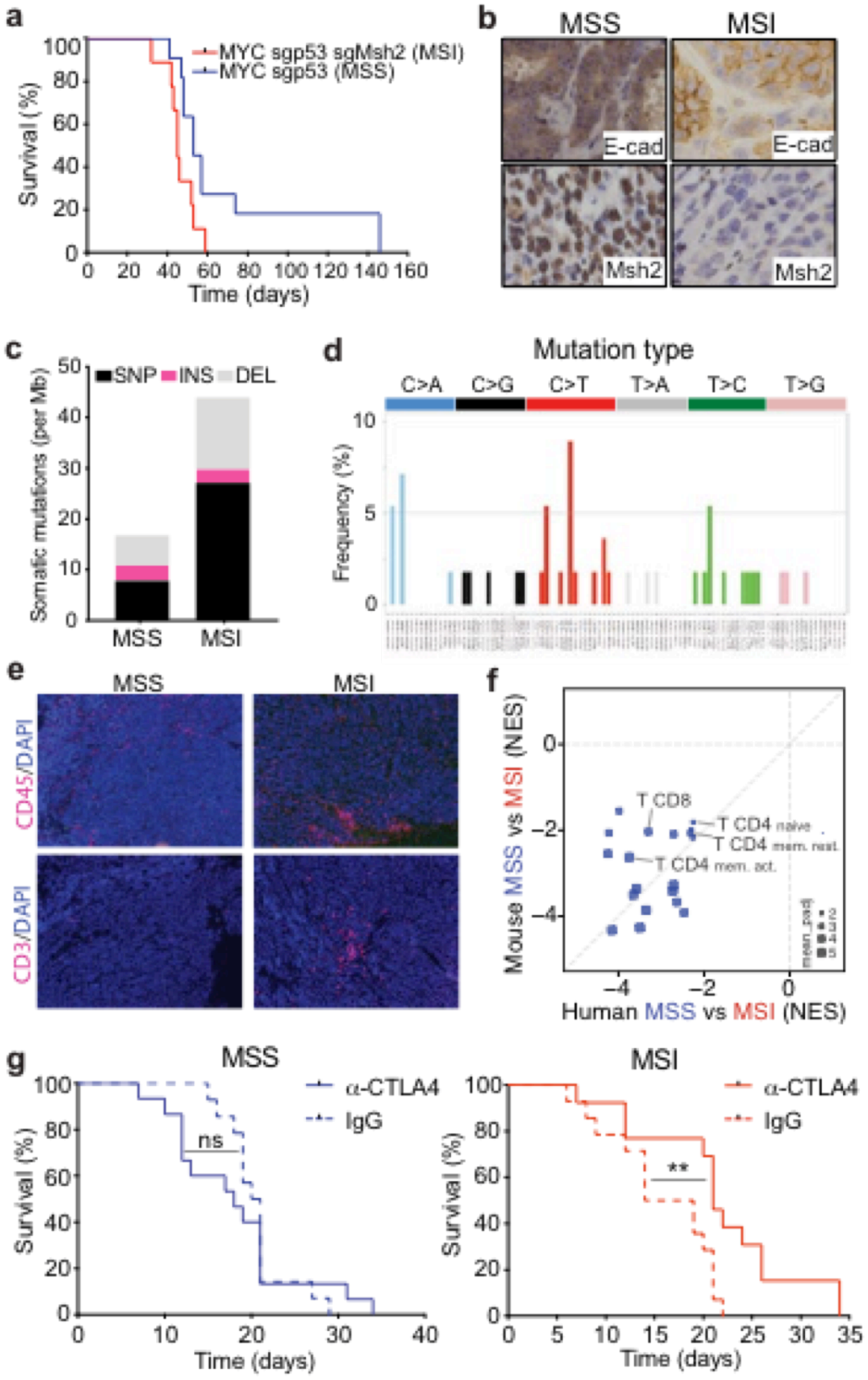

Figure 5.6. Engineering MSI gastric cancer de novo using EPO-GEMMs. (a) Kaplan-Meier survival curve of mice electroporated with the *MYC* transposon vector and a Sleeping Beauty transposase and a CRISPR/Cas9 vector targeting p*53* (MSS; blue) or with the *MYC* transposon vector and a Sleeping Beauty transposase and a CRISPR/Cas9 vector targeting *p53* and Msh2 (MSI; red). **(b)** Representative immunohistochemistry of E-cadherin (E-cad) and Msh2. **(c)** Number of somatic

mutations per Mb (single nucleotide polymorphisms, insertions or deletions) present in primary MSS and MSI tumors. **(d)** Mutational signature of the mutations presented in (c) for MSI tumors. **(e)** Immunofluorescence for CD45 and CD3 in MSS and MSI primary tumors. **(f)** Comparison of immune signaling pathways and infiltrates imputed from bulk RNA sequencing data of murine and human MSI vs. MSS tumors. **(g)** Kaplan-Meier survival curve of mice harboring MSS or MSI tumors treated with IgG control or anti-CTLA4**.**

5.3.-Discussion

The field of senogenic-senolytic strategies is rapidly expanding. There are still however, key fundamental biology questions that should be explored to optimize these approaches such as: 1) what are the key determinants of senescent cell immune surveillance? Are these effects cell type, or genotype dependent? 2) How does inducing senescence in the microenvironment vs in the tumor cells impact the final outcome? 3) what is the impact of inducing senescence on already established metastasis? The flexibility of genotypes and hosts provided by EPO-GEMMs could make it an ideal platform to explore some of these questions.

Regarding senolytic CAR T cells, our initial results support the notion that CAR T cells can effectively target uPAR positive tumors and provide therapeutic benefit in cancer adding to the growing repertoire of senolytic strategies in cancer. A key remaining question to explore is how do senescent cells modulate the activity of CAR T cells through their SASP. Many of these secreted factors are highly immunomodulatory and thus the effect of the SASP on the infiltrating senolytic CAR T cells warrants further study. In addition, given the heterogeneous composition of the SASP based on cell type and trigger of senescence (Hernandez-Segura et al., 2017) it is likely that these effects are context dependent. Gaining a better understanding of this regulation could lead to the generation of enhanced CAR designs that could counteract inhibitory or augment activating components of the SASP.

CHAPTER 6

DISCUSSION

6.1.-Concluding Remarks

In this work we study the expression of surface molecules on senescent cells. Our findings confirms previous reports (Hernandez-Segura et al., 2017) describing the heterogeneity of the senescent cell transcriptome but identifies for the first time uPAR as a protein preferentially upregulated on the surface of senescent cells. In addition, we show that owing to its cleavage and secretion, suPAR could potentially serve as a plasma biomarker of senescence burden.

Furthermore, our results show the feasibility of engineering CAR T cells that are selective against a specific cellular program, in this case senescence. CAR T cells directed against uPAR are able to infiltrate areas of senescence and efficiently target senescent cells without major toxicities. Therefore this work provides proof-of-principle of the therapeutic potential of senolytic CAR T cells in senescence-associated diseases such as liver fibrosis, age-related metabolic dysfunction and cancer.

Overall these findings have major relevance from both a therapeutic perspective but also from a pure basic biology point of view.

6.2 Implications for basic senescence biology and future directions

A major limitation in the field of senescence has been the lack of robust markers of this state. Historically, the field has only been able to identify senescent cells by using a combination of non-cell surface markers such as p16 or p21, assays for lysosomal SA-β-Gal activity, or the secretion of cytokines and chemokines as part of the SASP.

Identifying robust cell surface markers of senescence would allow us to, for the first time, isolate these cells from *in vivo* settings and study the molecular characteristics of the senescence program. While we expect that ours and others future work will identify additional surface markers beyond uPAR, this initial work makes it possible to already start isolating senescent cells from *in vivo* models by sorting uPAR-positive CD45-negative cells to isolate senescent cells excluding the uPAR positive immune populations. In addition, by using antibody-based approaches such as immunoPET, it could be possible now to perform intravital imaging studies to explore the dynamics of senescent cell induction and clearance *in vivo*.

In addition, by using cellular therapy to target senescent cells *in vivo*, we have generated a versatile tool for the effective elimination of senescent cells in models of senescence. They could be used to rapidly perform functional studies to understand the contribution of senescent cells to the phenotypes of cancer, aging-related disorders and aging itself. This could be particularly relevant in the setting of physiological aging where GEMMs that deplete $p16^{+}$ cells have shown that the accumulation of senescent cells is deleterious and that whole body elimination of these cells results in the amelioration of aging phenotypes (Baker et al., 2011; Xu et al., 2018). However, to date, there is little understanding about the contribution that senescent cells in different organs play in this phenotype; whether even if the net effect of eliminating all $p16^{+}$ cells is beneficial senescence in the context of aging could be favorable in certain cell types (Grosse et al., 2020), and whether certain senescent cell types are the major drivers of the observed deleterious effects. Answering these questions with the current technology in the field would require extensive breading of mice that would then have to be naturally aged consuming significant time and resources. Using double targeting senolytic CAR T cells that have been engineered to target cells expressing both uPAR as a marker of

senescence plus a second tissue specific marker would allow to deplete certain senescent populations without targeting the rest of senescent cells in the body. These studies would thus bypass the need to breed and then age GEMM mice as the CAR T cells could be administered in already aged WT mice. The flexibility of cellular therapy would allow us to optimize target, CAR design, dose and timing to the different experimental needs providing a valuable resource to streamline aging studies.

Regarding cancer, the development of our flexible, somatic EPO-GEMMs provides an ideal platform in which to harness uPAR and senolytic CAR T cells to better understand cancer senescence immune surveillance in future studies. By modeling different tumor genotypes in hosts with different levels of immune deficiency it could be possible to understand determinants of endogenous mechanism of immune surveillance. Potentially, these studies could be coupled with genetic screens. In addition, as an orthogonal approach it could be possible to utilize uPAR as a surface marker of senescence to allow the isolation and characterization of tumor senescent cells in models in which they are cleared and settings in which they are not targeted identifying molecular determinants of this effect. Knowledge derived from these studies will inform basic biology and will also potentially provide an opportunity to therapeutically restore immune surveillance through small molecule or antibody approaches. Regarding CAR T cells, this information could be used to enhance CAR design by generating “armed” CAR T cells that secrete specific cytokines that potentiate their activity or modified receptors that turn inhibitory signals into stimulatory ones (Sadelain et al., 2017) .

6.3.-Clinical Implications and future therapeutic directions

Our studies show the therapeutic activity of senolytic CAR T cells in preclinical models of chemically or diet induced liver fibrosis, age-dependent metabolic dysfunction, and

cancer. Given the contribution of senescent cells to multiple pathologies such as severe atherosclerosis, diabetes, osteoarthritis and neurodegenerative conditions, senolytic CAR T cells could have broad therapeutic applications. There are however, several aspects that should be studied before clinical trials.

First, our current senolytic CAR T cells target murine uPAR. Mouse uPAR and human uPAR share only 60% homology and the scFv of the anti mouse uPAR CAR does not cross-react with human uPAR. Ongoing efforts in the last year in collaboration with the Tri-institutional Discovery Institute and a external company (Abzena) have led to the development of several (19) monoclonal antibodies against human uPAR. The sequences of these scFvs have been used to engineer second generation 28z-based CAR T cells that have been tested *in vitro* to identify 4 highly specific and potent candidates. Future work is needed to test these constructs *in vivo* and to decide on the best CAR design.

Second, as with any new therapy it is imperative to characterize and understand side effects. The major toxicities observed with senolytic CAR T cells in immunocompetent mice relate to cytokine release syndrome (CRS). While these adverse effect can be treated with the concomitant administration of IL6R and IL1R inhibitors or completely avoided with the use of lower et effective CAR T doses, it is important to understand its pathophysiology. CRS results from cytokines (particularly IL6 and IL1) secreted by monocytes and macrophages that are recruited by the activity of the CAR T cells (Giavridis et al., 2018; Norelli et al., 2018). Since uPAR is expressed on a subset of monocytes and macrophages it is possible that the threshold to develop CRS could be lower with the uPAR CAR T cells if it gets triggered by engaging these uPAR positive

immune cells. Further work is needed to understand this as well as the phenotype of uPAR positive macrophages or monocytes. Curiously, macrophages and senescent cells share several markers/characteristics such as increased SA-B-Gal activity, phagocytic ability or expression of p16 (Hall et al., 2017; Tonnessen-Murray et al., 2019). Whether or not macrophages that are positive for these features are senescent or contribute to the deleterious effect of senescent cells has been controversial and additional work is needed (Childs et al., 2016; Hall et al., 2017). In any case, future strategies that could be employed to avoid targeting of immune cells by the senolytic CAR T cells could involve the use of AND/OR gate approaches (Srivastava et al., 2019) or, if identified, better surface targets that are not expressed on immune cells.

And additional consideration that warrants further study is the potential impact of senolytic CAR T cells on the function of the endogenous immune system. Previous studies on the CD19 CAR T have shown that they can not only directly target cells expressing their target antigen but can also stimulate endogenous tumor immune surveillance through several mechanisms such as by engaging conventional dendritic cell type 1 (cDC1) through CD40L-CD40 interaction which licenses cDC1 to secrete IL-12 to support $CD4^+$ T cell responses as well as to cross present antigens to endogenous $CD8^+$ T cells contributing alongside the CAR Ts to protective antitumor memory (Caux et al., 1994; Kuhn et al., 2019; Macatonia et al., 1995). Since the uPAR CAR Ts used in our aging studies were generated in CD45.1 mice and infused into aged 20 months old CD45.2 mice, we were able to perform flow cytometry in several organs and gain a preliminary insight into the effects of the uPAR CAR T cells in the endogenous immune system in aging. Interestingly, in this setting infusion of the uPAR CAR Ts led to an increase in the number of dendritic cells as well as endogenous $CD45.2^+$ $CD8^+$ T cells 20 days post infusion (Figure 6.1a,b). Furthermore, isolated $CD45.2^+$ T cells from aged

mice infused with either untransduced T cells or uPAR CAR T cells co-cultured with proliferating or senescent cells showed selected increased IFNγ production towards senescent cells in the uPAR CAR T treated groups (Figure 6.1c,d). These preliminary findings suggest that the uPAR CAR Ts could indeed be engaging dendritic cells and stimulating endogenous senescence immune surveillance. Future work is needed to confirm this effect, explore it *in vivo* (through uPAR negative senescent rechallenges) and to understand the mechanism. These studies will characterize the potential of senolytic CAR T cells in modulating the endogenous immune system, specially in the context of aging, and will guide new senolytic CAR designs that could improve *in vivo* potency in this setting. For example, the generation of uPAR CAR T cells that overexpress CD40L, or that secrete IL12 or IL18 (Kuhn et al., 2019; Yeku et al., 2017) could further potentiate the recruitment and activation of endogenous senescence reactive $CD8^+$ T cells. Ultimately, it would also be important to consider the long-term safety effects. On one hand such and engagement would contribute to senescent cell clearance possibly on the long term, on the other hand, it could be hypothesized that it could increase the risk of immune related adverse effects.

Finally, a highly relevant area that warrants further investigation pertains to the functional persistence of senolytic CAR T cells. Unlike tumor cells, senescent cells are constantly being generated in the organism, especially in the context of aging, which could potentially impact their persistence. The fact that in aging studies the observed improvements in fitness and metabolic profile are sustained up to 4 months after a single low dose of uPAR CAR T cells suggest a high persistence of the CAR T cells over time. Future work will include flow characterization of these cells over time as well as rechallenging experiments to test their functionality. Once the persistence of the current uPAR CAR T cells is characterized and understood in the different settings it would be

possible to consider whether such persistence is wanted/needed or not and tailor both CAR T cell dose and CAR designs accordingly. Strategies to further extend persistence could involve the use of CAR designs that have been shown to lead to enhanced functional persistence such as CARs harboring 4-1BB instead of 28z as costimulatory domain or the “IXX” CARs recently developed by the Sadelain lab that harbor only a single functional ITAM in their CD3ζ activation domain (Feucht et al., 2019). Another potential option could be to direct the uPAR-specific CAR to the endogenous T-cell receptor locus (TRAC) using a CRISPR/Cas9 mediated approach. Such an approach produces more uniform CAR expression in T cells as well as significantly higher T cell potency (Eyquem et al., 2017) and may extend CAR therapy to allogeneic settings. Approaches to provide a safety backup to deactivate the CAR T cells in case of toxicity development include the incorporation of safety switches such as iCaspase-9 (iCasp9) (Gargett and Brown, 2014) or EGFRt (Paszkiewicz et al., 2016).

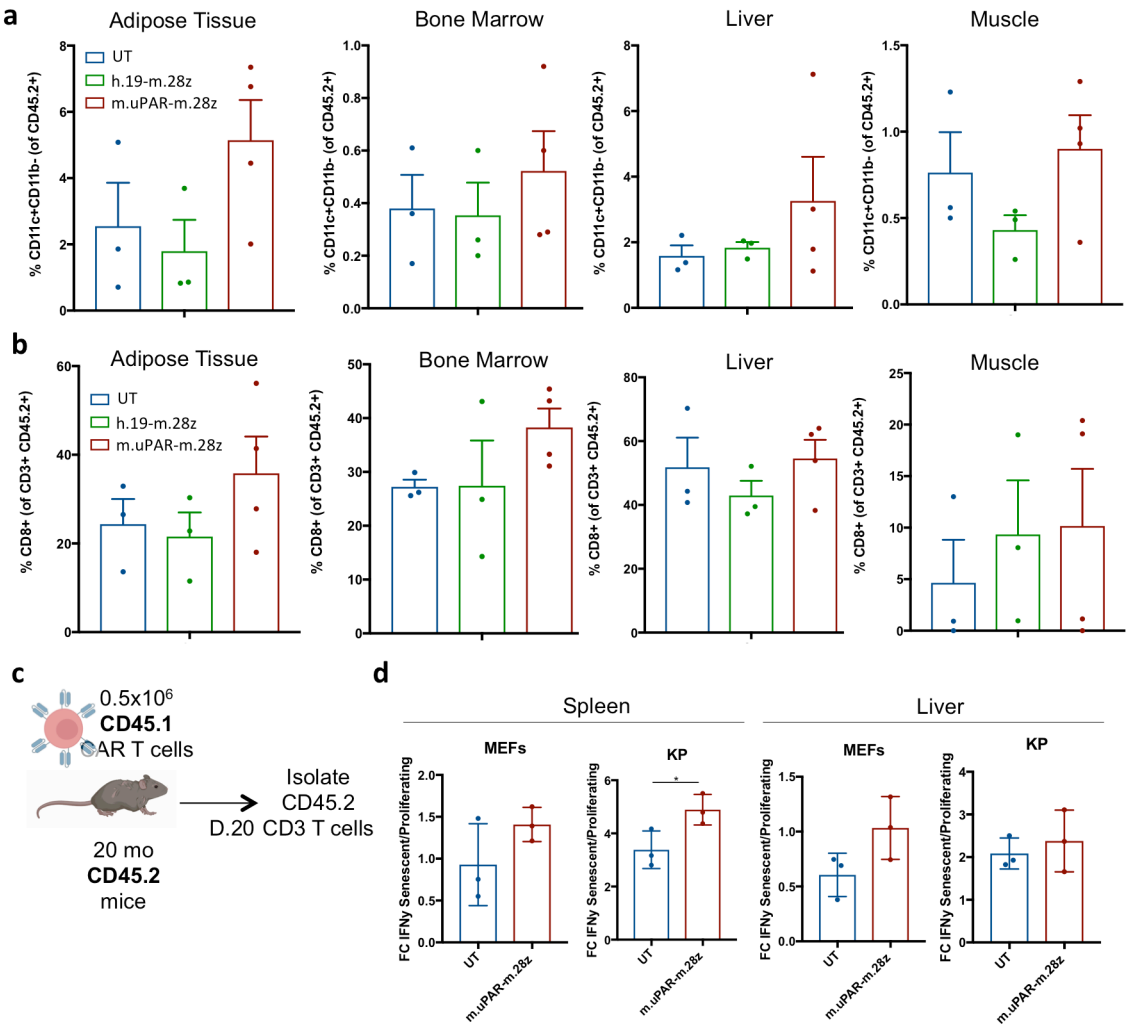

Figure 6.1. Modulation of the endogenous immune system by senolytic CAR T cells in aging (a) Abundance of dendritic cells and **(b)** endogenous CD45.2^{+} CD8^{+} T cells in the gonadal adipose tissue, bone marrow, liver and muscle of 20 months old mice 20 days after infusion of m.uPAR-m.28z or h.19-m.28z CAR Ts or untransduced T cells (UT). **(c)** Experimental scheme. CD45.2^{+} CD3^{+} T cells were isolated from the spleen and liver of 20 months old mice 20 days after infusion of m.uPAR-m.28z or untransduced T cells (UT) and co-cultured for 18h with senescent or proliferating mouse embryonic fibroblasts induced to senescence through irradiation (10Gy) or murine Kras^{G12D}, p53$^{-/-}$ lung cancer cells induced to senescence through combined Cdk4/6 and MEK inhibition. **(d)** Secretion of IFNγ of the endogenous T cells from the spleen or the liver after 18h of co-cultured as measured by ELISPOT.

BIBLIOGRAPHY

United States Census Bureau.

Acosta, J.C., Banito, A., Wuestefeld, T., Georgilis, A., Janich, P., Morton, J.P., Athineos, D., Kang, T.W., Lasitschka, F., Andrulis, M.*, et al.* (2013). A complex secretory program orchestrated by the inflammasome controls paracrine senescence. Nat Cell Biol *15*, 978-990.

Aghajanian, H., Kimura, T., Rurik, J.G., Hancock, A.S., Leibowitz, M.S., Li, L., Scholler, J., Monslow, J., Lo, A., Han, W.*, et al.* (2019). Targeting cardiac fibrosis with engineered T cells. Nature.

Ajani, J.A., D'Amico, T.A., Almhanna, K., Bentrem, D.J., Chao, J., Das, P., Denlinger, C.S., Fanta, P., Farjah, F., Fuchs, C.S.*, et al.* (2016). Gastric Cancer, Version 3.2016, NCCN Clinical Practice Guidelines in Oncology. J Natl Compr Canc Netw *14*, 1286-1312.

Ajani, J.A., Lee, J., Sano, T., Janjigian, Y.Y., Fan, D., and Song, S. (2017). Gastric adenocarcinoma. Nat Rev Dis Primers *3*, 17036.

Alexandrov, L.B., Nik-Zainal, S., Wedge, D.C., Aparicio, S.A., Behjati, S., Biankin, A.V., Bignell, G.R., Bolli, N., Borg, A., Borresen-Dale, A.L.*, et al.* (2013). Signatures of mutational processes in human cancer. Nature *500*, 415-421.

Andre, T., Shiu, K.K., Kim, T.W., Jensen, B.V., Jensen, L.H., Punt, C., Smith, D., Garcia-Carbonero, R., Benavides, M., Gibbs, P.*, et al.* (2020). Pembrolizumab in Microsatellite-Instability-High Advanced Colorectal Cancer. N Engl J Med *383*, 2207-2218.

Baar, M.P., Brandt, R.M.C., Putavet, D.A., Klein, J.D.D., Derks, K.W.J., Bourgeois, B.R.M., Stryeck, S., Rijksen, Y., van Willigenburg, H., Feijtel, D.A.*, et al.* (2017). Targeted Apoptosis of Senescent Cells Restores Tissue Homeostasis in Response to Chemotoxicity and Aging. Cell *169*, 132-147 e116.

Baker, D.J., Childs, B.G., Durik, M., Wijers, M.E., Sieben, C.J., Zhong, J., Saltness, R.A., Jeganathan, K.B., Verzosa, G.C., Pezeshki, A.*, et al.* (2016). Naturally occurring p16(Ink4a)-positive cells shorten healthy lifespan. Nature *530*, 184-189.

Baker, D.J., Wijshake, T., Tchkonia, T., LeBrasseur, N.K., Childs, B.G., van de Sluis, B., Kirkland, J.L., and van Deursen, J.M. (2011). Clearance of p16Ink4a-positive senescent cells delays ageing-associated disorders. Nature *479*, 232-236.

Belcher, C., Fawthrop, F., Bunning, R., and Doherty, M. (1996). Plasminogen activators and their inhibitors in synovial fluids from normal, osteoarthritis, and rheumatoid arthritis knees. Ann Rheum Dis *55*, 230-236.

Bolger, A.M., Lohse, M., and Usadel, B. (2014). Trimmomatic: a flexible trimmer for Illumina sequence data. Bioinformatics *30*, 2114-2120.

Brentjens, R.J., Davila, M.L., Riviere, I., Park, J., Wang, X., Cowell, L.G., Bartido, S., Stefanski, J., Taylor, C., Olszewska, M.*, et al.* (2013). CD19-targeted T cells rapidly induce molecular remissions in adults with chemotherapy-refractory acute lymphoblastic leukemia. Sci Transl Med *5*, 177ra138.

Brentjens, R.J., Latouche, J.B., Santos, E., Marti, F., Gong, M.C., Lyddane, C., King, P.D., Larson, S., Weiss, M., Riviere, I.*, et al.* (2003). Eradication of systemic B-cell tumors by genetically targeted human T lymphocytes co-stimulated by CD80 and interleukin-15. Nat Med *9*, 279-286.

Brentjens, R.J., Santos, E., Nikhamin, Y., Yeh, R., Matsushita, M., La Perle, K., Quintas-Cardama, A., Larson, S.M., and Sadelain, M. (2007). Genetically targeted T cells eradicate systemic acute lymphoblastic leukemia xenografts. Clin Cancer Res *13*, 5426-5435.

Brocker, T., and Karjalainen, K. (1995). Signals through T cell receptor-zeta chain alone are insufficient to prime resting T lymphocytes. J Exp Med *181*, 1653-1659.

Brocker, T., Peter, A., Traunecker, A., and Karjalainen, K. (1993). New simplified molecular design for functional T cell receptor. Eur J Immunol *23*, 1435-1439.

Brunt, E.M., Wong, V.W., Nobili, V., Day, C.P., Sookoian, S., Maher, J.J., Bugianesi, E., Sirlin, C.B., Neuschwander-Tetri, B.A., and Rinella, M.E. (2015). Nonalcoholic fatty liver disease. Nat Rev Dis Primers *1*, 15080.

Bugge, T.H., Suh, T.T., Flick, M.J., Daugherty, C.C., Romer, J., Solberg, H., Ellis, V., Dano, K., and Degen, J.L. (1995). The receptor for urokinase-type plasminogen activator is not essential for mouse development or fertility. J Biol Chem *270*, 16886-16894.

Bussian, T.J., Aziz, A., Meyer, C.F., Swenson, B.L., van Deursen, J.M., and Baker, D.J. (2018). Clearance of senescent glial cells prevents tau-dependent pathology and cognitive decline. Nature *562*, 578-582.

Cancer Genome Atlas Research, N. (2014). Comprehensive molecular characterization of gastric adenocarcinoma. Nature *513*, 202-209.

Caux, C., Massacrier, C., Vanbervliet, B., Dubois, B., Van Kooten, C., Durand, I., and Banchereau, J. (1994). Activation of human dendritic cells through CD40 cross-linking. J Exp Med *180*, 1263-1272.

Chao, J., Fuchs, C.S., Shitara, K., Tabernero, J., Muro, K., Van Cutsem, E., Bang, Y.J., De Vita, F., Landers, G., Yen, C.J.*, et al.* (2021). Assessment of Pembrolizumab Therapy for the Treatment of Microsatellite Instability-High Gastric or Gastroesophageal Junction Cancer Among Patients in the KEYNOTE-059, KEYNOTE-061, and KEYNOTE-062 Clinical Trials. JAMA Oncol.

Chen, E.Y., Tan, C.M., Kou, Y., Duan, Q., Wang, Z., Meirelles, G.V., Clark, N.R., and Ma'ayan, A. (2013). Enrichr: interactive and collaborative HTML5 gene list enrichment analysis tool. BMC Bioinformatics *14*, 128.

Childs, B.G., Baker, D.J., Wijshake, T., Conover, C.A., Campisi, J., and van Deursen, J.M. (2016). Senescent intimal foam cells are deleterious at all stages of atherosclerosis. Science *354*, 472-477.

Collado, M., Gil, J., Efeyan, A., Guerra, C., Schuhmacher, A.J., Barradas, M., Benguria, A., Zaballos, A., Flores, J.M., Barbacid, M.*, et al.* (2005). Tumour biology: senescence in premalignant tumours. Nature *436*, 642.

Coppe, J.P., Patil, C.K., Rodier, F., Sun, Y., Munoz, D.P., Goldstein, J., Nelson, P.S., Desprez, P.Y., and Campisi, J. (2008). Senescence-associated secretory phenotypes reveal cell-nonautonomous functions of oncogenic RAS and the p53 tumor suppressor. PLoS Biol *6*, 2853-2868.

Cristescu, R., Lee, J., Nebozhyn, M., Kim, K.M., Ting, J.C., Wong, S.S., Liu, J., Yue, Y.G., Wang, J., Yu, K.*, et al.* (2015). Molecular analysis of gastric cancer identifies subtypes associated with distinct clinical outcomes. Nat Med *21*, 449-456.

Davila, M.L., Kloss, C.C., Gunset, G., and Sadelain, M. (2013). CD19 CAR-targeted T cells induce long-term remission and B Cell Aplasia in an immunocompetent mouse model of B cell acute lymphoblastic leukemia. PLoS One *8*, e61338.

Davila, M.L., Riviere, I., Wang, X., Bartido, S., Park, J., Curran, K., Chung, S.S., Stefanski, J., Borquez-Ojeda, O., Olszewska, M.*, et al.* (2014). Efficacy and toxicity management of 19-28z CAR T cell therapy in B cell acute lymphoblastic leukemia. Sci Transl Med *6*, 224ra225.

Demaria, M., O'Leary, M.N., Chang, J., Shao, L., Liu, S., Alimirah, F., Koenig, K., Le, C., Mitin, N., Deal, A.M.*, et al.* (2017). Cellular Senescence Promotes Adverse Effects of Chemotherapy and Cancer Relapse. Cancer Discov *7*, 165-176.

Demaria, M., Ohtani, N., Youssef, S.A., Rodier, F., Toussaint, W., Mitchell, J.R., Laberge, R.M., Vijg, J., Van Steeg, H., Dolle, M.E.*, et al.* (2014). An essential role for senescent cells in optimal wound healing through secretion of PDGF-AA. Dev Cell *31*, 722-733.

Ding, L., Bailey, M.H., Porta-Pardo, E., Thorsson, V., Colaprico, A., Bertrand, D., Gibbs, D.L., Weerasinghe, A., Huang, K.L., Tokheim, C.*, et al.* (2018). Perspective on Oncogenic Processes at the End of the Beginning of Cancer Genomics. Cell *173*, 305-320 e310.

Dobin, A., Davis, C.A., Schlesinger, F., Drenkow, J., Zaleski, C., Jha, S., Batut, P., Chaisson, M., and Gingeras, T.R. (2013). STAR: ultrafast universal RNA-seq aligner. Bioinformatics *29*, 15-21.

Dobrenkov, K., Olszewska, M., Likar, Y., Shenker, L., Gunset, G., Cai, S., Pillarsetty, N., Hricak, H., Sadelain, M., and Ponomarev, V. (2008). Monitoring the efficacy of adoptively transferred prostate cancer-targeted human T lymphocytes with PET and bioluminescence imaging. J Nucl Med *49*, 1162-1170.

Du, H., Hirabayashi, K., Ahn, S., Kren, N.P., Montgomery, S.A., Wang, X., Tiruthani, K., Mirlekar, B., Michaud, D., Greene, K.*, et al.* (2019). Antitumor Responses in the Absence of Toxicity in Solid Tumors by Targeting B7-H3 via Chimeric Antigen Receptor T Cells. Cancer Cell *35*, 221-237 e228.

Egashira, M., Hirota, Y., Shimizu-Hirota, R., Saito-Fujita, T., Haraguchi, H., Matsumoto, L., Matsuo, M., Hiraoka, T., Tanaka, T., Akaeda, S.*, et al.* (2017). F4/80+ Macrophages Contribute to Clearance of Senescent Cells in the Mouse Postpartum Uterus. Endocrinology *158*, 2344-2353.

Eshhar, Z., Waks, T., Gross, G., and Schindler, D.G. (1993). Specific activation and targeting of cytotoxic lymphocytes through chimeric single chains consisting of antibody-binding domains and the gamma or zeta subunits of the immunoglobulin and T-cell receptors. Proc Natl Acad Sci U S A *90*, 720-724.

Eyquem, J., Mansilla-Soto, J., Giavridis, T., van der Stegen, S.J., Hamieh, M., Cunanan, K.M., Odak, A., Gonen, M., and Sadelain, M. (2017). Targeting a CAR to the TRAC locus with CRISPR/Cas9 enhances tumour rejection. Nature *543*, 113-117.

Feucht, J., Sun, J., Eyquem, J., Ho, Y.J., Zhao, Z., Leibold, J., Dobrin, A., Cabriolu, A., Hamieh, M., and Sadelain, M. (2019). Calibration of CAR activation potential directs alternative T cell fates and therapeutic potency. Nat Med *25*, 82-88.

Finney, H.M., Lawson, A.D., Bebbington, C.R., and Weir, A.N. (1998). Chimeric receptors providing both primary and costimulatory signaling in T cells from a single gene product. J Immunol *161*, 2791-2797.

Fujii, M., Shibazaki, Y., Wakamatsu, K., Honda, Y., Kawauchi, Y., Suzuki, K., Arumugam, S., Watanabe, K., Ichida, T., Asakura, H.*, et al.* (2013). A murine model for non-alcoholic steatohepatitis showing evidence of association between diabetes and hepatocellular carcinoma. Med Mol Morphol *46*, 141-152.

Gargett, T., and Brown, M.P. (2014). The inducible caspase-9 suicide gene system as a "safety switch" to limit on-target, off-tumor toxicities of chimeric antigen receptor T cells. Front Pharmacol *5*, 235.

Germano, G., Lamba, S., Rospo, G., Barault, L., Magri, A., Maione, F., Russo, M., Crisafulli, G., Bartolini, A., Lerda, G.*, et al.* (2017). Inactivation of DNA repair triggers neoantigen generation and impairs tumour growth. Nature *552*, 116-120.

Giavridis, T., van der Stegen, S.J.C., Eyquem, J., Hamieh, M., Piersigilli, A., and Sadelain, M. (2018). CAR T cell-induced cytokine release syndrome is mediated by macrophages and abated by IL-1 blockade. Nat Med *24*, 731-738.

Gonzalez-Gualda, E., Paez-Ribes, M., Lozano-Torres, B., Macias, D., Wilson, J.R., 3rd, Gonzalez-Lopez, C., Ou, H.L., Miron-Barroso, S., Zhang, Z., Lerida-Viso, A.*, et al.* (2020). Galacto-conjugation of Navitoclax as an efficient strategy to increase senolytic specificity and reduce platelet toxicity. Aging Cell *19*, e13142.

Gross, G., Waks, T., and Eshhar, Z. (1989). Expression of immunoglobulin-T-cell receptor chimeric molecules as functional receptors with antibody-type specificity. Proc Natl Acad Sci U S A *86*, 10024-10028.

Grosse, L., Wagner, N., Emelyanov, A., Molina, C., Lacas-Gervais, S., Wagner, K.D., and Bulavin, D.V. (2020). Defined p16(High) Senescent Cell Types Are Indispensable for Mouse Healthspan. Cell Metab *32*, 87-99 e86.

Grupp, S.A., Kalos, M., Barrett, D., Aplenc, R., Porter, D.L., Rheingold, S.R., Teachey, D.T., Chew, A., Hauck, B., Wright, J.F.*, et al.* (2013). Chimeric antigen receptor-modified T cells for acute lymphoid leukemia. N Engl J Med *368*, 1509-1518.

Guerrero, A., Herranz, N., Sun, B., Wagner, V., Gallage, S., Guiho, R., Wolter, K., Pombo, J., Irvine, E.E., Innes, A.J.*, et al.* (2019). Cardiac glycosides are broad-spectrum senolytics. Nat Metab *1*, 1074-1088.

Gust, J., Hay, K.A., Hanafi, L.A., Li, D., Myerson, D., Gonzalez-Cuyar, L.F., Yeung, C., Liles, W.C., Wurfel, M., Lopez, J.A.*, et al.* (2017). Endothelial Activation and Blood-Brain Barrier Disruption in Neurotoxicity after Adoptive Immunotherapy with CD19 CAR-T Cells. Cancer Discov *7*, 1404-1419.

Guthoff, M., Wagner, R., Randrianarisoa, E., Hatziagelaki, E., Peter, A., Haring, H.U., Fritsche, A., and Heyne, N. (2017). Soluble urokinase receptor (suPAR) predicts microalbuminuria in patients at risk for type 2 diabetes mellitus. Sci Rep *7*, 40627.

Hagani, A.B., Riviere, I., Tan, C., Krause, A., and Sadelain, M. (1999). Activation conditions determine susceptibility of murine primary T-lymphocytes to retroviral infection. J Gene Med *1*, 341-351.

Hall, B.M., Balan, V., Gleiberman, A.S., Strom, E., Krasnov, P., Virtuoso, L.P., Rydkina, E., Vujcic, S., Balan, K., Gitlin, II*, et al.* (2017). p16(Ink4a) and senescence-associated beta-galactosidase can be induced in macrophages as part of a reversible response to physiological stimuli. Aging (Albany NY) *9*, 1867-1884.

Harley, C.B., Futcher, A.B., and Greider, C.W. (1990). Telomeres shorten during ageing of human fibroblasts. Nature *345*, 458-460.

Hartmann Rasmussen, K.J.e.a. Association between elevated suPAR, a new biomarker of inflammation, an accelerated aging. The Journals of Gerontology *76*.

Hayek, S.S., Sever, S., Ko, Y.A., Trachtman, H., Awad, M., Wadhwani, S., Altintas, M.M., Wei, C., Hotton, A.L., French, A.L.*, et al.* (2015). Soluble Urokinase Receptor and Chronic Kidney Disease. N Engl J Med *373*, 1916-1925.

Hayflick, L., and Moorhead, P.S. (1961). The serial cultivation of human diploid cell strains. Exp Cell Res *25*, 585-621.

He, S., and Sharpless, N.E. (2017). Senescence in Health and Disease. Cell *169*, 1000-1011.

Hernandez-Segura, A., de Jong, T.V., Melov, S., Guryev, V., Campisi, J., and Demaria, M. (2017). Unmasking Transcriptional Heterogeneity in Senescent Cells. Curr Biol *27*, 2652-2660 e2654.

Heron, M. (2021). Deaths: Leading causes for 2019. National Vital Statistics Reports *70*.

Hombach, A., Wieczarkowiecz, A., Marquardt, T., Heuser, C., Usai, L., Pohl, C., Seliger, B., and Abken, H. (2001). Tumor-specific T cell activation by recombinant immunoreceptors: CD3 zeta signaling and CD28 costimulation are simultaneously required for efficient IL-2 secretion and can be integrated into one combined CD28/CD3 zeta signaling receptor molecule. J Immunol *167*, 6123-6131.

Huang, K.K., Ramnarayanan, K., Zhu, F., Srivastava, S., Xu, C., Tan, A.L.K., Lee, M., Tay, S., Das, K., Xing, M.*, et al.* (2018). Genomic and Epigenomic Profiling of High-Risk Intestinal Metaplasia Reveals Molecular Determinants of Progression to Gastric Cancer. Cancer Cell *33*, 137-150 e135.

Iannello, A., Thompson, T.W., Ardolino, M., Lowe, S.W., and Raulet, D.H. (2013). p53-dependent chemokine production by senescent tumor cells supports NKG2D-dependent tumor elimination by natural killer cells. J Exp Med *210*, 2057-2069.

Irving, B.A., and Weiss, A. (1991). The cytoplasmic domain of the T cell receptor zeta chain is sufficient to couple to receptor-associated signal transduction pathways. Cell *64*, 891-901.

June, C.H., and Sadelain, M. (2018). Chimeric Antigen Receptor Therapy. N Engl J Med *379*, 64-73.

Kang, T.W., Yevsa, T., Woller, N., Hoenicke, L., Wuestefeld, T., Dauch, D., Hohmeyer, A., Gereke, M., Rudalska, R., Potapova, A.*, et al.* (2011). Senescence surveillance of pre-malignant hepatocytes limits liver cancer development. Nature *479*, 547-551.

Kansal, R., Richardson, N., Neeli, I., Khawaja, S., Chamberlain, D., Ghani, M., Ghani, Q.U., Balazs, L., Beranova-Giorgianni, S., Giorgianni, F.*, et al.* (2019). Sustained B cell depletion by CD19-targeted CAR T cells is a highly effective treatment for murine lupus. Sci Transl Med *11*.

Kawaguchi, K., Komoda, K., Mikawa, R., Asai, A., and Sugimoto, M. (2021). Cellular senescence promotes cancer metastasis by enhancing soluble E-cadherin production. iScience *24*, 103022.

Kim, K.M., Noh, J.H., Bodogai, M., Martindale, J.L., Yang, X., Indig, F.E., Basu, S.K., Ohnuma, K., Morimoto, C., Johnson, P.F.*, et al.* (2017). Identification of senescent cell surface targetable protein DPP4. Genes Dev *31*, 1529-1534.

Kim, S.T., Cristescu, R., Bass, A.J., Kim, K.M., Odegaard, J.I., Kim, K., Liu, X.Q., Sher, X., Jung, H., Lee, M.*, et al.* (2018). Comprehensive molecular characterization of clinical responses to PD-1 inhibition in metastatic gastric cancer. Nat Med *24*, 1449-1458.

Kirkland, J.L., and Tchkonia, T. (2017). Cellular Senescence: A Translational Perspective. EBioMedicine *21*, 21-28.

Krizhanovsky, V., Yon, M., Dickins, R.A., Hearn, S., Simon, J., Miething, C., Yee, H., Zender, L., and Lowe, S.W. (2008). Senescence of activated stellate cells limits liver fibrosis. Cell *134*, 657-667.

Kuhn, N.F., Purdon, T.J., van Leeuwen, D.G., Lopez, A.V., Curran, K.J., Daniyan, A.F., and Brentjens, R.J. (2019). CD40 Ligand-Modified Chimeric Antigen Receptor T Cells Enhance Antitumor Function by Eliciting an Endogenous Antitumor Response. Cancer Cell *35*, 473-488 e476.

Kuwana, Y., Asakura, Y., Utsunomiya, N., Nakanishi, M., Arata, Y., Itoh, S., Nagase, F., and Kurosawa, Y. (1987). Expression of chimeric receptor composed of immunoglobulin-derived V regions and T-cell receptor-derived C regions. Biochem Biophys Res Commun *149*, 960-968.

Kwon, M., An, M., Klempner, S.J., Lee, H., Kim, K.M., Sa, J.K., Cho, H.J., Hong, J.Y., Lee, T., Min, Y.W.*, et al.* (2021). Determinants of Response and Intrinsic Resistance to PD-1 Blockade in Microsatellite Instability-High Gastric Cancer. Cancer Discov.

Laberge, R.M., Zhou, L., Sarantos, M.R., Rodier, F., Freund, A., de Keizer, P.L., Liu, S., Demaria, M., Cong, Y.S., Kapahi, P.*, et al.* (2012). Glucocorticoids suppress selected components of the senescence-associated secretory phenotype. Aging Cell *11*, 569-578.

Lasry, A., and Ben-Neriah, Y. (2015). Senescence-associated inflammatory responses: aging and cancer perspectives. Trends Immunol *36*, 217-228.

Lauren, P. (1965). The Two Histological Main Types of Gastric Carcinoma: Diffuse and So-Called Intestinal-Type Carcinoma. An Attempt at a Histo-Clinical Classification. Acta Pathol Microbiol Scand *64*, 31-49.

Le, D.T., Durham, J.N., Smith, K.N., Wang, H., Bartlett, B.R., Aulakh, L.K., Lu, S., Kemberling, H., Wilt, C., Luber, B.S.*, et al.* (2017). Mismatch repair deficiency predicts response of solid tumors to PD-1 blockade. Science *357*, 409-413.

Le, D.T., Uram, J.N., Wang, H., Bartlett, B.R., Kemberling, H., Eyring, A.D., Skora, A.D., Luber, B.S., Azad, N.S., Laheru, D.*, et al.* (2015). PD-1 Blockade in Tumors with Mismatch-Repair Deficiency. N Engl J Med *372*, 2509-2520.

Lee, D.W., Kochenderfer, J.N., Stetler-Stevenson, M., Cui, Y.K., Delbrook, C., Feldman, S.A., Fry, T.J., Orentas, R., Sabatino, M., Shah, N.N.*, et al.* (2015). T cells expressing CD19 chimeric antigen receptors for acute lymphoblastic leukaemia in children and young adults: a phase 1 dose-escalation trial. Lancet *385*, 517-528.

Leibold, J., Ruscetti, M., Cao, Z., Ho, Y.J., Baslan, T., Zou, M., Abida, W., Feucht, J., Han, T., Barriga, F.M.*, et al.* (2020). Somatic Tissue Engineering in Mouse Models Reveals an Actionable Role for WNT Pathway Alterations in Prostate Cancer Metastasis. Cancer Discov *10*, 1038-1057.

Lengauer, C., Kinzler, K.W., and Vogelstein, B. (1998). Genetic instabilities in human cancers. Nature *396*, 643-649.

Letourneur, F., and Klausner, R.D. (1991). T-cell and basophil activation through the cytoplasmic tail of T-cell-receptor zeta family proteins. Proc Natl Acad Sci U S A *88*, 8905-8909.

Leushacke, M., Tan, S.H., Wong, A., Swathi, Y., Hajamohideen, A., Tan, L.T., Goh, J., Wong, E., Denil, S., Murakami, K.*, et al.* (2017). Lgr5-expressing chief cells drive epithelial regeneration and cancer in the oxyntic stomach. Nat Cell Biol *19*, 774-786.

Liang, Q., Yao, X., Tang, S., Zhang, J., Yau, T.O., Li, X., Tang, C.M., Kang, W., Lung, R.W., Li, J.W.*, et al.* (2014). Integrative identification of Epstein-Barr virus-associated mutations and epigenetic alterations in gastric cancer. Gastroenterology *147*, 1350-1362 e1354.

Liao, Y., Smyth, G.K., and Shi, W. (2014). featureCounts: an efficient general purpose program for assigning sequence reads to genomic features. Bioinformatics *30*, 923-930.

Livshits, G., Alonso-Curbelo, D., Morris, J.P.t., Koche, R., Saborowski, M., Wilkinson, J.E., and Lowe, S.W. (2018). Arid1a restrains Kras-dependent changes in acinar cell identity. Elife *7*.

Lord, C.J., and Ashworth, A. (2012). The DNA damage response and cancer therapy. Nature *481*, 287-294.

Love, M.I., Huber, W., and Anders, S. (2014). Moderated estimation of fold change and dispersion for RNA-seq data with DESeq2. Genome Biol *15*, 550.

Lujambio, A. (2016). To clear, or not to clear (senescent cells)? That is the question. Bioessays *38 Suppl 1*, S56-64.

Lujambio, A., Akkari, L., Simon, J., Grace, D., Tschaharganeh, D.F., Bolden, J.E., Zhao, Z., Thapar, V., Joyce, J.A., Krizhanovsky, V.*, et al.* (2013). Non-cell-autonomous tumor suppression by p53. Cell *153*, 449-460.

Macatonia, S.E., Hosken, N.A., Litton, M., Vieira, P., Hsieh, C.S., Culpepper, J.A., Wysocka, M., Trinchieri, G., Murphy, K.M., and O'Garra, A. (1995). Dendritic cells produce IL-12 and direct the development of Th1 cells from naive CD4+ T cells. J Immunol *154*, 5071-5079.

Maher, J., Brentjens, R.J., Gunset, G., Riviere, I., and Sadelain, M. (2002). Human T-lymphocyte cytotoxicity and proliferation directed by a single chimeric TCRzeta /CD28 receptor. Nat Biotechnol *20*, 70-75.

Maldini, C.R., Claiborne, D.T., Okawa, K., Chen, T., Dopkin, D.L., Shan, X., Power, K.A., Trifonova, R.T., Krupp, K., Phelps, M.*, et al.* (2020). Dual CD4-based CAR T cells with distinct costimulatory domains mitigate HIV pathogenesis in vivo. Nat Med *26*, 1776-1787.

Mandal, R., Samstein, R.M., Lee, K.W., Havel, J.J., Wang, H., Krishna, C., Sabio, E.Y., Makarov, V., Kuo, F., Blecua, P.*, et al.* (2019). Genetic diversity of tumors with mismatch repair deficiency influences anti-PD-1 immunotherapy response. Science *364*, 485-491.

Maude, S.L., Frey, N., Shaw, P.A., Aplenc, R., Barrett, D.M., Bunin, N.J., Chew, A., Gonzalez, V.E., Zheng, Z., Lacey, S.F*., et al.* (2014). Chimeric antigen receptor T cells for sustained remissions in leukemia. N Engl J Med *371*, 1507-1517.

Maude, S.L., Laetsch, T.W., Buechner, J., Rives, S., Boyer, M., Bittencourt, H., Bader, P., Verneris, M.R., Stefanski, H.E., Myers, G.D*., et al.* (2018). Tisagenlecleucel in Children and Young Adults with B-Cell Lymphoblastic Leukemia. N Engl J Med *378*, 439-448.

Munoz-Espin, D., Rovira, M., Galiana, I., Gimenez, C., Lozano-Torres, B., Paez-Ribes, M., Llanos, S., Chaib, S., Munoz-Martin, M., Ucero, A.C*., et al.* (2018). A versatile drug delivery system targeting senescent cells. EMBO Mol Med *10*.

Murphy, K.M. (2012). Janeway's Immunobiology, Vol 8th Edition

Neelapu, S.S., Locke, F.L., Bartlett, N.L., Lekakis, L.J., Miklos, D.B., Jacobson, C.A., Braunschweig, I., Oluwole, O.O., Siddiqi, T., Lin, Y*., et al.* (2017). Axicabtagene Ciloleucel CAR T-Cell Therapy in Refractory Large B-Cell Lymphoma. N Engl J Med *377*, 2531-2544.

Norelli, M., Camisa, B., Barbiera, G., Falcone, L., Purevdorj, A., Genua, M., Sanvito, F., Ponzoni, M., Doglioni, C., Cristofori, P*., et al.* (2018). Monocyte-derived IL-1 and IL-6 are differentially required for cytokine-release syndrome and neurotoxicity due to CAR T cells. Nat Med *24*, 739-748.

Ovadya, Y., Landsberger, T., Leins, H., Vadai, E., Gal, H., Biran, A., Yosef, R., Sagiv, A., Agrawal, A., Shapira, A*., et al.* (2018). Impaired immune surveillance accelerates accumulation of senescent cells and aging. Nat Commun *9*, 5435.

Panda, A., Mehnert, J.M., Hirshfield, K.M., Riedlinger, G., Damare, S., Saunders, T., Kane, M., Sokol, L., Stein, M.N., Poplin, E*., et al.* (2018). Immune Activation and Benefit From Avelumab in EBV-Positive Gastric Cancer. J Natl Cancer Inst *110*, 316-320.

Park, J.H., Riviere, I., Gonen, M., Wang, X., Senechal, B., Curran, K.J., Sauter, C., Wang, Y., Santomasso, B., Mead, E*., et al.* (2018). Long-Term Follow-up of CD19 CAR Therapy in Acute Lymphoblastic Leukemia. N Engl J Med *378*, 449-459.

Paszkiewicz, P.J., Frassle, S.P., Srivastava, S., Sommermeyer, D., Hudecek, M., Drexler, I., Sadelain, M., Liu, L., Jensen, M.C., Riddell, S.R*., et al.* (2016). Targeted antibody-mediated depletion of murine CD19 CAR T cells permanently reverses B cell aplasia. J Clin Invest *126*, 4262-4272.

Pellegatta, S., Savoldo, B., Di Ianni, N., Corbetta, C., Chen, Y., Patane, M., Sun, C., Pollo, B., Ferrone, S., DiMeco, F*., et al.* (2018). Constitutive and TNFalpha-inducible expression of chondroitin sulfate proteoglycan 4 in glioblastoma and neurospheres: Implications for CAR-T cell therapy. Sci Transl Med *10*.

Perna, F., Berman, S.H., Soni, R.K., Mansilla-Soto, J., Eyquem, J., Hamieh, M., Hendrickson, R.C., Brennan, C.W., and Sadelain, M. (2017). Integrating Proteomics and Transcriptomics for Systematic Combinatorial Chimeric Antigen Receptor Therapy of AML. Cancer Cell *32*, 506-519 e505.

Puche, J.E., Lee, Y.A., Jiao, J., Aloman, C., Fiel, M.I., Munoz, U., Kraus, T., Lee, T., Yee, H.F., Jr., and Friedman, S.L. (2013). A novel murine model to deplete hepatic stellate cells uncovers their role in amplifying liver damage in mice. Hepatology *57*, 339-350.

Pule, M.A., Straathof, K.C., Dotti, G., Heslop, H.E., Rooney, C.M., and Brenner, M.K. (2005). A chimeric T cell antigen receptor that augments cytokine release and supports clonal expansion of primary human T cells. Mol Ther *12*, 933-941.

Ruscetti, M., Leibold, J., Bott, M.J., Fennell, M., Kulick, A., Salgado, N.R., Chen, C.C., Ho, Y.J., Sanchez-Rivera, F.J., Feucht, J*., et al.* (2018). NK cell-mediated cytotoxicity contributes to tumor control by a cytostatic drug combination. Science *362*, 1416-1422.

Ruscetti, M., Morris, J.P.t., Mezzadra, R., Russell, J., Leibold, J., Romesser, P.B., Simon, J., Kulick, A., Ho, Y.J., Fennell, M*., et al.* (2020). Senescence-Induced Vascular

Remodeling Creates Therapeutic Vulnerabilities in Pancreas Cancer. Cell *181*, 424-441 e421.
Sadelain, M., Riviere, I., and Riddell, S. (2017). Therapeutic T cell engineering. Nature *545*, 423-431.
Sagiv, A., Biran, A., Yon, M., Simon, J., Lowe, S.W., and Krizhanovsky, V. (2013). Granule exocytosis mediates immune surveillance of senescent cells. Oncogene *32*, 1971-1977.
Santos, E.B., Yeh, R., Lee, J., Nikhamin, Y., Punzalan, B., Punzalan, B., La Perle, K., Larson, S.M., Sadelain, M., and Brentjens, R.J. (2009). Sensitive in vivo imaging of T cells using a membrane-bound Gaussia princeps luciferase. Nat Med *15*, 338-344.
Schafer, M.J., White, T.A., Iijima, K., Haak, A.J., Ligresti, G., Atkinson, E.J., Oberg, A.L., Birch, J., Salmonowicz, H., Zhu, Y.*, et al.* (2017). Cellular senescence mediates fibrotic pulmonary disease. Nat Commun *8*, 14532.
Schnabl, B., Purbeck, C.A., Choi, Y.H., Hagedorn, C.H., and Brenner, D. (2003). Replicative senescence of activated human hepatic stellate cells is accompanied by a pronounced inflammatory but less fibrogenic phenotype. Hepatology *37*, 653-664.
Schuliga, M., Jaffar, J., Harris, T., Knight, D.A., Westall, G., and Stewart, A.G. (2017). The fibrogenic actions of lung fibroblast-derived urokinase: a potential drug target in IPF. Sci Rep *7*, 41770.
Scott, A.J., Ellison M., Sinclair, D.A. (2021). The economic value of targeting aging. Nat Aging *1*, 616-623.
Seehawer, M., Heinzmann, F., D'Artista, L., Harbig, J., Roux, P.F., Hoenicke, L., Dang, H., Klotz, S., Robinson, L., Dore, G.*, et al.* (2018). Necroptosis microenvironment directs lineage commitment in liver cancer. Nature *562*, 69-75.
Seidlitz, T., Chen, Y.T., Uhlemann, H., Scholch, S., Kochall, S., Merker, S.R., Klimova, A., Hennig, A., Schweitzer, C., Pape, K.*, et al.* (2019). Mouse Models of Human Gastric Cancer Subtypes With Stomach-Specific CreERT2-Mediated Pathway Alterations. Gastroenterology *157*, 1599-1614 e1592.
Serrano, M., Lin, A.W., McCurrach, M.E., Beach, D., and Lowe, S.W. (1997). Oncogenic ras provokes premature cell senescence associated with accumulation of p53 and p16INK4a. Cell *88*, 593-602.
Sharpless, N.E., and Sherr, C.J. (2015). Forging a signature of in vivo senescence. Nat Rev Cancer *15*, 397-408.
Simon, D.I., Rao, N.K., Xu, H., Wei, Y., Majdic, O., Ronne, E., Kobzik, L., and Chapman, H.A. (1996). Mac-1 (CD11b/CD18) and the urokinase receptor (CD87) form a functional unit on monocytic cells. Blood *88*, 3185-3194.
Smith, H.W., and Marshall, C.J. (2010). Regulation of cell signalling by uPAR. Nat Rev Mol Cell Biol *11*, 23-36.
Smyth, E.C., Nilsson, M., Grabsch, H.I., van Grieken, N.C., and Lordick, F. (2020). Gastric cancer. Lancet *396*, 635-648.
Srivastava, S., Salter, A.I., Liggitt, D., Yechan-Gunja, S., Sarvothama, M., Cooper, K., Smythe, K.S., Dudakov, J.A., Pierce, R.H., Rader, C.*, et al.* (2019). Logic-Gated ROR1 Chimeric Antigen Receptor Expression Rescues T Cell-Mediated Toxicity to Normal Tissues and Enables Selective Tumor Targeting. Cancer Cell *35*, 489-503 e488.
Sung, H., Ferlay, J., Siegel, R.L., Laversanne, M., Soerjomataram, I., Jemal, A., and Bray, F. (2021). Global cancer statistics 2020: GLOBOCAN estimates of incidence and mortality worldwide for 36 cancers in 185 countries. CA Cancer J Clin.
Tasdemir, N., Banito, A., Roe, J.S., Alonso-Curbelo, D., Camiolo, M., Tschaharganeh, D.F., Huang, C.H., Aksoy, O., Bolden, J.E., Chen, C.C.*, et al.* (2016). BRD4 Connects Enhancer Remodeling to Senescence Immune Surveillance. Cancer Discov *6*, 612-629.

Tavakoli, A., Monavari, S.H., Solaymani Mohammadi, F., Kiani, S.J., Armat, S., and Farahmand, M. (2020). Association between Epstein-Barr virus infection and gastric cancer: a systematic review and meta-analysis. BMC Cancer *20*, 493.

Till, B.G., Jensen, M.C., Wang, J., Qian, X., Gopal, A.K., Maloney, D.G., Lindgren, C.G., Lin, Y., Pagel, J.M., Budde, L.E.*, et al.* (2012). CD20-specific adoptive immunotherapy for lymphoma using a chimeric antigen receptor with both CD28 and 4-1BB domains: pilot clinical trial results. Blood *119*, 3940-3950.

Till, J.E., Yoon, C., Kim, B.J., Roby, K., Addai, P., Jonokuchi, E., Tang, L.H., Yoon, S.S., and Ryeom, S. (2017). Oncogenic KRAS and p53 Loss Drive Gastric Tumorigenesis in Mice That Can Be Attenuated by E-Cadherin Expression. Cancer Res *77*, 5349-5359.

Tonnessen-Murray, C.A., Frey, W.D., Rao, S.G., Shahbandi, A., Ungerleider, N.A., Olayiwola, J.O., Murray, L.B., Vinson, B.T., Chrisey, D.B., Lord, C.J.*, et al.* (2019). Chemotherapy-induced senescent cancer cells engulf other cells to enhance their survival. J Cell Biol *218*, 3827-3844.

Triana-Martinez, F., Picallos-Rabina, P., Da Silva-Alvarez, S., Pietrocola, F., Llanos, S., Rodilla, V., Soprano, E., Pedrosa, P., Ferreiros, A., Barradas, M.*, et al.* (2019). Identification and characterization of Cardiac Glycosides as senolytic compounds. Nat Commun *10*, 4731.

Van der Schueren, B., Vangoitsenhoven, R., Geeraert, B., De Keyzer, D., Hulsmans, M., Lannoo, M., Huber, H.J., Mathieu, C., and Holvoet, P. (2015). Low cytochrome oxidase 4I1 links mitochondrial dysfunction to obesity and type 2 diabetes in humans and mice. Int J Obes (Lond) *39*, 1254-1263.

Verdecchia, A., Francisci, S., Brenner, H., Gatta, G., Micheli, A., Mangone, L., Kunkler, I., and Group, E.-W. (2007). Recent cancer survival in Europe: a 2000-02 period analysis of EUROCARE-4 data. Lancet Oncol *8*, 784-796.

Wagner, A.D., Syn, N.L., Moehler, M., Grothe, W., Yong, W.P., Tai, B.C., Ho, J., and Unverzagt, S. (2017). Chemotherapy for advanced gastric cancer. Cochrane Database Syst Rev *8*, CD004064.

Wang, C., Vegna, S., Jin, H., Benedict, B., Lieftink, C., Ramirez, C., de Oliveira, R.L., Morris, B., Gadiot, J., Wang, W.*, et al.* (2019a). Inducing and exploiting vulnerabilities for the treatment of liver cancer. Nature *574*, 268-272.

Wang, J., Jensen, M., Lin, Y., Sui, X., Chen, E., Lindgren, C.G., Till, B., Raubitschek, A., Forman, S.J., Qian, X.*, et al.* (2007). Optimizing adoptive polyclonal T cell immunotherapy of lymphomas, using a chimeric T cell receptor possessing CD28 and CD137 costimulatory domains. Hum Gene Ther *18*, 712-725.

Wang, K., Yuen, S.T., Xu, J., Lee, S.P., Yan, H.H., Shi, S.T., Siu, H.C., Deng, S., Chu, K.M., Law, S.*, et al.* (2014). Whole-genome sequencing and comprehensive molecular profiling identify new driver mutations in gastric cancer. Nat Genet *46*, 573-582.

Wang, L., Yang, R., Zhao, L., Zhang, X., Xu, T., and Cui, M. (2019b). Basing on uPAR-binding fragment to design chimeric antigen receptors triggers antitumor efficacy against uPAR expressing ovarian cancer cells. Biomed Pharmacother *117*, 109173.

Wang, R., Yu, Z., Sunchu, B., Shoaf, J., Dang, I., Zhao, S., Caples, K., Bradley, L., Beaver, L.M., Ho, E.*, et al.* (2017). Rapamycin inhibits the secretory phenotype of senescent cells by a Nrf2-independent mechanism. Aging Cell *16*, 564-574.

Wang, X., Zheng, Z., Caviglia, J.M., Corey, K.E., Herfel, T.M., Cai, B., Masia, R., Chung, R.T., Lefkowitch, J.H., Schwabe, R.F.*, et al.* (2016). Hepatocyte TAZ/WWTR1 Promotes Inflammation and Fibrosis in Nonalcoholic Steatohepatitis. Cell Metab *24*, 848-862.

Xu, M., Pirtskhalava, T., Farr, J.N., Weigand, B.M., Palmer, A.K., Weivoda, M.M., Inman, C.L., Ogrodnik, M.B., Hachfeld, C.M., Fraser, D.G.*, et al.* (2018). Senolytics improve physical function and increase lifespan in old age. Nat Med *24*, 1246-1256.

Xu, M., Tchkonia, T., Ding, H., Ogrodnik, M., Lubbers, E.R., Pirtskhalava, T., White, T.A., Johnson, K.O., Stout, M.B., Mezera, V.*, et al.* (2015). JAK inhibition alleviates the

cellular senescence-associated secretory phenotype and frailty in old age. Proc Natl Acad Sci U S A *112*, E6301-6310.

Xue, W., Zender, L., Miething, C., Dickins, R.A., Hernando, E., Krizhanovsky, V., Cordon-Cardo, C., and Lowe, S.W. (2007). Senescence and tumour clearance is triggered by p53 restoration in murine liver carcinomas. Nature *445*, 656-660.

Yeku, O.O., Purdon, T.J., Koneru, M., Spriggs, D., and Brentjens, R.J. (2017). Armored CAR T cells enhance antitumor efficacy and overcome the tumor microenvironment. Sci Rep *7*, 10541.

Zhao, Z., Condomines, M., van der Stegen, S.J.C., Perna, F., Kloss, C.C., Gunset, G., Plotkin, J., and Sadelain, M. (2015). Structural Design of Engineered Costimulation Determines Tumor Rejection Kinetics and Persistence of CAR T Cells. Cancer Cell *28*, 415-428.

Zhu, C., Kim, K., Wang, X., Bartolome, A., Salomao, M., Dongiovanni, P., Meroni, M., Graham, M.J., Yates, K.P., Diehl, A.M.*, et al.* (2018). Hepatocyte Notch activation induces liver fibrosis in nonalcoholic steatohepatitis. Sci Transl Med *10*.

Zhu, Y., Tchkonia, T., Fuhrmann-Stroissnigg, H., Dai, H.M., Ling, Y.Y., Stout, M.B., Pirtskhalava, T., Giorgadze, N., Johnson, K.O., Giles, C.B.*, et al.* (2016). Identification of a novel senolytic agent, navitoclax, targeting the Bcl-2 family of anti-apoptotic factors. Aging Cell *15*, 428-435.

Zhu, Y., Tchkonia, T., Pirtskhalava, T., Gower, A.C., Ding, H., Giorgadze, N., Palmer, A.K., Ikeno, Y., Hubbard, G.B., Lenburg, M.*, et al.* (2015). The Achilles' heel of senescent cells: from transcriptome to senolytic drugs. Aging Cell *14*, 644-658.